Investigation on the electrical and electrochemical properties of conducting polymer coated aCNT- bismuth ferrite nanocomposites

A thesis submitted toward partial fulfilment of the requirements for the degree of

Master of Technology in
Nanoscience and Technology
Course affiliated to Faculty of Engineering & Technology
Jadavpur University

Submitted by

Name*:* Tuhin Roychowdhury

ROLL NO.: M4NST14-10

Under the guidance of

Dr. Kalyan Kumar Chattopadhyay

Jadavpur University

SCHOOL OF MATERIALS SCIENCE AND NANOTECHNOLOGY
M.Tech (Nanoscience and Technology) course affiliated to
Faculty of Engineering and Technology
Jadavpur University
Kolkata-700032
India

2014

M.Tech. (Nanoscience and Technology) course affiliated to
Faculty of Engineering and Technology
Jadavpur University
Kolkata, India

CERTIFICATE OF RECOMMENDATION

This is to certify that the thesis entitled **"Investigation on the electrical and electrochemical properties of conducting polymer coated aCNT-bismuth ferrite nanocomposites"** is a bonafide work carried out by **Tuhin Roychowdhury** under our supervision and guidance for partial fulfilment of the requirement for Post Graduate Degree of Master of Technology in Nanoscience and Technology during the academic session 2013-2014.

THESIS ADVISOR
Dr. Kalyan Kumar Chattopadhyay
Director
School of Materials Science and Nanotechnology
Jadavpur University,
Kolkata-700032

DIRECTOR
School of Materials Science and Nanotechnology
Jadavpur University,
Kolkata-700 032

DEAN
Faculty Council of Interdisciplinary Studies, Law and Management
Jadavpur University,
Kolkata-700 032

M.Tech. (Nanoscience and Technology) course affiliated to
Faculty of Engineering and Technology
Jadavpur University
Kolkata, India

CERTIFICATE OF APPROVAL **

This foregoing thesis is hereby approved as a credible study of an engineering subject carried out and presented in a manner satisfactorily to warranty its acceptance as a prerequisite to the degree for which it has been submitted. It is understood that by this approval the undersigned do not endorse or approve any statement made or opinion expressed or conclusion drawn therein but approve the thesis only for purpose for which it has been submitted.

Committee of final examination for evaluation of Thesis

** Only in case the thesis is approved.

DECLARATION OF ORIGINALITY AND COMPLIANCE OF ACADEMIC ETHICS

I hereby declare that this thesis contains literature survey and original research work by the undersigned candidate, as part of his **Master of Technology in Nanoscience and Technology** studies during academic session 2013-2014.

All information in this document has been obtained and presented in accordance with academic rules and ethical conduct.

I also declare that, as required by this rules and conduct, I have fully cited and referred all material and results that are not original to this work.

NAME: Tuhin Roychowdhury

ROLL NUMBER: M4NST14-10

THESIS TITLE: Investigation on the electrical and electrochemical properties of conducting polymer coated aCNT-bismuth ferrite nanocomposites.

SIGNATURE: DATE:

Dedicated to parents and grandparents

"Be yourself ; everyone else is undertaken."

Oscar Wilde

Abstract

In the present work, the composite materials consist of noble carbon material (a-CNT) and conducting polymer reinforced with ferrite material have been synthesized using low temperature simple sol-gel procedure which incorporates gelation followed by polymerization. The crystallization of BFO is supposed to be completed at the temperature of 170 °C due to citric acid which used as chelating agent. The as synthesized samples were characterized by field emission scanning electron microscopy (FESEM), high resolution transmission electron microscopy (HRTEM), fourier transform infra-red spectroscopy (FTIR) and X-ray diffraction spectroscopy (XRD). FESEM study has been done due to analyse surface morphology and dispersion of ferrite. HRTEM study is used to observe the dispersion of nanoparticles in the CNT-Polymer matrix. FTIR study is carried out to study of chemical composition of the as prepared samples. For the application purpose we chose the electrochemical analysis of samples as well as current-voltage characteristics. We believe that the results show new possibilities towards the direction of electrochemistry as well as charge transport.

***Keywords**: In-situ polymerization, gelation, ferrite, electrochemistry, current-voltage, transport.*

Acknowledgement

This work described in the thesis titled "Investigation on the electrical and electrochemical properties of conducting polymer coated aCNT-bismuth ferrite nanocomposites" was started in the Thin Film & Nanoscience Laboratory, Jadavpur University in 2013 and would not have been what it is today without the support and advice of others. It was an opportunity to work under the guidance of Dr. K. K. Chattopadhyay, Director, School of Materials Science & Nanotechnology. I sincerely would like to thank him for his support and experienced guidance throughout the project work and for allowing me to utilize the valuable resources and necessary instrumental, laboratory and library facilities. I accept this opportunity to thank all members of Thin Film and Nanoscience Laboratory of Physics Department for giving me the golden opportunity to work with Nirmalya da, Debabrata da, Soumen da, Saswati di, Biswajit da for helping me to carry out some key characterization studies. I am deeply indebted to Supratim da for his invaluable contribution to complete my project work. I also acknowledge the help rendered by Mr Subhasis Das and Mr Pankaj Bhadra during my execution of work. I take this occasion also to thank all my classmates namely Debanjan, Poulomi, Parthajeet, Subhronil da, Dheeraj etc whose cooperative attitude helped me very much. Among them, especially Subhajit has contributed the backbone of my project work. I also like to acknowledge the cooperation of all the staff members of department during my project work.

Finally, I pay my indebt acknowledgement to my parents for providing me inspiration and supporting me throughout my carrier.

Date : Tuhin Roychowdhury

CONTENTS:

Chapter 1:
Introduction

1. Introduction:

1.1. Definition of nanoscience:

Nanoscience is an emerging area of science which concerns itself with the study of materials that have very small dimensions, in the range of nano scale. *The word itself is a combination of nano, from the Greek "nanos" (or Latin "nanus"), meaning "Dwarf", and the word "Science" meaning knowledge*[1]. It is an interdisciplinary field that seeks to bring about mature nanotechnology, focusing on the nanoscale intersection of fields such as physics, biology, engineering, chemistry, computer science and more.

Physics is the mother of natural sciences. In principle, physics can be used to explain everything that goes on at the nanoscale. There is active physics research going on in nanomechanics, quantum computation, quantum teleportation, artificial atoms etc. At nanometer scale physics is different. Properties not seen on a macroscopic scale now become important- such as quantum mechanical and thermodynamic properties. Rather than working with bulk materials, one works with individual atoms and molecules. By learning about an individual molecule's properties, we can put them together in very well-defined ways to produce new materials with new and amazing characteristics.

Nanoscience is the study of phenomena on a nanometer scale. Atoms are a few tenths of a nanometer in diameter and molecules are typically a few nanometers in size. Nanometer is a magical point on the length scale, for this is the point where the smallest man-made devices meet the atoms and molecules of the natural world. Typically nano means 10^{-9}. So, a nanometer is one billionth of a meter and is the unit of length that is generally most appropriate for describing the size of single molecule.

Nanometer objects are too small to be seen with naked eye. In fact, if one wanted to see a 10 nm sized marble in his hand, his eye would have to be smaller than a human hair. Anyhow the rough definition of nanoscience could be anything which has at least one dimension less than 100 nanometer[2].

1.2. Definition of nanotechnology:

The nanoworld provides scientists with a rich set of materials useful for probing the fundamental nature of matter. These materials have unique structures and tunable properties. This makes them valuable for many different real world applications. Nanotechnology is currently in a very infantile stage. It is basically the creation of useful/functional materials, devices and systems through control of matter on the nanometer length scale and exploitation of novel phenomena and properties (physical, chemical, biological) at that length scale.

1.3. History:

The first mention of nanotechnology (not yet using that name) was in a talk given by Richard Feynman in 1959, entitled ***there's plenty of Room at the Bottom***. Feynman suggested a means to develop the ability to manipulate atoms and molecules directly, by developing a set of one-tenth-scale machine tools analogous to those found in any machine shop. These small tools would be used to develop and operate a next generation of one-hundredth-scale machine tools, and so forth. As the sizes get smaller, it would be necessary to redesign some tools because the relative strength of various forces would change. Gravity would become less important, surface tension would become more important, van der Waals attraction would become important,

etc. Feynman mentioned these scaling issues during his talk. The feasibility of his proposal has never been effectively refuted.

1.4. What distinguishes nanomaterials from bulk ?

While most microstructured materials have similar properties to the corresponding bulk materials, the properties of materials with nanometer dimensions are significantly different from those of atoms and bulk materials. Among the characteristics of nanomaterials that distinguish them from bulk materials, it is important to note the following:

(1) large fraction of surface atoms;

(2) high surface energy;

(3) spatial confinement;

(4) reduced numbers of imperfections that do not exist in the corresponding bulk materials (Cao 2004).

The use of nanomaterials provides the following advantages. First, all nanomaterials consist of very small particles. This is the first advantage of nanomaterials and nanotechnologies, promoting attainment of super miniaturization. Because they are small, nanostructures can be packed very closely together. As a result, on a given unit of area one can locate more functional nanodevices, which is very important for nanoelectronics. Their high packing density has the potential to bring higher area and volume capacity to information storage and higher speed to information processing (because electrons require much less time to move between components). Thus, new electronic device concepts, smaller and faster circuits, more

sophisticated functions, and greatly reduced power consumption can all be achieved simultaneously by controlling nanostructure interactions and complexity.

Second, because of their small dimensions, nanomaterials have large specific surface areas, accelerating interactions between them and the environment in which they are located. For example, nanoparticles with a radius of 2.5 nm and a density of 5 gcm^{-3} have a surface of 240 m^2g^{-1} when assuming a ball-like shape. For comparison, a dense (compact) material with a weight of 1 g and the same density has a surface area of 2×10^{-6} m^2. Thus, nanoparticles have a much larger surface area per unit of mass compared with larger particles. Because growth and catalytic chemical reactions occur at surfaces, this means that materials in nanoparticle form will be much more reactive than the same mass of material made up of larger particles.

A strong increase in the participation of surface atoms in the physical and chemical properties of nanomaterials is another consequence of a decrease in particle size. It is known that the volume of an object decreases as the third power of its linear dimensions, but the surface area decreases only as its second power. In case of nanoparticles, the surface area-to-volume ratio (the ratio between surface and bulk atoms) increases that bulk.

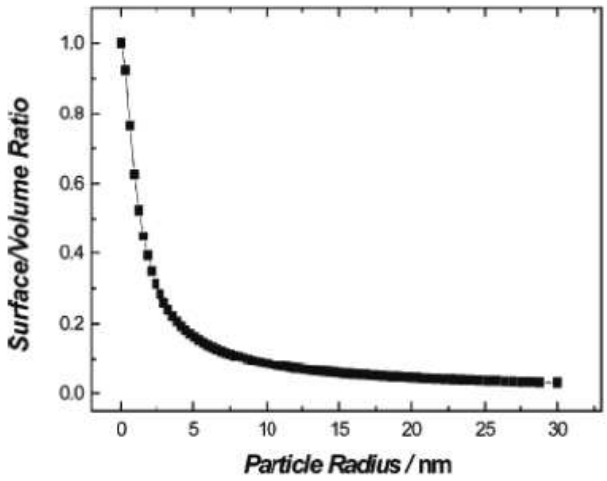

Figure 1.1 : Surface/volume ratio as a function of particle size. (Reprinted from Burda et al. 2005)

This effect is especially strong when the sizes of nanomaterials are comparable to the Debye length (Ogawa et al. 1982; Luth 1995). Simple calculations show that a particle of size 30 nm has 5% of its atoms on its surface; at 10 nm, 20% of its atoms; and at 3 nm, 50% of its atoms (Royal Society 2004) (see Figure 1.1).

It is known that atoms on the surface of nanoparticles have unusual properties and (relatively speaking) there are a lot of them. These surface atoms make nanoparticles very different from just small particles, because not all bonds of surface atoms with neighbouring atoms are enabled. For atoms on uneven surfaces, no saturation of the bonds is even higher. For this reason, corner atoms normally have the highest affinity to form bonds to adsorbate molecules, followed by edge and in-plane surface atoms, a fact that is of great importance for catalytic activity. Alternatively, because of their low stabilization due to low coordination, edge and in particular corner atoms are often missing on single crystals, even in thermodynamic equilibrium (Roduner 2006). Recently, size-dependent variation in oxidation state and lattice parameter has been reported for cerium oxide nanoparticles (Deshpande et al. 2005) (see Figure 1.2).

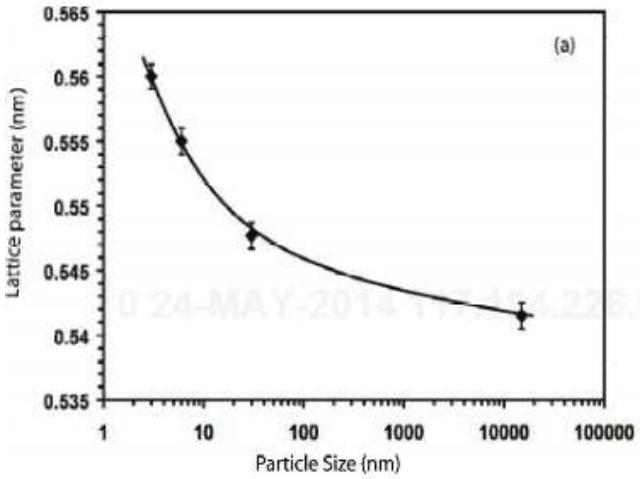

Figure 1.2 : Semilog plot of lattice parameter as a function of particle size. (Reprinted from Deshpande et al. 2005)

As a result of the changes that occur in particles with a decrease of particle size, nanomaterials can have extremely high biological and chemical reactivity (Eustis and El-Sayed 2006). For example, catalytically active nanomaterials allow accelerating either chemical or biochemical reactions by tens of thousands, and even a million times. This attribute explains even 1 g of nanomaterial can be more effective than 1 ton of a similar but macro substance. As will be shown later, the high chemical and catalytic activity of nanomaterials opens up fundamentally new opportunities for elaboration next-generation chemical sensors.

Another aspect we must consider is that the free surface is a place of accumulation (sink) of crystallographic defects. At small particles sizes, the surface concentration of such defects increases considerably. Classical calculations of van Hardeveld and Hartog (1969) showed that the largest changes of proportions between facets, edges, corners, and micro defects at the surface occur between 1 and 5 nm. As a result, strong lattice distortion and even a change of lattice type can take place on the surface layer. In fact, due to accumulation of structural defects and chemical

impurities on the surface, we can observe purification of the bulk area of the nanoparticles.

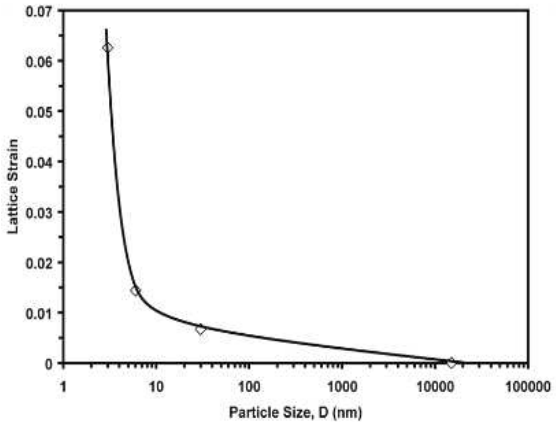

Figure 1.3 : Semilog plot of lattice strain as a function of particle size. (Reprinted from Deshpande et al. 2005).

An important specific characteristic of nanomaterial properties (we mean here polycrystalline materials with grain size less than 40 nm) is an increase of the role of interfaces with decrease of the size of grains or crystallites in nanomaterials. Experimental research has shown that the state of grain boundaries has a non-equilibrium character, conditioned by the presence of the high concentration of grain boundary defects. This non-equilibrium is characterized by extra energy of the grain boundaries and by the presence of long-range elastic stress (see Figure 1.3). At the same time, the grains have ordered crystallographic structure, while the grain boundary defects act as a source of elastic strains. Non-equilibrium of the grain boundaries initiates the occurrence of the lattice distortion, the change of interatomic distances, and the appearance of sufficient displacement of atoms, right up to loss of an ordered state.

Another important factor peculiar to nanoparticles is their tendency to aggregation. The possibility of migration (diffusion) of either atoms or groups of

atoms along the surface and the boundaries, as well as the presence of attractive forces between them, often leads to processes of self-organization into various cluster structures. This effect has already been used for creation of ordered nanostructures in optics and electronics.

One more important aspect of nanomaterial properties is connected with the fact that, during transport processes (diffusion, electro- and thermal conductivity, etc.), there are certain effective lengths of free path of a carrier of this transport (Le), such as phonon and electron mean free paths, the Debye length, and the exciton diffusion length for certain polymers (see Figure 1.4). While proceeding to sizes smaller than Le, transport speed starts to depend on both the size and the shape of the nanomaterial; generally, the transport speed increases sharply. For example, in some cases the length of the electron free path can be considered as Le. As can be seen in Figure 1.4, chemically synthesized nanowires 5–100 nm in diameter allow experimental access to a rich spectrum of mesoscopic phenomena.

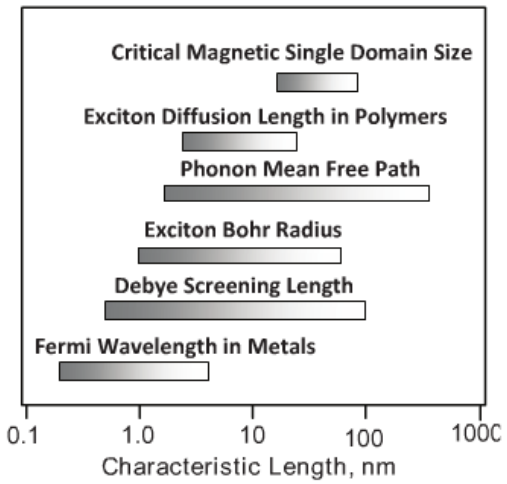

Figure 1.4 : A few characteristic length scales for condensed systems at 300 K. (Data from Law et al. 2004.)

The principal characteristics of nanomaterials are conditioned by not only by their small the size, but also by the appearance of new quantum mechanical effects in

a dominating role at the interface (Esaki 1991; Gimzewski and Welland 1995; Serena and Garcia 1997; Ciraci et al. 2001). Those quantum size effects occur at a critical size, which is commensurate with the so-called correlative radius of one or another physical phenomena, for example, with the length of the free path of electrons or photons, the length of coherence in a superconductor, sizes of magnetic domains, and so on. As a rule, quantum size effects appear in materials with crystallite sizes in the nanorange $D < 10$ nm. As a result, in nanomaterials with characteristic size, one can expect the appearance of effects which cannot be observed in bulk materials.

In particular, quantum effects may appear in the form of an oscillating change of electric properties for example, conductivity—or the appearance of new energetic states for electrons. At nanoscale dimensions the normally collective electronic properties of the solid become severely distorted, and the electrons at this length scale tend to follow the ‘‘particle-in-a-box’’ model, so that they often require higher-order calculations to account for band structure (Law et al. 2004). The electronic states are more like those found in localized molecular bonds than in macroscopic solids. The main implication of this confinement is a change in the system total energy, and hence the overall thermodynamic stability. These effects thus create conditions for the elaboration of chemical sensors based on entirely new principles.

Absence of point defects is another characteristic property of some nanomaterials, such as nanotubes. For example, because of the absence of point defects, individual carbonic nanotubes have strength that exceeds the strength of the best steel. At the same time, they are much lighter in weight than steel, such that nanotubes may be 6 times lighter in weight and 50–100 times stronger than steel.

1.5. Classification of nanomaterials:

Nanomaterials can be classified dimension wise into following categories.

Table 1.1 : Categories of Nanomaterials

Classification	Examples
1 dimension < 100nm 2 dimensions < 100nm. 3 Zero or 3 dimensions < 100nm	nanorods, nanowires etc. Tubes, fibers, platelets, etc Particles, quantum dots, hollow Spheres, etc.

On the basis of phase composition, nanomaterials in different phases can be classified as,

1. Single phase solids include crystalline, amorphous particles and layers, etc.
2. Multi phase solids include matrix composites, coated particles, etc.
3. Multi phase systems include colloids, aero gels, Ferro fluids, etc

.

1.6. Some applications of nanomaterials:

The potential applications of nanotechnology in different fields are the following:

1. Electronics :

- Improving display screens on electronics devices. This involves reducing power consumption while decreasing the weight and thickness of the screens. This can be achieved using **carbon nanotubes (CNT)**. They can be used as field emitters with extremely high efficiency for field emission displays (FED).

- Increasing the density of memory chips. Researchers are developing a type of memory chip with a projected density of one terabyte of memory per square inch or greater. Integrated nanosensors are used for collecting, processing and communicating massive amounts of data with minimal size, weight, and power consumption

- Reducing the size of transistors used in integrated circuits. One researcher believes it may be possible to "put the power of all of today's present computers in the palm of your hand". Processors with declining energy use and cost per gate, thus increasing efficiency of computer by 106.

- Allowing the refrigeration without the need of refrigeration fluids. This can be done if nanoparticles with large magnetic moments and adequate coericivity can be obtained then the magnetocaloric effect may allow refrigeration on a practical scale.

2. Health and Medicine :

- Nanomedicine has the potential to enable early detection and prevention, and to essentially improve diagnosis, treatment and follow-up of diseases.

- Biological tests measuring the presence or activity of selected substances become quicker, more sensitive and more flexible when certain nano scale particles are put to work as tags and labels.

- Nanodevices can make gene sequencing more efficient. Gold nanoparticles tagged with short segments of DNA can be used for detection of genetic sequence in a sample.

- Nanotechnology can help to reproduce or to repair damaged tissue. This so called tissue engineering makes use of artificially stimulated cell. It might replace today’s conventional treatments, e.g. transplantation of organs or artificial implants.

Carbon nanotubes have recently become promising functional materials for the development of advanced biosensors with novel features. These sensors are being used for astrobiology to study origins of life. The technology is also being used to develop sensors for cancer diagnostics. CNT, though inert, can be functionalized at the tip with a probe molecule. Their study uses AFM as an experimental platform.

3. Transportation

4. Energy and Environment

5. Space exploration etc.

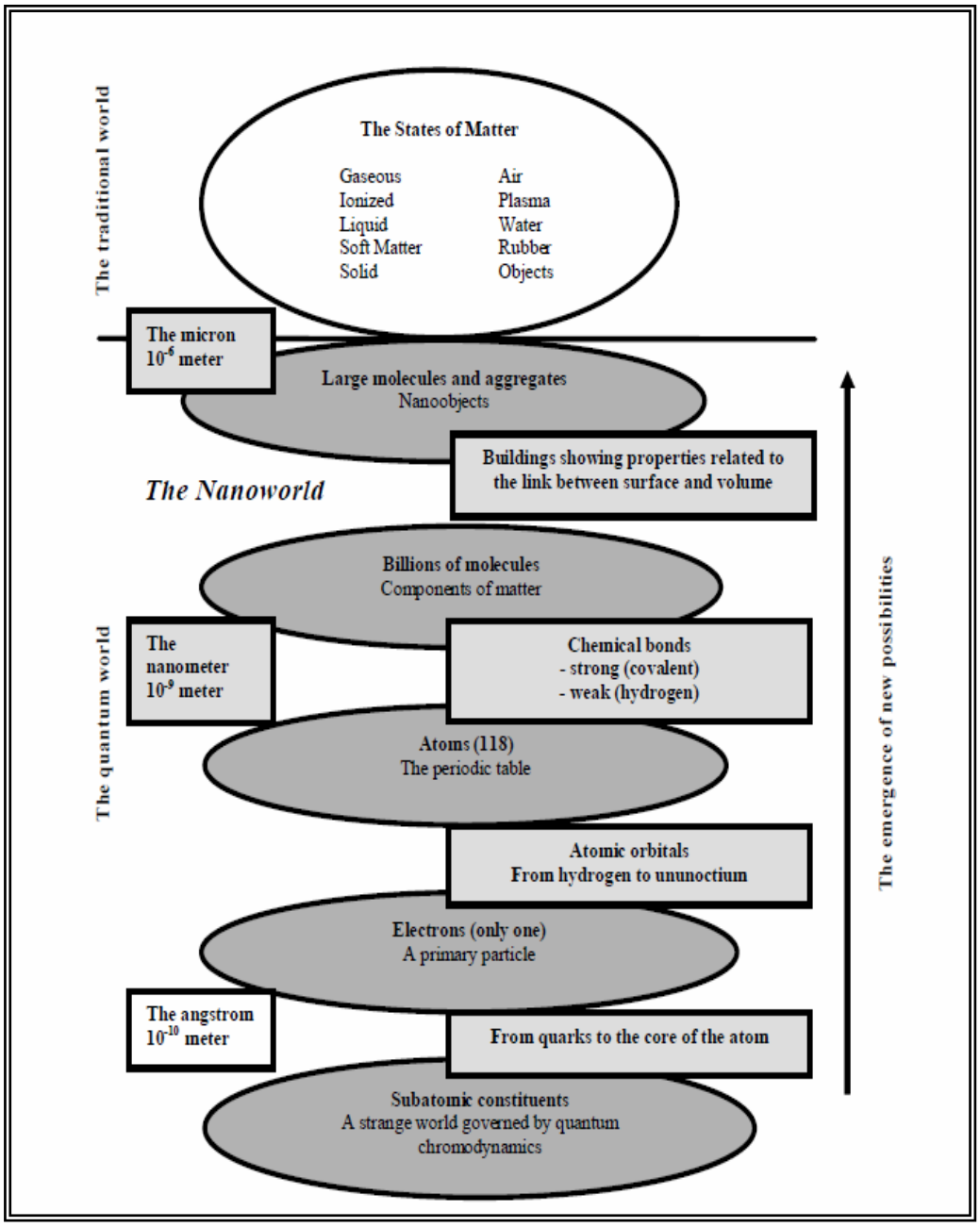

Figure 1.5 : A short overview of nano world.

1.7. Definition of Carbon nanotubes(CNTs):

A Carbon Nanotube is a tube-shaped material, made of carbon, having a diameter measuring on the nanometer scale. A nanometer is one-billionth of a meter, or about one ten-thousandth of the thickness of a human hair. The graphite layer appears somewhat like a rolled-up chicken wire with a continuous unbroken hexagonal mesh and carbon molecules at the apexes of the hexagons. Carbon Nanotubes have many structures, differing in length, thickness, and in the type of helicity and number of layers. Although they are formed from essentially the same graphite sheet, their electrical characteristics differ depending on these variations, acting either as metals or as semiconductors.

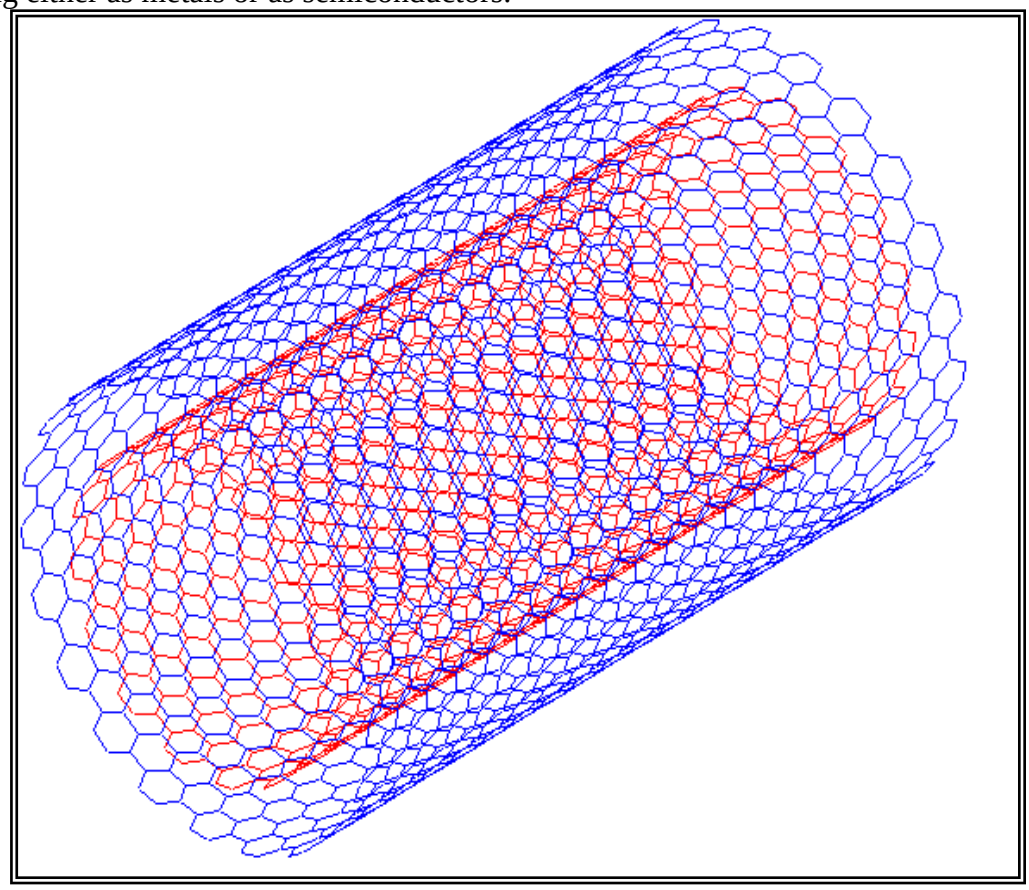

Figure 1.6 : An image of CNT.

Carbon Nanotubes can be categorized by their structures:

a) Single-wall nanotubes : Single-wall nanotubes (SWNT) are tubes of graphite that are normally capped at the ends. They have a single cylindrical wall. The structure of a SWNT can be visualized as a layer of graphite, a single atom thick, called graphene, which is rolled into a seamless cylinder. Most SWNT typically have a diameter of close to 1 nm. The tube length, however, can be many thousands of times longer. SWNT are more pliable yet harder to make than MWNT. They can be twisted, flattened, and bent into small circles or around sharp bends without breaking. SWNT have unique electronic and mechanical properties which can be used in numerous applications, such as field-emission displays, nanocomposite materials, nanosensors, and logic elements. These materials are on the leading-edge of electronic fabrication, and are expected to play a major role in the next generation of miniaturized electronics.

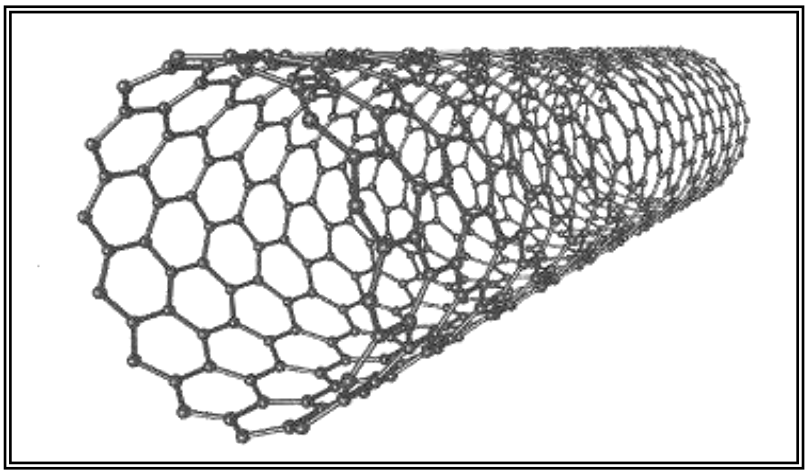

Figure 1.7 : An image of SWCNT.

b) Multi-wall nanotubes : Multi-wall nanotubes can appear either in the form of a coaxial assembly of SWNT similar to a coaxial cable, or as a single sheet of

graphite rolled into the shape of a scroll. The diameters of MWNT are typically in the range of 5 nm to 50 nm. The interlayer distance in MWNT is close to the distance between graphene layers in graphite. MWNT are easier to produce in high volume quantities than SWNT. However, the structure of MWNT is less well understood because of its greater complexity and variety. Regions of structural imperfection may diminish its desirable material properties. The challenge in producing SWNT on a large scale as compared to MWNT is reflected in the prices of SWNT, which currently remain higher than MWNT. SWNT, however, have a performance of up to ten times better, and are outstanding for very specific applications.

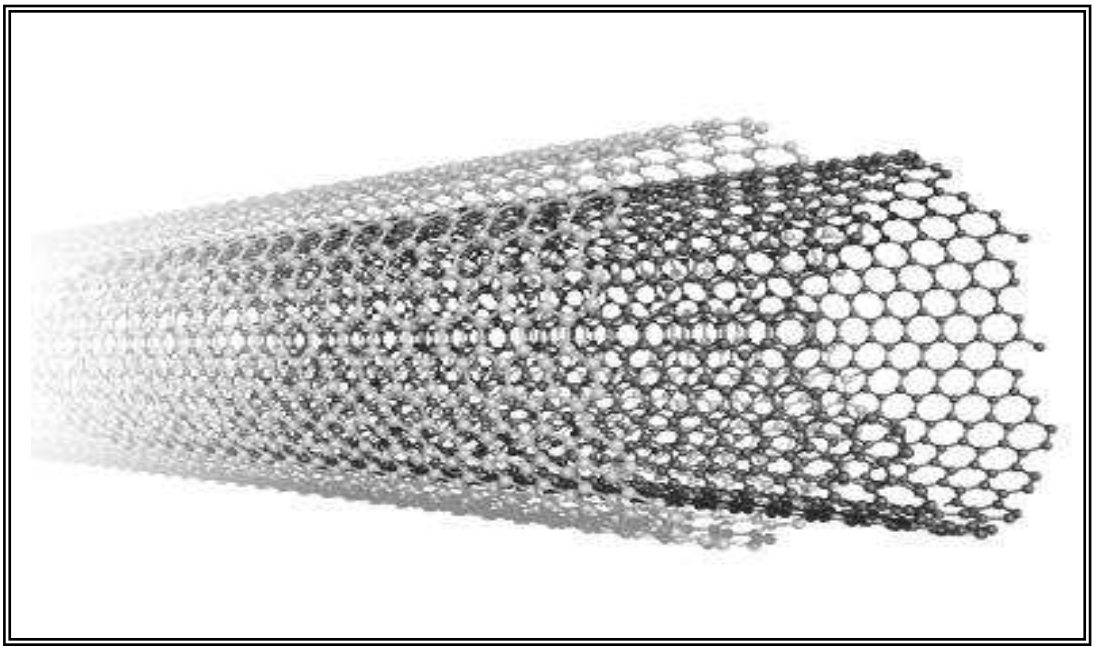

Figure 1.8 : An image of MWCNT.

c) Double-wall nanotubes : Double-wall nanotubes (DWNT) are an important sub-segment of MWNT. These materials combine similar morphology and other properties of SWNT, while significantly improving their resistance to chemicals. This property is especially important when functionality is required to add

new properties to the nanotube. Since DWNT are a synthetic blend of both SWNT and MWNT, they exhibit the electrical and thermal stability of the latter and the flexibility of the former. Because they are developed for highly specific applications, SWNT that have been functionalized are more susceptible to breakage. Creating any structural imperfections can modify their mechanical and electrical properties. However, with DWNT, only the outer wall is modified, thereby preserving the intrinsic properties. Also, research has shown that DWNT have better thermal and chemical stability than SWNT. DWNT can be applied to gas sensors and dielectrics, and to technically-demanding applications like field-emission displays, nanocomposite materials, and nanosensors.

1.8. Background of Carbon nanotubes(CNTs):

The history of carbon nanotubes is not entirely clear even for those in the science therefore giving proper credit to the person that invented the carbon nanotube has been the subject of several high tech debates among the scientific communities. The initial history of nanotubes started in the 1970s. A preparation of the planned carbon filaments was completed by Morinobu Endo who was earning his Ph.D. at the University of Orleans, France. The growth of these carbon filaments were initially thought to be the first carbon nanotubes. However, they failed to meet the measurement requirements for width and thus were deemed. This was still a highly important development in the history of carbon nanotubes, but it just wasn't the right time to be considered the first recognized invention. Giving the proper credit to who invented carbon nanotubes would not come along for another 20 years. In 1991 the true first invention of nanotube was finally made. It seems as though there was a race between Russian nanotechnologists and Sumio Iijima of IBM. The first observation of

the multiwalled carbon nanotubes was credited to Iijima. There are some that hold the belief that in the 1950s there was an initial discovery of what could have possibly been seen as the first carbon nanotubes had Roger Bacon had the high powered electron microscope that would have been necessary. He was credited with the first visual impression of the tubes of atoms that roll up and are capped with fullerene molecules by many scientists in the field. Some state that his discovery just wasn't taken very seriously at the time because science did not know how this discovery could impact scientific research. It would be in 1993 that Iijima and Donald Bethune found single walled nanotubes known as buckytubes. This helped the scientific community make more sense out of not only the potential for nanotube research, but the use and existence of fullerenes. With this information, the complete discovery of carbon nanotubes was realized and Iijima and Bethune were ultimately credited with their discovery in their entirety. Russian nanotechnologists were independently discovering the same visual affirmation. They were just a little bit later in their announcement and the potential affect of this discovery. The continuation of research revealed a great deal about nanotubes and their place in scientific discovery. The research has indicated that there are three basic types of nanotubes (zigzag, armchair, and chiral) as well as single walled and multiwalled nanotubes. There are buckytubes, which are completely hollow molecules that are crafted from pure carbon and are bonded together in a pattern of specific hexagon patterns. The multiwalled nanotubes are likely to suffer from defects. These defects happen in more than half of all multiwalled nanotubes. The multiwalled nanotubes have already made appearances in practical applications like creating tennis rackets that are stronger than steel but are ultra light in weight. These nanotubes are also responsible for creating sunscreen and other skin care products that are clear or able to be blended into the skin without leaving behind residue as well as the creation of UV protective clothing. As

nanotechnologists continue to research nanotubes, there is still a race to discover something new within the science. Scientists are researching the potential for life saving techniques as well as the potential to create nanotubes that can be tailored toward specific designated jobs. With the creation of specified nanotubes, the potential for their use will become unlimited and there will be a nanotechnology world hard at work crafting all kinds of products from the convenient to the life saving. While Roger Bacon might not have been completely aware of the impact his discovery had on the scientific world, he is technically the first scientist to discover these hollow tubes of carbon that are changing lives on a daily basis. Since the initial rediscovery of the nanotubes in 1991, who discovered carbon nanotubes is no longer as important as who can come up with the most practical applications. The nanotube is a molecular structure that can be manufactured, or discovered. In reality, the nanotube is invariable and cannot be anything other than a hollow tube of carbon that remains within the specified single molecule width requirement. With its invariability comes the potential for scientists to create a wide variety of practical applications by testing their potential for directivity and versatility.

1.9. Structure and Properties of Carbon nanotubes(CNTs):

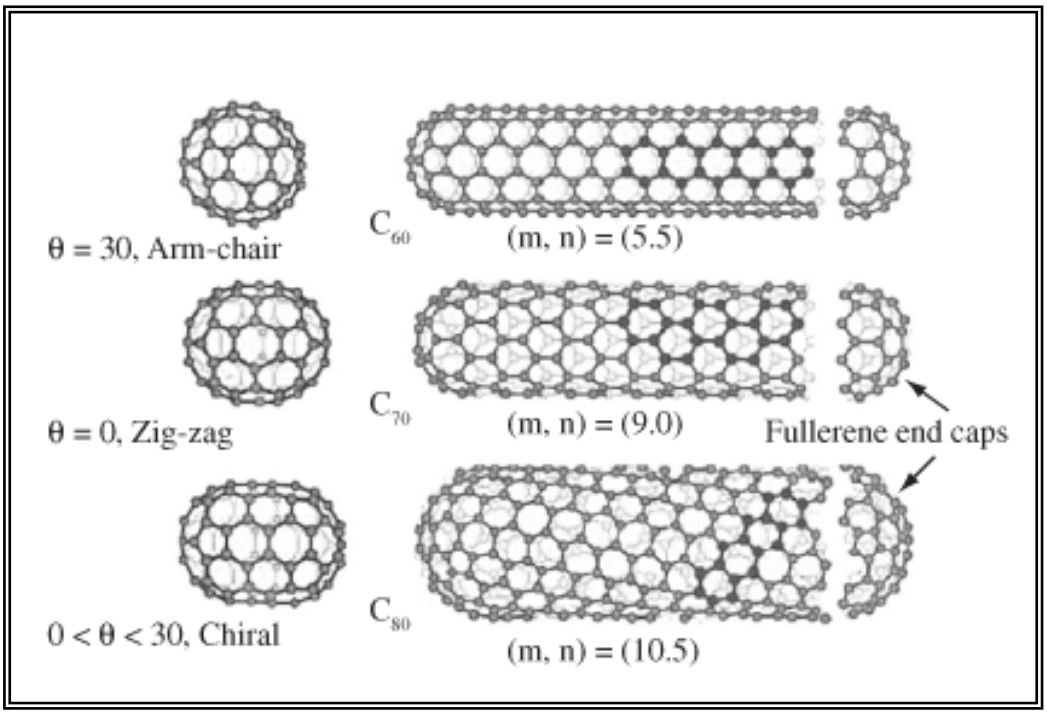

Figure 1.9 : Different structural formation of CNTs.

The structure of carbon nanotubes can be visualized by rolling up a graphite sheet plane to a tube. According to Dresselhaus and co-workers, the crystalline structure of CNTs can be characterized by the (chiral) roll-up vector R within a corresponding graphite sheet plane. R = ma + nb (m,n∈ N), with vectors a and b describing the base unit of the graphite sheet plane. The roll-up vector results from the difference between the two grid points of the graphite lattice that coincide in a single grid point of the nanotube on the imaginary roll-up. The length defines the perimeter, the angle, the helicity (chirality) of the nanotube.

Aside from chiral CNTs, two achiral highly symmetric types of nanotubes can be determined. For m = n (θ = 30°) the tubes are called *"armchair"-nanotubes* and

for either m or n = 0 (θ = 0°) they are referred to as *"zig-zag"-nanotubes*, following the hexagonal arrangement of the carbon atoms along the perimeter, respectively.

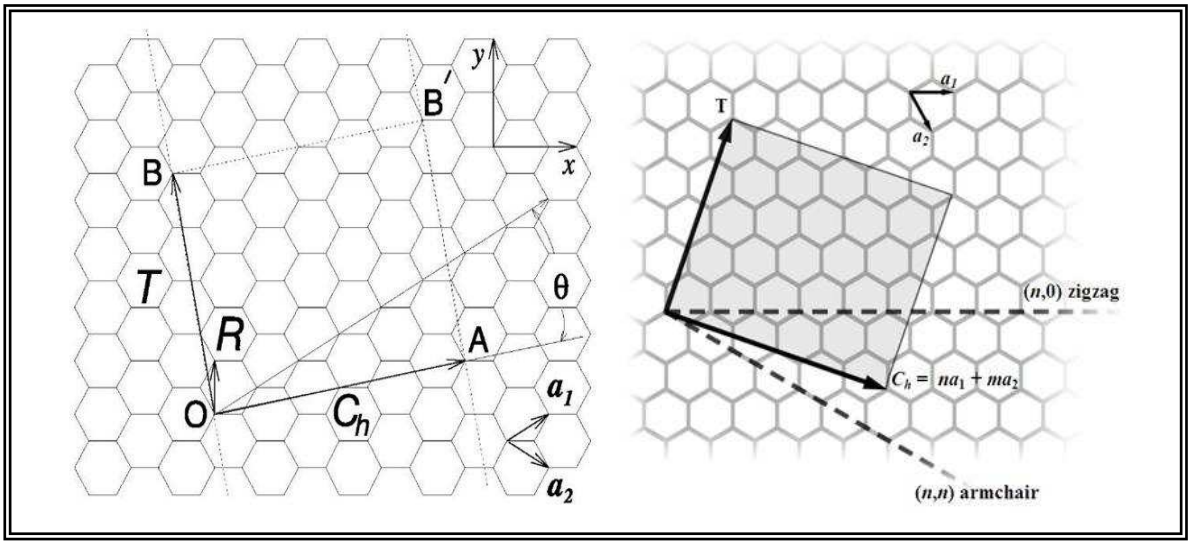

Figure 1.10 : Vector OA is called the chiral vector. It can be defined by the vector Ch=na1+ma2 and the chiral angle with the zigzag axis. Vectors a1 and a2 are the lattice vectors.

The diameter of an ideal nanotube can be calculated from its (n,m) indices as follows

$$d = \frac{a}{\pi}\sqrt{(n^2 + nm + m^2)}.$$

where*a* = 0.246 nm.

.

SWNTs are an important variety of carbon nanotube because most of their properties change significantly with the (n,m) values, and this dependence is non-monotonic. Armchair nanotubes (n=m) are metallic, zigzag nanotube (m=0) is semiconductor and chiral tubes are metallic or semiconductor.

Properties change significantly with the (n,m) values, and this dependence is non-monotonic. Armchair nanotubes (n=m) are metallic, zigzag nanotube (m=0) is semiconductor and chiral tubes are metallic or semiconductor.

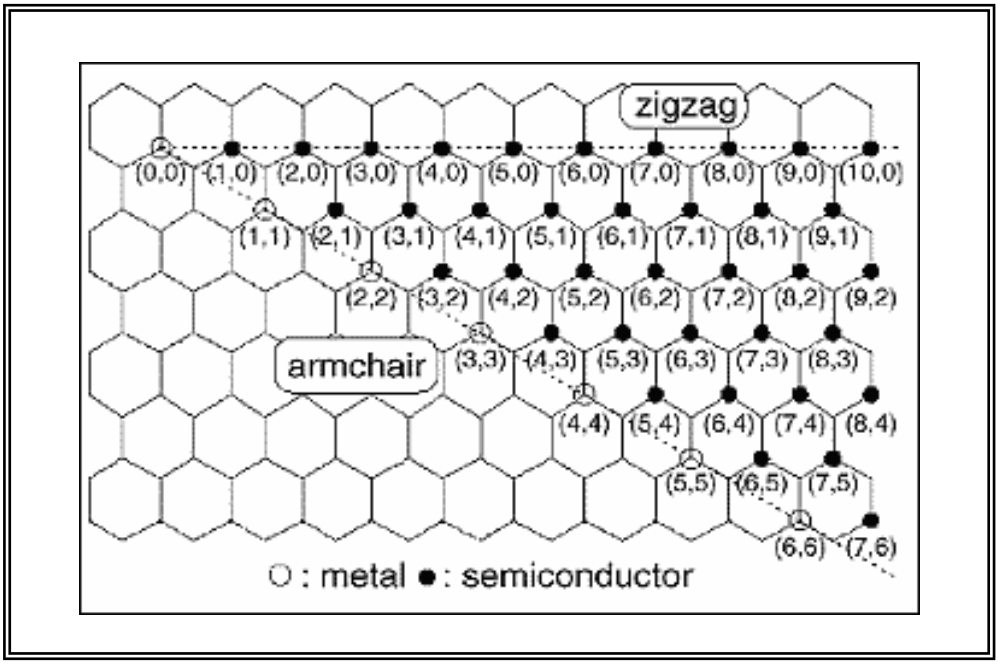

Figure 1.11 : Labelling convention for nanotubes.

Electronic, molecular and structural properties of carbon nanotubes are determined to a large extent by their nearly one dimensional structure. The most important properties of CNTs and their molecular background are stated below.

High electric conductivity : Because of the symmetry and unique electronic structure of graphene, the structure of a nanotube strongly affects its electrical properties. For a given (*n*,*m*) nanotube, if $n = m$, the nanotube is metallic; if $n - m$ is a multiple of 3, then the nanotube is semiconducting with a very small band gap, otherwise the nanotube is a moderate semiconductor. Thus all armchair ($n = m$) nanotubes are metallic, and nanotubes (6,4), (9,1), etc. are semiconducting[3]. However, this rule has exceptions, because curvature effects in small diameter carbon nanotubes can strongly influence electrical properties. Thus, a (5,0) SWCNT that should be semiconducting in fact is metallic according to the calculations. Likewise, *vice versa*—zigzag and chiral SWCNTs with small diameters that should be metallic have

finite gap (armchair nanotubes remain metallic). In theory, metallic nanotubes can carry an electric current density of 4×10^9 A/cm^2, which is more than 1,000 times greater than those of metals such as copper,[4] where for copper interconnects current densities are limited by electro migration. Because of their nanoscale cross-section, electrons propagate only along the tube's axis. As a result, carbon nanotubes are frequently referred to as one-dimensional conductors. The maximum electrical conductance of a single-walled carbon nanotube is $2G_0$, where $G_0 = 2e^2/h$ is the conductance of a single ballistic quantum channel. There have been reports of intrinsic superconductivity in carbon nanotubes.[5][6][7] Many other experiments, however, found no evidence of superconductivity, and the validity of these claims of intrinsic superconductivity remains a subject of debate.[8]

High thermal conductivity : All nanotubes are expected to be very good thermal conductors along the tube, exhibiting a property known as "ballistic conduction", but good insulators laterally to the tube axis. Measurements show that a SWNT has a room-temperature thermal conductivity along its axis of about 3500 $W \cdot m^{-1} \cdot K^{-1}$;[9] compare this to copper, a metal well known for its good thermal conductivity, which transmits 385 $W \cdot m^{-1} \cdot K^{-1}$. A SWNT has a room-temperature thermal conductivity across its axis (in the radial direction) of about 1.52 $W \cdot m^{-1} \cdot K^{-1}$,[10] which is about as thermally conductive as soil. The temperature stability of carbon nanotubes is estimated to be up to 2800 °C in vacuum and about 750 °C in air.

Mechanical strength : Carbon nanotubes are the strongest and stiffest materials yet discovered in terms of tensile strength and elastic modulus respectively. This strength results from the covalent sp^2 bonds formed between the individual carbon atoms. In 2000, a multi-walled carbon nanotube was tested to have a tensile strength of 63 GPa.

(For illustration, this translates into the ability to endure tension of a weight equivalent to 6422 kg (14,158 lbs) on a cable with cross-section of 1 mm^2.) Further studies, such as one conducted in 2008, revealed that individual CNT shells have strengths of up to ~100 GPa, which is in agreement with quantum/atomistic models. Since carbon nanotubes have a low density for a solid of 1.3 to 1.4 g/cm^3, its specific strength of up to 48,000 $kN \cdot m \cdot kg^{-1}$ is the best of known materials, compared to high-carbon steel's 154 $kN \cdot m \cdot kg^{-1}$.Under excessive tensile strain, the tubes will undergo plastic deformation, which means the deformation is permanent. This deformation begins at strains of approximately 5% and can increase the maximum strain the tubes undergo before fracture by releasing strain energy. Although the strength of individual CNT shells is extremely high, weak shear interactions between adjacent shells and tubes leads to significant reductions in the effective strength of multi-walled carbon nanotubes and carbon nanotube bundles down to only a few GPa's. This limitation has been recently addressed by applying high-energy electron irradiation, which crosslinks inner shells and tubes, and effectively increases the strength of these materials to ~60 GPa for multi-walled carbon nanotubes and ~17 GPa for double-walled carbon nanotube bundles.

Table 1.2: Mechanical parameters of CNT

Material	Young's modulus (TPa)	Tensile strength (GPa)	Elongation at break (%)
SWNT	~1 (from 1 to 5)	13–53	16
Armchair SWNT	0.94	126.2	23.
Zigzag SWNT	0.94	94.5	15.6–17.5
Chiral SWNT	0.92		
MWNT	0.2–0.8–0.95	11–63–150	
Stainless steel	0.186–0.214	0.38–1.55	15–50
Kevlar–29&149	0.06–0.18	3.6–3.8	~2

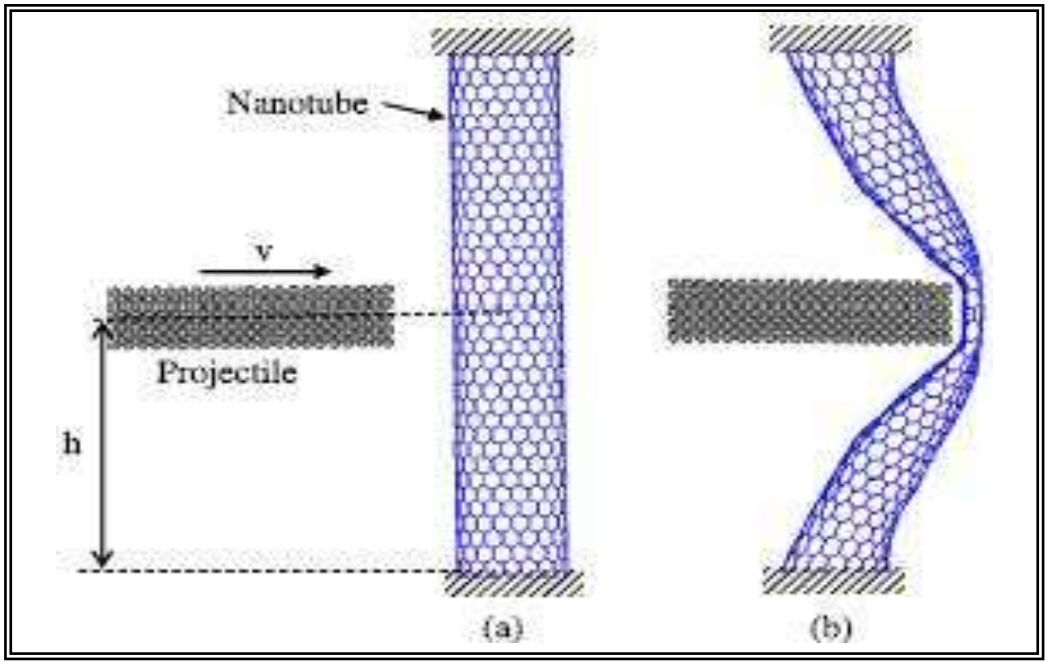

Figure 1.12 :Mechanical property of CNT.

Thermal resistivity / stability : All nanotubes are expected to be very good thermal conductors along the tube, exhibiting a property known as "ballistic conduction", but good insulators laterally to the tube axis. Measurements show that a SWNT has a room-temperature thermal conductivity along its axis of about 3500 $W \cdot m^{-1} \cdot K^{-1}$;

compare this to copper, a metal well known for its good thermal conductivity, which transmits 385 $W \cdot m^{-1} \cdot K^{-1}$. A SWNT has a room-temperature thermal conductivity across its axis (in the radial direction) of about 1.52 $W \cdot m^{-1} \cdot K^{-1}$, which is about as thermally conductive as soil. The temperature stability of carbon nanotubes is estimated to be up to 2800 °C in vacuum and about 750 °C in air.

Optical property : The optical properties of CNTs refer to the absorption, photoluminescence, and Raman spectroscopy. Whereas mechanical, electrical and electrochemical (super capacitor) properties of the carbon nanotubes are well established and have immediate applications, the practical use of optical properties is yet unclear. In particular, light-emitting diodes (LEDs) and photo-detectors based on a single nanotube have been produced in the lab. Their unique feature is not the efficiency, which is yet relatively low, but the narrow selectivity in the wavelength of emission and detection of light and the possibility of its fine tuning through the nanotube structure. In addition, bolometer and optoelectronic memory devices have been realized on ensembles of single-walled carbon nanotubes.

Field emission : Carbon nanotubes have many potential applications. One of these is the use of nanotubes as electron beam sources. A typical nanotube has a diameter of only a few nanometers, but can be microns long. Applying a voltage to such an object causes electrons to be field emitted right off the end of the tube. The effect is due to the intense electric field concentrated at the ultra sharp tip of the nanotube. Many researchers have shown that a viable field emission electron beam source can be fabricated from carbon nanotubes. The tubes are simply mixed into an epoxy matrix to produce a conducting matrix of tube tips. No matter how the surface is cut, it bristles with the ends of nanotubes, which are typically stronger than any cutting

mechanism. Applying a voltage to this epoxy matrix in turn causes these nanotube tips to field emit a stable electron beam.

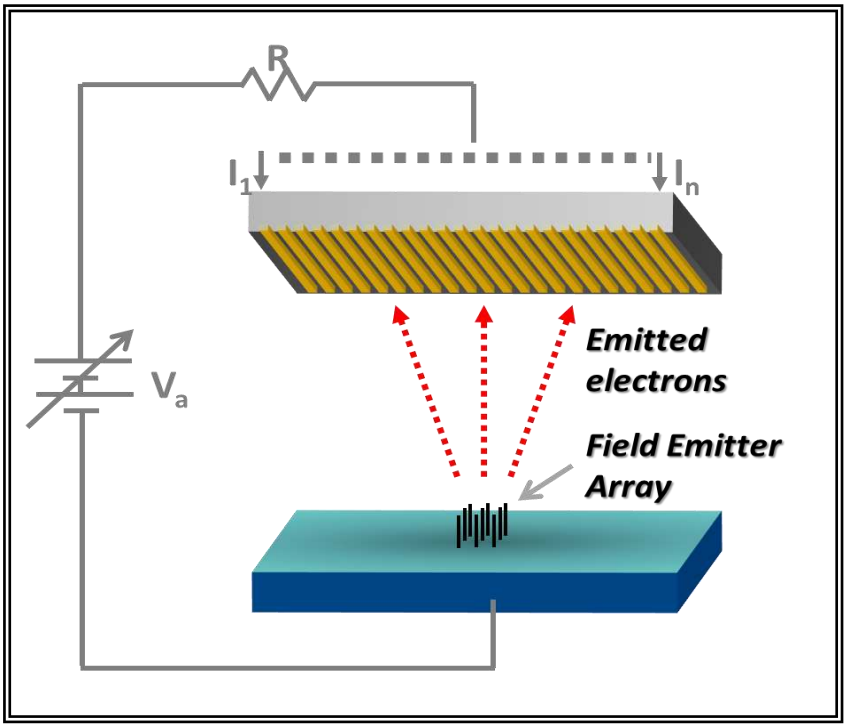

Figure 1.13 :Field emission property of CNT

Chemical reactivity : The chemical reactivity of a CNT is, compared with a grapheme sheet, enhanced as a direct result of the curvature of the CNT surface. Carbon nanotube reactivity is directly related to the pi-orbital mismatch caused by an increased curvature. Therefore, a distinction must be made between the sidewall and the end caps of a nanotube. For the same reason, a smaller nanotube diameter results in increased reactivity. For example, the solubility of CNTs in different solvents can be controlled this way. Though, direct investigation of chemical modifications on nanotube behaviour is difficult as the crude nanotube samples are still not pure enough.

1.10. Applications of Carbon nanotubes(CNTs):

Carbon Nanotube Technology can be used for a wide range of new and existing applications:

- Conductive plastics
- Structural composite materials
- Flat-panel displays
- Gas storage
- Antifouling paint
- Micro- and nano-electronics
- Radar-absorbing coating
- Technical textiles
- Ultra-capacitors
- Atomic Force Microscope (AFM) tips
- Batteries with improved lifetime
- Biosensors for harmful gases
- Extra strong fibers

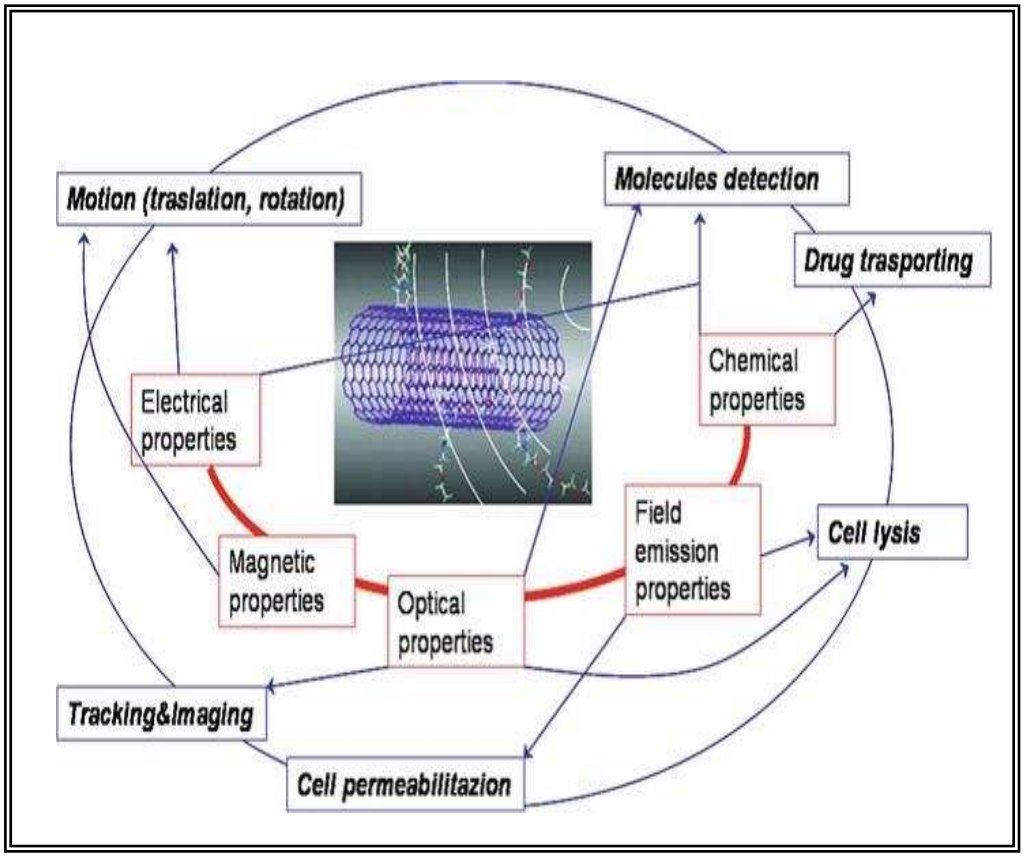

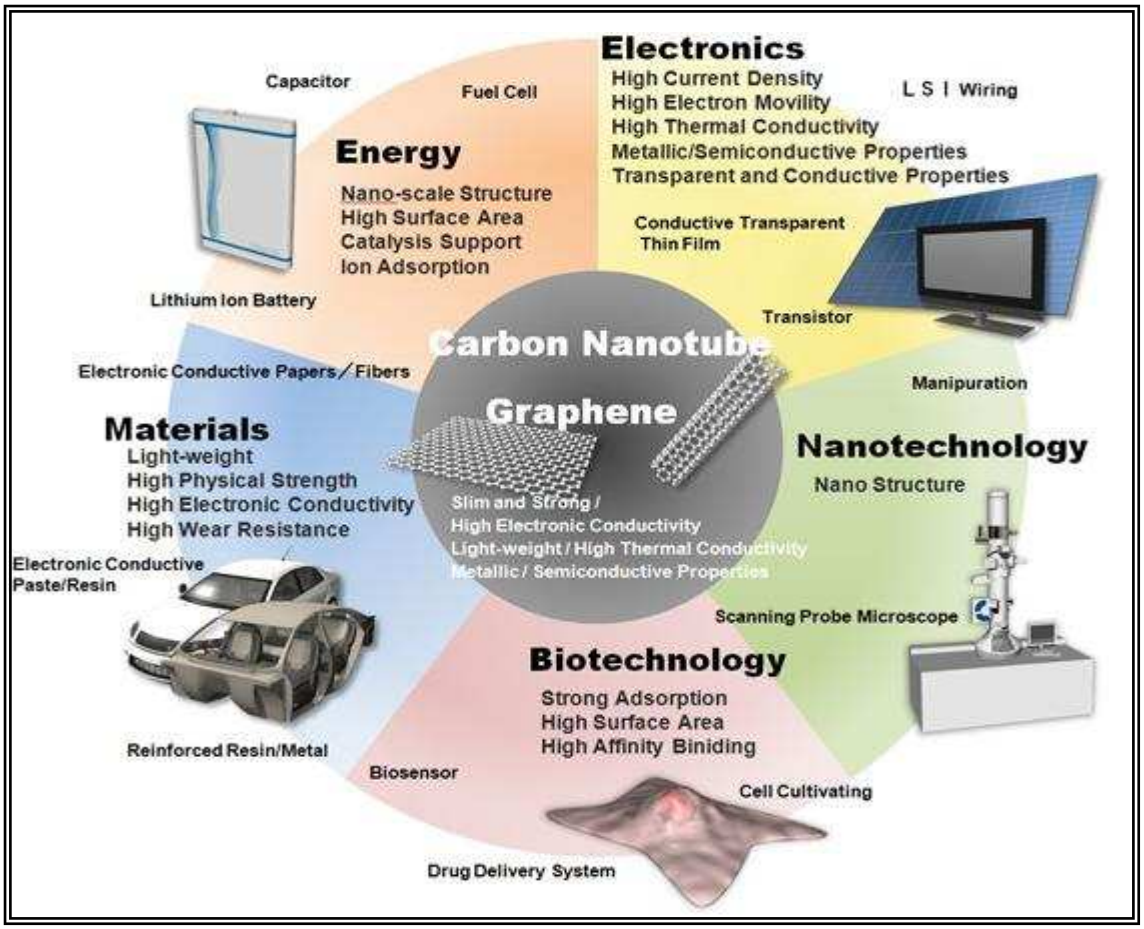

Figure 1.14 : Applications of CNT.

1.11. Introduction to Multiferroic Materials :

Multiferroic materials that exhibit long range electric as well as magnetic orderings have been studied for a new type of memory application using a combination of ferroelectric and ferromagnetic properties. Among them, $BiFeO_3$ (BFO) with a rhombohedrally distorted simple perovskite structure, has been of much interest due to its antiferromagnetic behaviour with a relatively high Néel temperature ($T_N \sim 380$ ° C and its ferroelectric behaviour with a high Curie temperature $T_C \sim 810$ ° C. The spontaneous polarization of bulk BFO was expected to be $\sim 91.5\ \mu C/cm^2$ because of large atomic displacements and a high Curie temperature. However, the spontaneous polarizations reported in the literature were much lower than the theoretical ideal one. This can be attributed to the high leakage current densities of BFO, since the ferroelectric properties of BFO disappeared with the high bias electric fields due to the high leakage current.

1.12. Bismuth Ferrite :

Bismuth Ferrite ($BiFeO_3$) is a multiferroic materials which shows simultaneous coexistence of ferroelectric with high Curie temperature (T C = 810-830˚C) and anti-ferromagnetic order parameters in perovskite structure. However, these two ordering parameters are mutually exclusive in principle because ferroelectricity and magnetism require different filling states of d shells of transition metal ions. Empty d shells mainly exist in Ferro-electricity, while partially filled d shells are required in magnetism. Multiferroic exhibits weak magnetism at room temperature.

Multiferroics have been known as materials exhibiting ferromagnetic and ferroelectric properties at the same time, which have exhibited interesting physical properties as well as possibility of practical applications for new memory devices. The rhombohedrally distorted simple perovskite structure of $BiFeO_3$ is one of the representative multiferroic materials. It is interesting due to the antiferromagnetic behaviour with a relatively high Neel temperature and the ferroelectric behaviour with a high Curie temperature. Although rhombohedral $BiFeO_3$ (BFO R-phase) has been studied extensively since first discovery in 1960s, electrical properties of the pure BFO R-phase have been rarely reported due to its high conductivity, which may originated from uncertain oxygen stoichiometry, high defect density and poor sample quality. In order to understand the properties of multiferroic BFO, it is very important that the fabrication procedure of pure BFO phase should be established. If temperature and oxygen partial pressure were not controlled accurately during crystallization of the BFO R-phase, the kinetics of phase formation always lead to other impurity phases in Bi–Fe–O system, such as $Bi_2Fe_4O_9$,$Bi_2O_{2.75}$, and $Bi_{46}Fe_2O_{72}$. Recently, pure BFO ceramics, including ferroelectric hysteresis loops at room temperature, have been independently synthesized by the solid state reaction method followed with leaching out the impurity phases using diluted nitric acid and by a rapid liquid phase sintering technique [11]. In spite of these preparation techniques for pure BFO, studies on the phase evolution, microstructure, and electrical properties of the BFO prepared by a solgel method, which has great advantages on thin film fabrications, are still rare in the literature.

1.13. Introduction to Polymers :

A **polymer** is a large molecule, or macromolecule, composed of many repeated subunits, known as monomers. Polymers, both natural and synthetic, are created via polymerization of many monomers. Their consequently large molecular mass relative to small molecule compounds produces unique physical properties, including toughness, viscoelasticity, and a tendency to form glasses and semicrystalline structures rather than crystals. Polymers have the advantage that they are so much more easily to be processed than metals for example. One can very easily cover large surfaces with a spin-coated polymer solution. Once the solvent has evaporated one is left with a layer of polymer chains. Most plastics can be deformed reversibly and they also do not break easily, which is not true for metals.

1.14. Conducting Polymers :

Conducting polymers (CPs) were first produced in the 1960s and they are the most recent generation of polymers. CPs have both electrical and optical properties similar to those of metals and inorganic semiconductors, but they also exhibit the attractive properties associated with conventional polymers, such as ease of synthesis and flexibility in processing. This primer presents an introduction to the physical and electrochemical properties and covers main applications of CPs in many fields. The first part is focused on the charge transport mechanism of CPs. Synthesis strategies applied to CPs are reviewed in the second part. The following sections are focused on the ion transport kinetics during redox processes of CPs and the advantages of use

functionalized monomer in order to obtain CPs with desirable properties. Finally some applications of CPs are reviewed.

Polymers have always been considered as insulators of electricity. No one would have believed 30 years ago that polymers could conduct as good as metals. But now such feats have been achieved and that through simple modification of ordinary organic conjugated polymers called electrically conducting polymers or synthetic metals, these materials combine the electrical properties of metals with the advantages of polymers such as, lighter weight, greater workability, resistance to corrosion and chemical attack and the lower cost and have infiltrated our day-to-day life with a wide range of products, extending from most common consumer goods to highly specialized applications in space, aeronautics, electronics, and non-linear optics. It is, therefore, no wonder that these polymers are called the Materials of the twenty first century.

1.15. Discovery of some useful polymers :

The discovery of highly conducting PA led to a sudden spurt in research activity directed towards the study of new conducting polymeric systems. The instability of PA in air further intensified this research (on exposure to air, covalent bonds are formed between oxygen and carbon atoms and these bonds lower the conductivity of PA because of their interruption of conjugated double bonds) The result is that at present many novel conducting systems are known and these include polypyrrole(PPY), poly(*p*-phenylenesulphide)(PPS), poly(*p*-phenylene)(PPP), polythiophene(PTP), polyfuran(PFU), polyaniline(PAN), polyisothianaphthene(PIN) and their derivatives. These polymers, though they share many structural features

such as a conjugated backbone, planarity and large anisotropy ratio(i.e. the intrachain conductivity is much larger than the inter-chain conductivity),however have a wide range of conductivity depending upon; (i) The doping percent, (ii) The alignment of polymer chains, (iii) The conjugation length, and (iv) The purity of the sample.

1.16.Polypyrrole:

Polypyrrole (PPy) is a type of organic polymer formed from by polymerization of pyrrole. Polypyrroles are conducting polymers, related members being polythiophene, polyaniline, and polyacetylene. The some of the first examples of polypyrroles were reported in 1963 by Weiss and co-workers. These workers described the pyrolysis of tetraiodopyrrole to produce highly conductive materials. Most commonly Ppy is prepared by oxidation of pyrrole, which can be achieved using ferric chloride in methanol. Films of PPy are yellow but darken in air due to some oxidation. Doped films are blue or black depending on the degree of polymerization and film thickness. They are amorphous, showing only weak diffraction. PPy is described as "quasi-one-dimensional" vs one-dimensional since there is some crosslinking and chain hopping. Undoped and doped films are insoluble in solvents but swellable. Doping makes the materials brittle. They are stable in air up to 150 °C at which temperature the dopant starts to evolve (e.g., as HCl).

PPy is an insulator, but its oxidized derivatives are good electrical conductors. The conductivity of the material depends on the conditions and reagents used in the oxidation. Conductivities range from 2 to 100 S/cm. Higher conductivities are associated with larger anions, such as tosylate. Doping the polymer requires that the material swell to accommodate the charge-compensating anions. PPy and related conductive polymers have two main applications in electronic devices and for

chemical sensors. PPy is also potential vehicle for drug delivery. The polymer matrix serves as a container for proteins

1.17. Introduction to I-V Characteristics:

A **current–voltage characteristic** or **I–V curve** (current–voltage curve) is a relationship, typically represented as a chart or graph, between the electric current through a circuit, device, or material, and the corresponding voltage, or potential difference across it.

Ohm's law states that the current through a conductor between two points is directly proportional to the potential difference across the two points. Introducing the constant of proportionality, the resistance one arrives at the usual mathematical equation that describes this relationship:

$$I = \frac{V}{R} \qquad \text{.....(1.1)}$$

Where, I is the current through the conductor in units of amperes, V is the potential difference measured *across* the conductor in units of volts, and R is the resistance of the conductor in units of ohms. More specifically, Ohm's law states that the R in this relation is constant, independent of the current.

Many resistors and conductors have a uniform cross section with a uniform flow of electric current, and are made of one material. In this case, the electrical resistivity ρ (Greek: rho) is defined as:

$$\rho = R\frac{A}{\ell}, \qquad \text{.....(1.2)}$$

Where R is the electrical resistance of a uniform specimen of the material (measured in ohms, Ω)

ℓ is the length of the piece of material (measured in metres, m)

A is the cross-sectional area of the specimen (measured in square metres, m^2).

The reason resistivity is defined this way is that it makes resistivity an intrinsic property, unlike resistance. All copper wires, irrespective of their shape and size, have approximately the same resistivity, but a long, thin copper wire has a much larger resistance than a thick, short copper wire. Every material has its own characteristic resistivity – for example, rubber's resistivity is far larger than copper's.

In a hydraulic analogy, passing current through a high-resistivity material is like pushing water through a pipe full of sand, while passing current through a low-resistivity material is like pushing water through an empty pipe. If the pipes are the same size and shape, the pipe full of sand has higher resistance to flow. But resistance is not solely determined by the presence or absence of sand; it also depends on the length and width of the pipe: short or wide pipes will have lower resistance than narrow or long pipes.

The above equation can be transposed to get **Pouillet's law** (named after Claude Pouillet):

$$R = \rho\frac{\ell}{A}. \qquad \text{……(1.3)}$$

The resistance of a given material will increase with the length, but decrease with increasing cross-sectional area. From the above equations, resistivity has SI units of ohm·metre. Other units like ohm·cm or ohm·inch are also sometimes used.

The formula $R = \rho\ell/A$ can be used to intuitively understand the meaning of a resistivity value. For example, if $A = 1\text{m}^2$ and $\ell = 1\text{m}$ (forming a cube with perfectly-conductive contacts on opposite faces), then the resistance of this element in ohms is numerically equal to the resistivity of the material it is made of in ohm-meters. Likewise, a 1 ohm·cm material would have a resistance of 1 ohm if contacted on opposite faces of a 1 cm×1 cm×1 cm cube.

Conductivity σ (Greek: sigma) is defined as the inverse of resistivity:

$$\sigma = \frac{1}{\rho}. \qquad \text{……(1.4)}$$

Conductivity has SI units of siemens per meter (S/m).

1.18. Introduction to Cyclic Voltammetry:

Electrochemical analyses can be thought of in terms of two broad classes of measurement, one in which the potential that develops between two electrodes is measured (potentiometry) and another in which the current that flows between two electrodes is measured (amperometry). The electrochemical potential of one electrode (the reference electrode) is usually fixed, so the measured cell potential can be interpreted in terms of an equilibrium half-cell reaction involving an analyte species in contact with the other electrode (the working electrode).In many situations, it is instead more appropriate to control the potential of the working electrode (relative to a reference electrode) and to measure the resulting current as current is simply the flow rate of electrons in a circuit. The magnitude of the resulting current and its dependence on the applied potential then provide the analytical information. ***An***

experiment in which the potential applied to the working electrode is swept at a constant sweep rate and the resulting current measured as a function of potential is called a voltammetry experiment, and much of the recent interest in electroanalytical chemistry stems from the use of voltammetry to obtain analytical (e.g., concentration), thermodynamic (e.g., redox potentials and equilibrium constants), kinetic (e.g., rate constants for reactions involving electrogenerated species) and mechanistic information about chemical systems in which redox chemistry plays a role from Nernst equation.

$$E = E^{0'} + \frac{RT}{nF}\ln\left(\frac{C_O}{C_R}\right) \quad \text{.....(1.5)}$$

E^o is the redox potential for the couple involving O and R, C_O is the concentration of the oxidized "half" of the couple and C_R is the concentration of the reduced half. (For example, in the case of the $Fe^{3+/2+}$couple, Fe^{3+} corresponds to "O", and Fe^{2+} to "R".) One could think of either O or R as the "analyte" in such an experiment. The concentrations C_O and C_R in the Nernst equation apply to the solution immediately adjacent to the surface of the electrode. The concentrations near the electrode surface may or may not be the same as the corresponding concentrations in the bulk of solution (i.e., far from the electrode surface). If the concentrations at the electrode surface happen to be the same as those in bulk solution, then there is no driving force for transport of analyte to or from the electrode surface.

1.18.i. The basics of voltammetry:

Voltammetry is one of the techniques which electrochemists employ to investigate electrolysis mechanisms. Here we incorporated this technique to analyse electrochemical properties of our as prepared samples. There are numerous forms of voltammetry are :

- **Potential Step**
- **Linear sweep**
- **Cyclic Voltammetry**

For each of these cases a voltage or series of voltages are applied to the electrode and the corresponding current that flows monitored. In this section we will examine Cyclic Voltammetry. For the moment we will focus on voltammetry in stagnant solution. There is a working electrode which is hooked up to an external electrical circuit. Obviously there must be more than one electrode for current to flow. There are another counter electrode and one reference electrode which is to kept in separate cell connected through a salt bridge with main cell. The counter electrode here is platinum electrode and reference electrode is saturated calomel electrode (Ag/AgCl). The essential elements needed for an electrolysis measurement are as follows:

- **The electrodes:**1) working electrode: material

  2) counter electrode: platinum electrode

  3) reference electrode: saturated calomel electrode (Ag/AgCl)

- **The solvent:** This usually has a high dielectric constant (example: water or acetonitrile) to enable the electrolyte to dissolve and help aid the passage of current.
- **The reactant:** Typically in low concentration 10^{-3} M.

1.18.ii. Cyclic voltammetry:

Cyclic voltammetry is the most widely used technique for acquiring qualitative information about electrochemical reactions. it offers a rapid location of *redox potentials* of the electro active species. A few concepts have to be introduced before talking about this method.

In CV measurements the current response is plotted as a function of voltage rather than time. The scan begins from the left hand side of the current/voltage plot where no current flows. As the voltage is swept further to the right (to more reductive values) a current begins to flow and eventually reaches a peak before dropping. To rationalise this behaviour one needs to consider the influence of voltage on the equilibrium established at the electrode surface. Here the rate of electron transfer is fast in comparison to the voltage sweep rate. Therefore at the electrode surface equilibrium is established identical to that predicted by thermodynamics. The exact form of the voltammogram can be rationalised by considering the voltage and mass transport effects. As the voltage is initially swept from $V1$ the equilibrium at the surface begins to alter and the current begins to flow. However now when the voltage reaches $V2$ the scan is reversed and the voltage is swept back to $V1$. The current rises as the voltage is swept further from its initial value as the equilibrium position is shifted further to the right hand side, thus converting more reactant. The peak occurs, since at some point the diffusion layer has grown sufficiently above the electrode so that the flux of reactant to the electrode is not fast enough to satisfy. In this situation the current begins to drop. The above voltammogram was recorded at a single scan rate. If the scan rate is altered the current response also changes. This again can be rationalised by considering the size of the diffusion layer and the time taken to record the scan. Clearly the cyclic voltammogram will take longer to record as the scan rate

is decreased. Therefore the size of the diffusion layer above the electrode surface will be different depending upon the voltage scan rate used. In a slow voltage scan the diffusion layer will grow much further from the electrode in comparison to a fast scan. Consequently the flux to the electrode surface is considerably smaller at slow scan rates than it is at faster rates. As the current is proportional to the flux towards the electrode, the magnitude of the current will be lower at slow scan rates and higher at high rates. A final point to note is that it is clear that the peak occurs at the same voltage and this is a characteristic of electrode reactions which have rapid electron transfer kinetics. These rapid processes are often referred to as reversible electron transfer reactions.

.

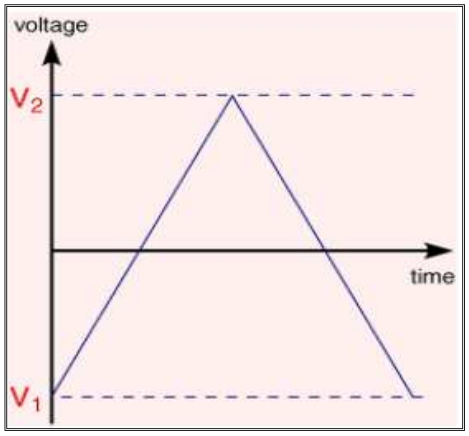

Figure 1.15 : Current as a function of voltage for CV.

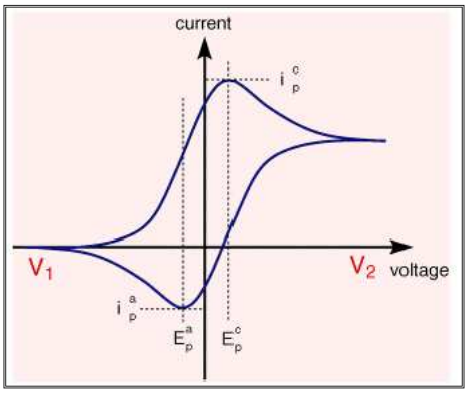

Figure 1.16 : Voltage as a function of time.

The characteristics of the cyclic voltammogram depend on a number of factors including:

- **The rate of the electron transfer reaction(s)**
- **The chemical reactivity of the electro active species**
- **The voltage scan rate**

In this section a quantitative model for the influence of the electrode voltage on the rate of electron transfer has been developed. For simplicity we will consider a single electron transfer reaction between two species (O) and (R)

$$O + e^- \xrightarrow{k_{red}} R$$
$$R \xrightarrow{k_{ox}} O + e^- \quad \text{.....(1.6,1.7)}$$

The current flowing in either the reductive or oxidative steps can be predicted using the following expressions,

$$i_O = FAk_{ox}c_R$$
$$i_R = -FAk_{red}c_O \quad \text{.....(1.8,1.9)}$$

For the reduction reaction the current $i_R$is related to the electrode area A, the surface concentration of the reactant c_O, the rate constant for the electron transfer k_{red} and Faraday's constant F. A similar expression is valid for the oxidation, now the current is labelled i_O, with the surface concentration that of the species R. Similarly the rate constant for electron transfer corresponds to that of the oxidation process. Note that by definition the reductive current is negative and the oxidative positive, the difference in sign simply tells us that current flow in opposite directions across the interface depending upon whether one is studying an oxidation or reduction. To

establish how the rate constants *k*ox and *k*red are influenced by the applied voltage. In transition state theory the reaction is considered to proceed via an energy barrier, as shown in Figure 1.17. The summit of this barrier is referred to as the transition state. Using this picture the corresponding reaction rates are given by

$$k_{\mathrm{red,ox}} = Z \exp\left(\frac{-\Delta G_{\mathrm{red,ox}}}{k_B T}\right) \quad \text{.....(1.10)}$$

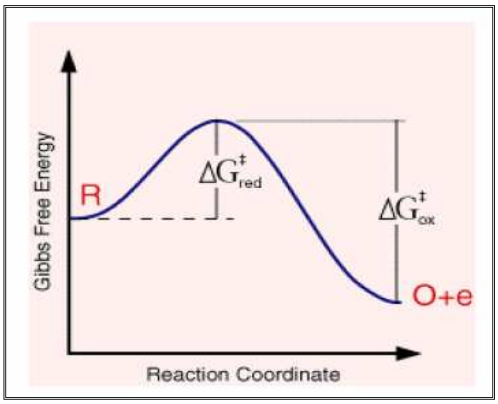

Figure 1.17 : Transition occurs via barrier ΔG.

It has already seen that a typical electrolysis reaction involves the transfer of charge between an electrode and a species in solution. This whole process due to the interfacial nature of the electron transfer reactions typically involves a series of steps. This is an exponential relationship, so we would predict from the electron transfer model that as the voltage is increased the reaction rate and therefore the current will increase exponentially. This would mean that it is possible to pass unlimited quantities of current. Of course in reality this does not arise and this can be rationalized by considering the expression for the current that we encountered in the electrode kinetics section. Clearly for a fixed electrode area (A) the reaction can be controlled by two factors. First the rate constant *k*red and second the surface concentration of the reactant (C^{surf}_{O}). If the rate constant is large, such that any reactant close to the interface is immediately converted into products then the current

will be controlled by the amount of fresh reactant reaching the interface from the bulk solution above. Thus movement of reactant in and out of the interface is important in predicting the current flowing. There are various ways in which material can move within solution so called mass transport : **Diffusion**, **Convection** and **Migration**.

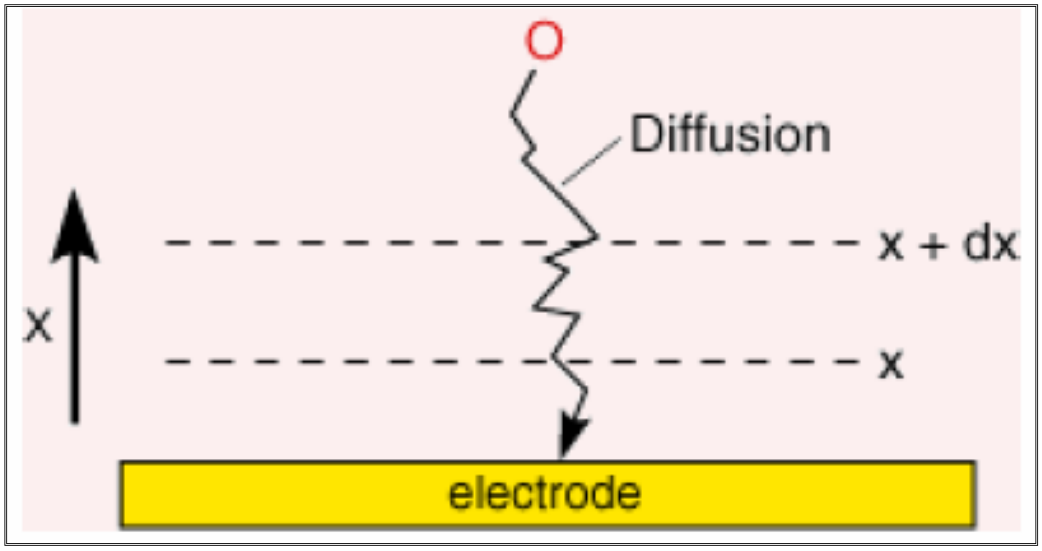

Figure 1.18 : Diffusion of the reactants to the electrode.

1.19. Objectives :

Carbon nanotubes (CNT) have shown great interest for their potential applications in electrochemistry, conductivity, field emission, dielectric etc. At the same time conducting polymer have attracted much attention because of their applications in electronic and electro-optical devices. Among conducting polymers, polypyrrole (PPY) has superiority for commercial applications because of its unique properties, such as high conductivity, stability in air, and ease of preparation. Hence, it is expected that their hybrid structure may show some distinguished properties and applications. But the yield of crystalline CNT is still a big problem. On the other hand use of nearly equivalent one dimensional nanoform of

carbon which has significantly large yield is very much attractive for industrial point of view. Also very little is known about the composite formation of amorphous carbon nanotubes with polymers. In this study, within the amorphous CNT-PPY complex, a ferrite material (Bismuth Ferrite) showing dielectric behaviour is attached. Also, there is no much development in the composite of a ferrite material with CNT-PPy. This is one of the novel approach to synthesis this type of complex and to investigate the interaction between the constituents which may lead to different unique properties. On the hunch of discovering new properties, a composite is made with a dielectric material and a conducting polymer. The electrochemical and I-V characteristics of the composites made from these extreme end materials have been studied. An improvement of conductivity and specific capacitance of these nanostructure composites are the most undertaken issue. In short the objective can be summarised as follows:

- Synthesis of phase-pure BFO and amorphous CNT (aCNT)
- To develop a successful preparation method of aCNT with ferrite and conducting polymer composites.
- Characterizations of the synthesized samples in detail to confirm their successful synthesis.
- Investigation on the electrical & electrochemical properties of the samples.

References:

[1] http://www.nanoscience.com/education/overview.html

[2] http://powersof10.com

[3] Lu, X.; Chen, Z. ,"Curved Pi-Conjugation, Aromaticity, and the Related Chemistry of Small Fullerenes (C_{60}) and Single-Walled Carbon Nanotubes" (2005).

[4] Hong, Seunghun; Myung, "Nanotube Electronics: A flexible approach to mobility", Nature Nanotechnology 2 (2007) 4.

[5] Tang, Z. K.; Zhang, L; Wang, N; Zhang, XX; Wen, GH; Li, GD; Wang, JN; Chan, CT; Sheng, P, "Superconductivity in 4 Angstrom Single-Walled Carbon Nanotubes". Science 292 (2001) 5526.

[6] Takesue, I.; Haruyama, J.; Kobayashi, N.; Chiashi, S.; Maruyama, S.; Sugai, T.; Shinohara, H. Phys. Rev. Lett. 96 (2006) 5.

[7] Lortz, R.; Zhang, Q; Shi, W; Ye, J. T.; Qiu, C. Y.; Wang, Z.; He, H. T.; Sheng, P; Qian, T. Z.; Tang, Z. K.; Wang, N.; Zhang, X. X.; Wang, J; Chan, C. T. (2009).

[8] M. Bockrath, "Carbon nanotubes: The weakest link", Nature Physics 2 (2006) 3.

[9] Pop, Eric; Mann, David; Wang, Qian; Goodson, Kenneth; Dai, Hongjie, "Thermal conductance of an individual single-wall carbon nanotube above room temperature". Nano Letters 6 (2005) 96.

[10] Sinha, Saion; Barjami, Saimir; Iannacchione, Germano; Schwab, Alexander; Muench, George, "Off-axis thermal properties of carbon nanotube films", Journal of Nanoparticle Research 7 (2005) 651.

[11]Jong KukKim, Sang Su Kim, Won-Jeong Kim, Sol–gel synthesis and properties of multiferroic $BiFeO_3$, (2005) 641.

[12] A. G. MacDiarmid, ""Synthetic metals": A novel role for organic polymers (Nobel Lecture)", Angew. Chem., Int. Ed. 40 (2001) 2581.

Chapter 2:
Literature review

2.Literature review:

Since the discovery of carbon nanotubes (CNT), great interest has been stimulated for their potential applications in electrochemistry, conductivity, field emission, dielectric etc. At the same time conducting polymer microtubes have attracted much attention because of their applications in electronic and electro-optical devices . Among conducting polymers, polypyrrole (PPY) has superiority for commercial applications because of its unique properties, such as high conductivity, stability in air, and ease of preparation. Thus, it is expected that complex of carbon nanotubes with conducting polypyrrole may be an effective way to synthesize new type of nanometer materials. Here some of the reviews of the past work on this topic have been discussed briefly.

The synthesis of CNT-PPy can be done by in-situ polymerization technique. The conductivity of the composite should be higher that of their constituents. **Fanet al.** in **1999** synthesized polypyrrole (PPY) on crystalline carbon nanotubes (CNT) using in-situ polymerization method. On calculating the conductivity at room temperature the composite had shown temperature is about 16 S/cm, which is higher than that of pure PPy (-3.0 S/cm) synthesized without carbon nanotubes under the same conditions, while lower than that of unaligned carbon nanotubes pellet (-40 S/cm) [1].

In-situ polymerization of technique is one of the pronounced synthesis processes of CNT-PPy composites. The addition of a conducting polymer to CNT enhances the conductivity**.** In **2000, Chang and co-workers** developed a method to

produce a carbon nanotube/conducting polymer nano-composite through in-situ polymerization of pyrrole in the carbon nanotube template. Conductivity measurements show that the conductivity of CNT/PPY was improved compared with that of PPY. The semiconductor-like conductivity of the composite is larger than for PPy[2].

Along with conductivity, the effects of the conducting agent (PPy) added in the nanocomposite on specific capacitance and internal resistance of supercapacitors are needed to be investigated. **Hyeok An et al.** in**2002** fabricated a nanocomposite electrode of single-walled carbon nanotube (SWNT) and polypyrrole (PPy) to improve the specific capacitance of the supercapacitor. The individual nanotubes and nanoparticles are uniformly coated with PPy by in-situ chemical polymerization of pyrrole. The SWNT-PPy nanocomposite electrode had shown much higher specific capacitance than pure PPy and as-grown SWNT electrodes, due to the uniformly coated PPy on the SWNTs[3].

Temperature dependent electrical conductivity can also be a major field of study when dealing with conducting polymer nanocomposites. **Zhang et al.** in **2005** reported the template-directed synthesis, characterization, and electric properties of single-walled carbon nanotube-core (SWNT)-shell (conducting polypyrrole and polyaniline) nanowires. The SWNTs were first dispersed in aqueous solutions containing cationic surfactant cetyltrimethylammonium bromide (CTAB) or nonionic surfactant poly(ethylene glycol) mono-p-nonyl phenyl ether (Oπ-10). Each individual nanotube (or small bundle) was then encased in its own micelle like envelope with hydrophobic surfactant groups orientated toward the nanotube and hydrophilic groups orientated toward the solution. And thus a hydrophobic region within the micelle/SWNT (called a micelle/SWNT hybrid template) was formed. Insertion and

growth of pyrrole or aniline monomers in this hybrid template, upon removal of the surfactant, produce coaxial structures with a SWNT centre and conducting polypyrrole or polyaniline coating. Electric properties testing indicated that the SWNTs played the key roles in the conducting polymer/SWNT composites during electron transfer in the temperature range 77 K to room temperature. Compared with the CNT network embedded in the conducting polymers, the composites within which CNTs were coated perfectly by the identical conducting polymers exhibited higher barrier heights during electron transfer[4].

Microemulsion is one of the synthesis techniques to develop CNT-PPy nanocomposites. These composites show an enhancement in the specific charge capacity with respect to that of pure PPy**. Yu et al.** in **2005** demonstrated a feasible approach to the preparation of multiwalled carbon nanotube (MWNT)/polypyrrole (PPy) core–shell nanowires by in-situ inverse microemulsion. The thermal stability and electrical conductivity of the MWNT/PPy composites were examined with thermogravimetric analysis and a conventional four-probe method. In comparison with pure PPy, the decomposition temperature of the MWNT/PPy (1 wt % MWNT) composites increased from 305ºC to 335ºC, and the electrical conductivity of the MWNT/PPy (1 wt % MWNT) composites increased by 1 order of magnitude. The current–voltage curves of the MWNT/PPy nanocomposites followed Ohm's law, reflecting its metallic character. The cyclic voltammetry measurements revealed that PPy/MWNT composites showed an enhancement in the specific charge capacity with respect to that of pure PPy[5].

Anglada et al. in **2006** used thin film Carbon Nanotube (CNT) networks as a conductive, transparent and flexible electrode for electrochemically depositing a conducting polymer on it, polypyrrole or polyaniline. They had constructed a solid

state pH sensor, depositing polypyrrole or polyaniline on single walled CNT networks. It was shown that CNT/Polypyrrole and CNT/Polyaniline can be used as solid state pH sensors: the response was linear, fast and reproducible. Compared to pure CNT networks, the linearity and stability were improved[6].

On doping with a oxide material, the investigation of electrochemical behaviour has been done in the past. **Sivakkumar et al.** in **2007** prepared a ternary composite of CNT/polypyrrole/hydrous MnO_2 is prepared by in-situ chemical method and its electrochemical performance is evaluated by using cyclic voltammetry (CV), impedance measurement and constant-current charge/discharge cycling techniques. For comparative purpose, binary composites such as CNT/hydrous MnO_2 and polypyrrole/hydrous MnO_2 are prepared and also investigated for their physical and electrochemical performances. The specific capacitance (SC) values of the ternary composite, CNT/hydrous MnO_2 and polypyrrole/hydrous MnO_2 binary composites estimated by CV technique in 1.0 M Na_2SO_4 electrolyte are 281, 150 and 35 Fg^{-1}at 20 mV s^{-1} and 209, 75 and 7 Fg^{-1} at 200 mVs^{-1}, respectively. The electrochemical stability of ternary composite electrode is investigated by switching the electrode back and forth for 10,000 times between 0.1 and 0.9 V versus Ag/AgCl at 100 mVs^{-1}. The electrode exhibits good cycling stability, retaining up to 88% of its initial charge at 10,000th cycle. A full cell assembled with the ternary composite electrodes shows a SC value of 149 Fg^{-1}at a current loading of 1.0 mA cm^{-2} during initial cycling, which decreased drastically to a value of 35 Fg^{-1} at 2000th cycle. The actual reason(s) for the poor cyclability behaviour of the ternary composite electrode(s) in the full cell, in contrast to the half cell, is unclear from the attempts made in this study[7].

Wang and co-workers in **2007** measured electrochemical capacitance properties of composite films prepared from electrically conducting polypyrrole (PPy)

and single walled carbon nanotubes (SWNTs). The composite films were electropolymerized from homogenous mixture of pyrrole (Py) and raw SWNTs, or suspension of PPy and functionalized SWNTs. The SWNTs were functionalized and cut by suspending in concentrated H_2SO_4/HNO_3solution and sonicating in a water bath. Electrochemical capacitance properties of the composite films were measured by cyclic voltammetry (CV) and electrochemical impedance spectroscopy (EIS) techniques in 1 M KCl aqueous solutions. Due to the mesoporous structure of carbon nanotubes (CNTs), the easily accessible electrode/electrolyte interface allowed very fast charging/discharging process. Moreover, owing to the high electrical conductivity of CNTs and the mesoporous structure, the composite films had very low resistance and almost ideal capacitance behaviour even on deeply discharged states. On the contrary, the pure PPy films had much larger resistance and worse capacitance properties due to the low conductance and contracted volume on discharging (reduced)states. On the other hand, in PPy/functionalized CNTs composite films, the PPy was doped by immobile functionalized CNTs. On reduced state, the PPy chains become neutral and the negative charge on functionalized CNTs must be balanced by cations with smaller size. The balancing behaviour of cations could diminish ion-transfer polarization further. Therefore, the specific capacitance of PPy/SWNTs and PPy/functionalized SWNTs composite films would reach 144 Fg^{-1} and 200 Fg^{-1}at scanning rate of 200 mVs^{-1}, respectively. All of the above implies that the PPy/SWNTs composite, especially PPy/functionalized SWNTs composite, was a kind of promising electrode material of supercapacitor[8].

Previously, experiments on the capacitance behaviour of oxide doped CNT-PPy composites were shown. The study of the electrochemical properties of the ferrite-CNT-PPy composites is under progress. **Wu et al.** in **2008** described the preparation of a nanocomposites fabricated from monodispersed 4nm iron oxide

(Fe_3O_4) coated on the surface of carboxylic acid containing multi-walled carbon nanotube (c-MWCNT) and polypyrrole (PPy) by in-situ chemical oxidative polymerization. Structural and morphological analysis showed that the fabricated Fe_3O_4 coated c-MWCNT/PPy nanocomposites are core (Fe_3O_4coated c-MWCNT)-shell (PPy) structures. The conductivities of these Fe_3O_4 coated c-MWCNT/PPy nanocomposites are about four times higher than those of pure PPy matrix. The magnetic properties of Fe_3O_4coated cMWCNT/PPy nanocomposites show ferromagnetic behaviour[9].

Miet al. in **2009** was to successfully develop thorn-like, organometallic-functionalized carbon nanotubes via a novel microwave hydrothermal route. The organometallic complex with methyl orange and iron (III) chloride served as reactive seed template, resulting in the oriented polymerization of pyrrole on the modified carbon nanotubes without the assistance of other oxidants. The electrochemical performance indicated that the prepared composites had a specific capacitance of 304 Fg^{-1}. Through a series of chemical characterizations, it was clear that the growth of granular-like PPy was closely related to the shape and size of the oxidative compounds on CNTs. If the thorns could be developed into long fibers, the highly oriented PPy nanofibers or nanotubes covered on the CNTs could be expected, which will result in a significant improvement of electrochemical performance[10].

Talemi et al. in **2010** presented a novel method for the electropolymerization of polypyrrole/carbon nanotube composites on an electrically insulating, porous membrane. In order to study the mechanisms relating to this process, different samples using carbon nanotubes with varying concentrations of functional groups were prepared. The underlying efficacy of this process is based on the use of a solid, bulky particle (functionalized nanotubes) as the counter ion for the polymerization of

an intrinsically conducting polymer, a counter ion system which cannot penetrate a porous membrane for steric reasons. Morphological, thermal, electrical, and spectroscopic analyses of the prepared samples confirm the proposed mechanism, and the degree of functionalization of the nanotube provides a route for controlling the relative concentration of PPy and nanotubes in the final nanocomposite hybrid[11].

Hu et al. in **2010** synthesized nanoparticles (NPs) of multiferroic bismuth ferrite with narrow size distributions via a wet chemical route using bismuth nitrate and iron nitrate as starting materials and excess tartaric acid and citric acid as chelating agent, respectively, followed by thermal treatment. It was found that $BiFeO_3$ NPs crystallized at 350°C when using citric acid as chelating agent. Such crystallization temperature is much lower than that of conventional chemical process in which other types of chelating agent are used. $BiFeO_3$ NPs with different sizes distributions show obvious ferromagnetic properties, and the magnetization is increased with reducing the particle size[12].

Kan et al. in **2012** developed an electrochemical sensor combining a molecular imprinted technique and an electropolymerization method. A molecular imprinted polymer (MIP) film was fabricated by electropolymerizing pyrrole in the presence of dopamine (DA) after electrodepositing carboxyl functionalized multi-walled carbon nanotubes (MWNTs-COOH) onto a glassy carbon electrode (GCE) surface. Scanning electron microscopy (SEM), differential pulse voltammetry (DPV), and electrochemical impedance spectroscopy (EIS) were employed to characterize the constructed sensor. The effects of pH, the monomer concentration, the number of cycles for the electropolymerization, and the scan rate for the sensor preparation were optimized. The MIP-based sensor displayed an excellent recognition capacity

toward DA compared with other structurally similar molecules. Additionally, the DPV peak current was linear to the DA concentration in the range from 6.25×10^{-7} to 1×10^{-4} mol/L, with a detection limit of 6×10^{-8} mol/L. The prepared sensor also showed stable reproducibility and regeneration capacity[13].

Lu et al. in **2012** successfully prepared flexible films with polypyrrole/carbon nanotube (PPy/CNT) composite homogeneously distributed between graphene (GN) sheets by flow-assembly of the mixture dispersion of GN and PPy/CNT. In such layered structure, the coaxial PPy/CNT nanocables can not only enlarge the space between GN sheets but also provide pseudo-capacitance to enhance the total capacitance of electrodes. According to the galvanostatic charge/discharge analysis, the mass and volume specific capacitances of GN-PPy/CNT (52 wt% PPy/CNT) are 211 Fg^{-1} and 122 $F\,cm^{-3}$ at a current density of 0.2 $A\,g^{-1}$, higher than those of the GN film (73 Fg^{-1} and 79 $F\,cm^{-3}$) and PPy/CNT (164 Fg^{-1} and 67 Fcm^{-3}). Significantly, the GN-PPy/CNT electrode shows excellent cycling stability (5% capacity loss after 5000 cycles) due to the flexible GN layer and the rigid CNT core synergistically releasing the intrinsic differential strain of PPy chains during long-term charge/discharge cycles[14].

Li et al. in **2013** presented a rational strategy to fabricate a unique CNT-polypyrrole (PPy) core–shell sponge, and demonstrated its application as a highly compressible supercapacitor electrode with high performance. A PPy layer with optimal thickness was coated uniformly on individual CNTs and inter-CNT contact points by electrochemical deposition and crosslinking of pyrrole monomers, resulting in a core–shell configuration. The PPy coating significantly improves specific capacitance of the CNT sponge to above 300 F/g, and simultaneously reinforces the

porous structure to achieve better strength and fully elastic structural recovery after compression. The CNT-PPy sponge can sustain 1,000 compression cycles at a strain of 50% while maintaining a stable capacitance (> 90% of initial value). Their CNT-PPy core–shell sponges with a highly porous network structure may serve as compressible, robust electrodes for supercapacitors and many other energy devices[15].

Liu et al. in **2013** reported the fabrication of well-defined carboxylated carbon nanotubes/polypyrrole composite (CNTs/PPy) hollow microspheres via chemical oxidative interfacial polymerization of pyrrole in the presence of the carboxylated carbon nanotubes (CNT-COOH). It was found that the presence of the carboxylated carbon nanotubes greatly improved their morphological, thermal, and electrical conductive properties. The cycling stability as electrode materials for supercapacitors had been evidently improved by introducing the CNT-COOH, although the presence of the CNT-COOH had slightly enhanced their specific capacitance. It makes the CNTs/PPy hollow microspheres potential electrode materials for supercapacitors or other devices[16].

Johari et al. synthesized nanoparticles (NPs) of multiferroic bismuth ferrite ($BiFeO_3$) via a wet chemical route using bismuth nitrate and iron nitrate as starting materials and excess citric acid as chelating agent, respectively, followed by thermal treatment at 350°C, 450°C and 550°C. It was found that $BiFeO_3$ nanoparticles crystallized at 350°C when using citric acid as chelating agent. $BiFeO_3$ nanoparticles with different sizes distributions show obvious ferromagnetic properties, and the magnetization is increased with reducing the particle size. The prepared samples were characterized by X-ray diffraction of powder (XRD), scanning electron microscope (SEM) for extracting their surface morphology and

their crystallographic structure. The surface morphology studies confirm the growth of bismuth ferrite nanoparticles with their diameters in the range of 200nm to 500nm. The XRD analysis concludes the rhombocentered structure of synthesized nanoparticles[17].

From the review of past-work we have seen that CNT-PPy nanostructure was synthesized by various methods like in-situ polymerization[1], microemulsion[5], electrochemically[6] etc. Among these synthesis methods in-situ polymerization of pyrrole is an easy process to prepare CNT-PPy composite. But all the reported results used crystalline carbon nanotubes which has several limitations particularly for large scale application. This is because the yield of crystalline CNT is still a big problem. On the other hand use of nearly equivalent one dimensional nanoform of carbon which has significantly large yield is very much attractive for industrial point of view. Also very little is known about the composite formation of amorphous carbon nanotubes with polymers. In this work an attempt has been made in this direction for synthesizing composites of amorphous carbon nanotubes with conducting polymers like PPy and also inorganic materials like BFO. Two of the standout applications of this hybrid structure are electrochemical and electrical and from literature survey it can be stated that these crystalline CNT-PPy nanostructures show a lot of improvement in conductivity and electrochemical performance from many of their counterparts. Similarly as no data are available for the above applications using amorphous carbon nanostructures hence one of the major aims of the thesis is to develop the technology route for such composite fabrication as well as understanding its physical properties for specific applications.

References:

[1] Junhua Fan, Meixisang Wan, Baoben Zhu, Haohe Chang, Zhenwei Pan, SishenXie, Synthetic Metals 102 (1999) 1266.

[2] B. H. Chang, Z. Q. Liu, L. F. Sun , D. S. Tang, W. Y. Zhou, G. Wang, L. X. Qian, S. S. Xie, J. H. Fen, and M. X. Wan, Journal of Low Temperature Physics,

119 (2000) 1.

[3] Kay Hyeok An, Kwan Ku Jeon, Jeong Ku Heo, Seong Chu Lim, Dong Jae Bae, and Young Hee Lee, J. Electrochem. Soc. 149 (2002) 8

[4] Xuetong Zhang, Zhou Lu, Mengting Wen, Hailin Liang, Jin Zhang* and Zhongfan Liu, J. Phys. Chem. B 109 (2005) 1101.

[5] Yijun Yu, Chu Ouyang, Yun Gao, Zhihuai Si, Wei Chen, Zhaoqun Wang, Gi Xue, Journal of Polymer Science: Part A: Polymer Chemistry, 43 (2005) 6105.

[6] N. Ferrer-Anglada, M. Kaempgen and S. Roth, phys. stat. sol. (b) 243 (2006) 3519.

[7] S.R. Sivakkumar, Jang Myoun Ko, Dong Young Kim, B.C. Kim, G.G. Wallace, Electrochimica Acta 52 (2007) 7377.

[8] Jie Wang, Youlong Xu, Xi Chen, Xiaofei Sun, Composites Science and Technology 67 (2007) 2981.

[9] Tzong-Ming Wu, Shiang-Jie Yen, Erh-Chiang Chen, Ray-Kuang Chiang, Journal of Polymer Science: Part B: Polymer Physics, 46 (2008) 727.

[10] Hongyu Mi, Xiaogang Zhang, Youlong Xu, Fang Xiao, Applied Surface Science 256 (2010) 2284.

[11] Pejman Hojati-Talemi and George P. Simon, J. Phys. Chem. C 114 (2010) 13962.

[12] Yongming Hu, Linfeng Fei, Yiling Zhang, Jikang Yuan, Yu Wang andHaoshuang Gu, Journal of Nanomaterials 2011 (2011) 1.

[13] Xianwen Kan, Hong Zhou, Chen Li, Anhong Zhu, Zonglan Xing, Zhe Zhao, Electrochimica Acta 63 (2012) 69.

[14] Xiangjun Lu, Hui Doua, Changzhou Yuan, Sudong Yang, Liang Haoa, Fang Zhang, Laifa Shen, Luojiang Zhang, Xiaogang Zhang, Journal of Power Sources 197 (2012) 319.

[15] Peixu Li, Enzheng Shi, Yanbing Yang, Yuanyuan Shang, Qingyu Peng, Shiting Wu, Jinquan Wei, Kunlin Wang, Hongwei Zhu, Quan Yuan, Anyuan Cao, and Dehai Wu, Nano Research DOI : 10.1007/s12274-013-0388-5.

[16] Peng Liu, Xue Wang, Haidong Li, Synthetic Metals 181 (2013) 72.

[17] Anoopshi Johari, Synthesis and Characterization of Bismuth Ferrite Nanoparticles, AKGEC INTERNATIONAL JOURNAL OF TECHNOLOGY, Vol. 2 No. 2, 17-20.

Chapter 3:
Characterisation tools

3.1. FESEM (Field-emission Scanning Electron Microscope):

An FESEM is microscope instead of light it works with electrons, liberated by a field emission source.

3.1.1 Principle

Under vacuum, electrons generated by a Field Emission Source are accelerated in afield gradient. The beam passes through electromagnetic lenses, focusing onto the specimen. As result of this bombardment different types of electrons are emitted from the specimen. A detector catches the secondary electrons and an image of the sample surface is constructed by comparing the intensity of these secondary electrons to the scanning primary electron beam. Finally the image is displayed on a monitor. A FESEM is used to visualize very small topographic details on the surface or entire or fractioned objects. Researchers in biology, chemistry and physics apply this technique to observe structures that may be as small as 1 nanometer. The FESEM may be employed for example to study organelles and DNA material in cells, synthetic polymers, and coatings on microchips.

3.1.2. Preparation

In order to be observed with a SEM objects are first made conductive for current. This is done by coating them with an extremely thin layer (1.5 - 3.0 nm) of gold or palladium. Further on, objects must be able to sustain the high vacuum and should not alter the vacuum, for example by losing water molecules or gasses. Metals, polymers and crystals are usually little problematic and keep their structure in the

SEM. Biological material, however, requires a prefixation, e.g. with cold slush nitrogen (cryo-fixation) or with chemical compounds. This particular microscope is foreseen of a special cryo-unit where frozen objects can be fractured and coated for direct observation in the FESEM. Chemically fixed material needs first to be washed and dried below the critical point to avoid damage of the fine structures due to surface tension. Coating is then performed in a separate device.

- **Source of electrons**

In standard electron microscopes electrons are mostly generated by heating a tungsten filament by means of a current to a temperature of about 2800°C. Sometimes electrons are produced by a crystal of lanthanum hexaboride (LaB_6) that is mounted on a tungsten filament. This modification results in a higher electron density in the beam and a better resolution than with the conventional device. In a field emission (FE) scanning electron microscope no heating but a so-called "cold" source is employed. An extremely thin and sharp tungsten needle (tip diameter 10^{-7} –10^{-8} m) functions as a cathode in front of a primary and secondary anode. The voltage between cathode and anode is in the order of magnitude of 0.5 to 30 KV. Because the electron beam produced by the FE source is about 1000 times smaller than in a standard microscope, the image quality is markedly better. As field emission necessitates an extreme vacuum (10^{-8}Torr) in the column of the microscope, a device is present that regularly decontaminates the electron source by a current flash. In contrast to a conventional tungsten filament, a FE tip last theoretically for a lifetime, provided the vacuum is maintained stable.

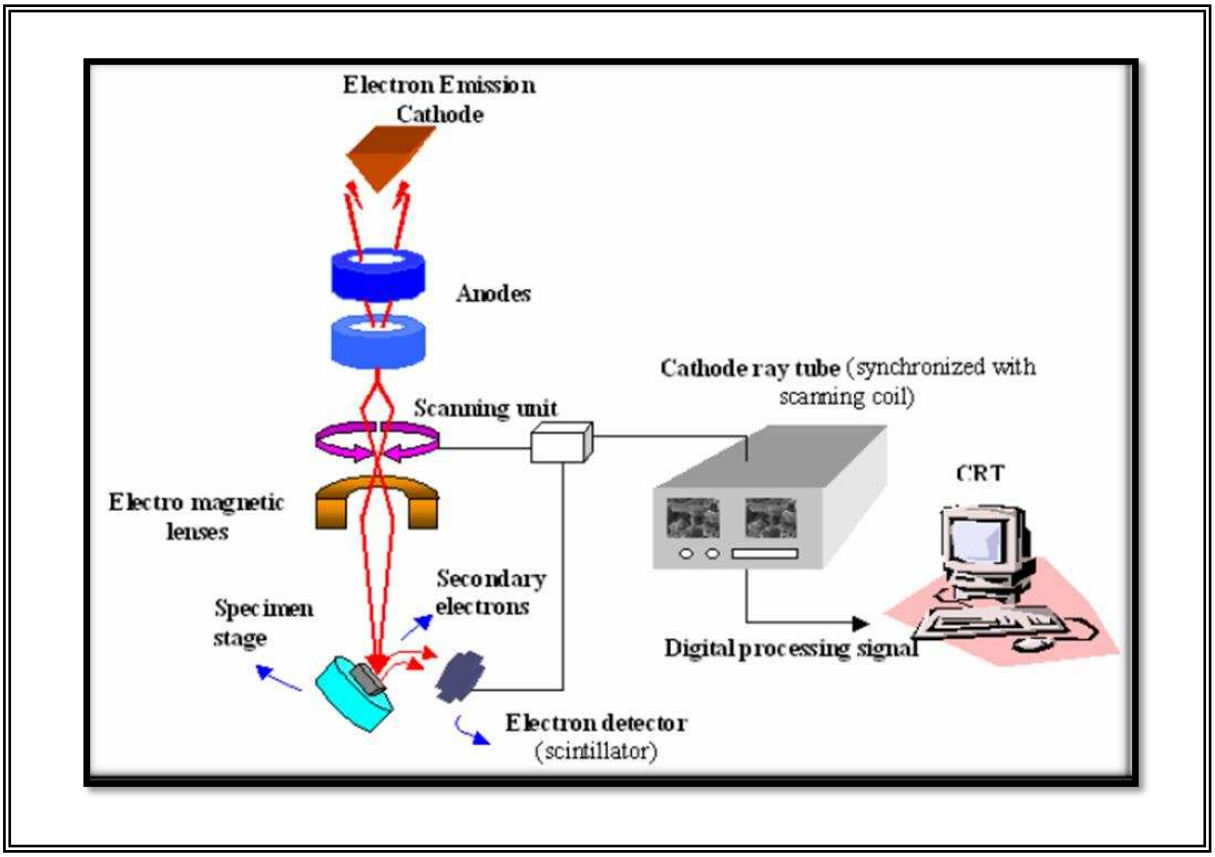

Figure 3.1 : Schematic diagram of FESEM.

The electron beam is focused by the electro-magnetic lenses (condenser lens, scancoils, stigmator coils and objective lens) and the apertures in the column to a tiny sharp spot.

- **Condenser lens**

The current in the condenser determines the diameter of the beam: a low current result in a small diameter, a higher current in a larger beam. A narrow beam has the advantage that the resolution is better, but the disadvantage that the signal to noise ratio is worse. The situation is reversed when the beam has a large diameter. The condenser lens is consisting mostly out of two parts.

- **Scan coils**

The scan coils deflect the electron beam over the object according to a zig-zag pattern. The formation of the image on the monitor occurs in synchrony with this scan movement. The scan velocity determines the refreshing rate on the screen and the amount of noise in the image (rapid scan = rapid refreshing = low signal = much noise; see SCANMODE in the virtual FESEM). The smaller the scanned region on the object, the larger the magnification becomes at a constant window size (see MAGNIFICATION in the virtual FESEM). Scan coils often consist of upper and lower coils, which prevent the formation of a circular shadow at low magnification.

- **The objective lens**

The objective lens is the lowest lens in the column. The objective focuses the electron beam on the object (see FOCUS in the virtual FESEM). At a short working distance(= object in a higher position, that is closer to the objective lens) the objective lens needs to apply a greater force to deflect the electron beam. The shortest working distance produces the smallest beam diameter, the best resolution, but also the poorest depth of field. (The depth of field indicates which range in vertical direction in the object can still be visualized sharply).

- **The stigmator coils**

The stigmator coils are utilized to correct irregularities in the x and y deflection of the beam and thus to obtain a perfectly round-shaped beam. When the beam is not circular, but ellipsoidal, the image looks blurred and stretched.

- **Object chamber**

After the object has been covered by a conductive layer it is mounted on a special holder. The object is inserted through an exchange chamber into the high

vacuum part of the microscope and anchored on a moveable stage. In the virtual FESEM the object can be moved in horizontal and vertical direction on the screen by operating the arrows in the POSITION box. In the real microscope the object can be repositioned in the chamber by means of a joy stick that steers in left right axis, or forward and backward. In addition, the object can be tilted (e.g. for stereo views), rotated and moved in Z direction (= closer or further away to the Objective lens). The "secondary electron emission" detector (scintillator) is located at the rear of the object holder in the chamber.

- **Image formation**

When the primary probe bombards the object, secondary electrons are emitted from the object surface with a certain velocity that is determined by the levels and angles at the surface of the object. The secondary electrons, which are attracted by the Corona, strike the scintillator (fluorescing mirror) that produces photons. The location and intensity of illumination of the mirror vary depending on the properties of the secondary electrons. The signal produced by the scintillator is amplified and transduced to a video signal that is fed to a cathode ray tube in synchrony with the scan movement of the electron beam. The contrast in the "real time" image that appears on the screen reflects the structure on the surface of the object. Parallel to the analog image, a digital image is generated which can be further processed.

Figure 3.2 : Experimental Set-up of FESEM HITACHI S4800

3.2. HRTEM (High Resolution Transmission Electron Microscope):

Transmission electron microscopy (TEM) is a microscopy technique whereby a beam of electrons is transmitted through an ultra thin specimen, interacting with the specimen as it passes through. An image is formed from the interaction of the electrons transmitted through the specimen; the image is magnified and focused onto an imaging device, such as a fluorescent screen, on a layer of photographic film, or to be detected by a sensor such as a CCD camera. TEMs are capable of imaging at a significantly higher resolution than light microscopes, owing to the small de Broglie wavelength of electrons.

3.2.1. Principle

(1) The "Virtual Source" at the top represents the electron gun, producing a stream of monochromatic electrons.

(2) This stream is focused to a small, thin, coherent beam by the use of condenser lenses 1and 2. The first lens (usually controlled by the "spot size knob") largely determines the "spotsize"; the general size range of the final spot that strikes the sample. The second lens(usually controlled by the "intensity or brightness knob" actually changes the size of the spot on the sample; changing it from a wide dispersed spot to a pinpoint beam.

(3) The beam is restricted by the condenser aperture (usually user selectable), knocking out high angle electrons (those far from the optic axis, the dotted line down the centre).

(4) The beam strikes the specimen and parts of it are transmitted.

(5) This transmitted portion is focused by the objective lens into an image.

(6) Optional Objective and Selected Area metal apertures can restrict the beam; the Objective aperture enhancing contrast by blocking out high-angle diffracted electrons, the Selected Area aperture enabling the user to examine the periodic diffraction of electrons by ordered arrangements of atoms in the sample.

(7) The image is passed down the column through the intermediate and projector lenses, being enlarged all the way.

(8) The image strikes the phosphor image screen and light is generated, allowing the user to see the image.

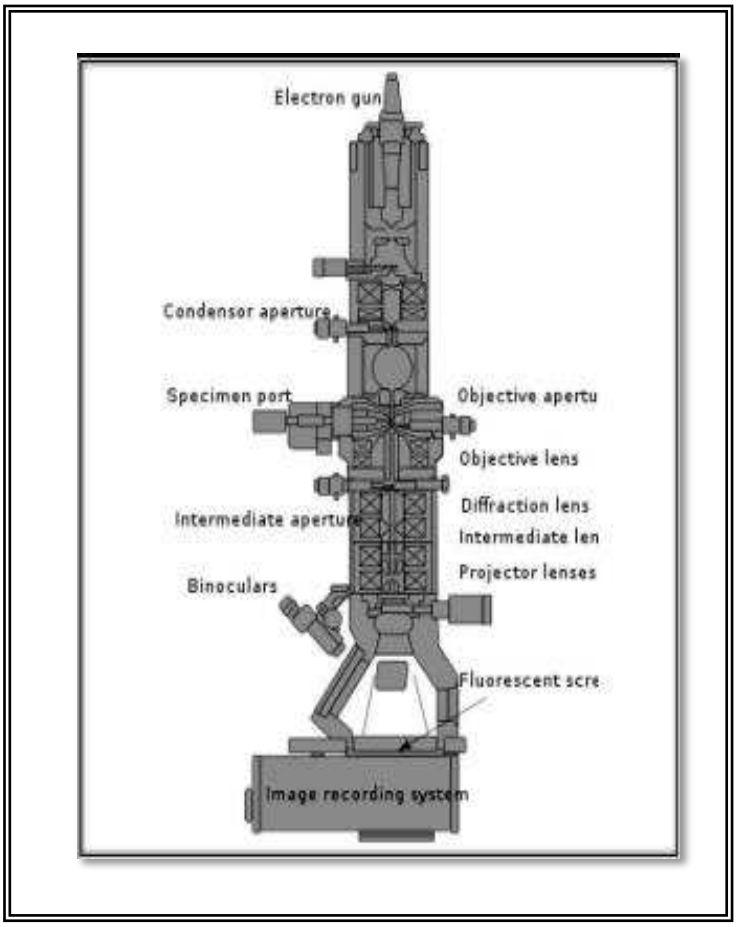

Figure 3.3 : Schematic diagram of FESEM

3.2.2. Restriction of samples:

Sample preparation for TEM generally requires more time and experience than for most other characterization techniques. A TEM specimen must be approximately 1000 Å or less in thickness in the area of interest. The entire specimen must fit into a 3 mm diameter up and be less than about 100 microns in thickness. A thin, disc shaped sample with a hole in the middle, the edges of the hole being thin enough for TEM viewing, is typical. The initial disk is usually formed by cutting and grinding from bulk or thin film/substrate material, and the final thinning done by ion milling. Other specimen preparation possibilities include direct deposition onto a TEM-thin substrate (Si_3N_4, carbon); direct dispersion of powders on such a substrate; grinding and polishing using special devices like tripod; chemical etching and electro-polishing; and lithographic patterning of walls and pillars for cross-section viewing. A focused ion beam (FIB) may be used to make cross-sections; however this capability is not currently available at HUJ.

Figure 3.4 : HRTEM (JEOL 200 kV) SET UP

- **Applications**

  - **Morphology**

The size, shape and arrangement of constituent particles as well as their relationship with each other on the scale of atomic diameters can be predicted.

  - **Crystallographic Information**

The arrangement of atoms in the specimen and their degree of order, detection of atomic scale defects in areas a few nanometers in diameter.

  - **Compositional Information (if so equipped)**

The elements and compounds, the sample is composed of and their relative ratios, in areas a few nanometers in diameter.

3.3. XRD (X-ray Diffractometer):

The atomic planes of a crystal cause an incident beam of X-rays to interfere with one another as they leave the crystal. The phenomenon is called X-ray diffraction.

3.3.1. Production of X-ray:

X-rays are produced whenever high-speed electrons collide with a metal target. A source of electrons – hot W filament, a high accelerating voltage between the cathode (W)and the anode and a metal target, Cu, Al, Mo, Mg. The anode is a water-cooled block of Cu containing desired target metal.

3.3.2. Importance of XRD:

- Measure the average spacing between layers or rows of atoms
- Determine the orientation of a single crystal or grain
- Find the crystal structure of an unknown material
- Measure the size, shape and internal stress of small crystalline regions

3.3.3.Determination of interplaner spacing:

Diffraction occurs only when Bragg's Law is satisfied Condition for constructive interference (X-rays) from planes with spacing d. The inter planer spacing calculated from **Bragg's Law**

$$n\lambda = 2d_{hkl} \sin\theta \quad \text{.....(3.1)}$$

where **'n'** is any integer, **'λ'** is the x-ray wave length, **'θ'** is the Bragg's angle, **'d'** is the inter planer spacing.

3.3.4. Determination of lattice parameter:

A crystal consists of a periodic arrangement of the unit cell into a lattice. The unit cell can contain a single atom or atoms in a fixed arrangement. Crystals consist of planes of atoms that are spaced a distance d apart, but can be resolved into many atomic planes, each with a different d-spacing. a,b and c (length) and α, β and γ(angles between a,b and c) are lattice constants or parameters which can be determined by XRD. Miller indices are the reciprocals of the fractional intercepts which the plane makes with crystallographic axes.

For **cubic system** lattice parameter has been calculated from the following equation:

For **(hkl)** planes,

$$\mathbf{1/d^2_{hkl} = (h^2+k^2+l^2)/a^2} \quad \text{.....(3.2)}$$

Where **'d_{hkl}'** is the inter planer distance, **'a'** is the lattice parameter, **'h', 'k', 'l'** is known as **Miller indices.**

3.3.5. Determining the particle size or grain size:

The mean crystalline sizes of the powders are calculated using Scherrer formula : $D = 0.9\lambda/ \beta \cos\theta$, ...(3.3)

Where D is the average crystallite size, λ =1.541 A° (X-ray wavelength**),** β = $\sqrt{(B^2-b^2)}$, being the width of the diffraction peak at half maximum for the diffraction angle 2θ, b is calculated from the peak width of single crystal silicon wafer.

Figure 3.5 : Photograph of Rigaku Ultima III X-ray Diffractometer

3.3.6. Phase identification:

• Measure d-spacing from the obtained XRD pattern.

• Obtain integrated intensities.

• Compare data with known standards in the JCPDS file, which are for random orientations(there are more than 50,000 JCPDS cards of inorganic materials).

3.4. FTIR (Fourier Transform Infrared Spectroscopy):

Fourier Transform Infrared Spectroscopy (FTIR) is a technique which is used to analyze the chemical composition of many organic chemicals, polymers, paints, coatings, adhesives, lubricants, semiconductor materials, coolants, gases, biological samples, inorganics and minerals. FTIR can be used to analyze a wide range of materials in bulk or thin films, liquids, solids, pastes, powders, fibers, and other forms. FTIR analysis not only gives qualitative (identification) analysis of materials, but with relevant standards, can be used for quantitative (amount) analysis. FTIR can be used to analyze samples up to ~11millimeters in diameter, and either measure in bulk or the top ~1 micrometer layer. An FTIR Spectrometer is an instrument which acquires broadband NIR to FIR spectra. Unlike a dispersive instrument, i.e. grating mono-chromator or spectrograph, a FT-IR Spectrometer collects all wavelengths simultaneously. An FT-IR (Fourier Transform Infra-Red) is a method of obtaining infrared spectra by first collecting an interferogram of a sample signal using an interferometer, and then performing a Fourier Transform (FT) on the interferogram to obtain the spectrum. An FTIR Spectrometer collects and digitizes the interferogram, performs the FT function, and displays the spectrum.

3.4.1. Principle of operation:

An FTIR is typically based on a Michelson Interferometer the interferometer consists of abeam splitter, a fixed mirror, and a mirror that translates back and forth, very precisely. The beam splitter is made of a special material that transmits half of the radiation striking it and reflects the other half. Radiation from the source strikes the beam splitter and separates into two beams. One beam is transmitted through the

beam splitter to the fixed mirror and the second is reflected off the beam splitter to the moving mirror. The fixed and moving mirrors reflect the radiation back to the beam splitter. Again, half of this reflected radiation is transmitted and half is reflected at the beam splitter, resulting in one beam passing to the detector and the second back to the source.

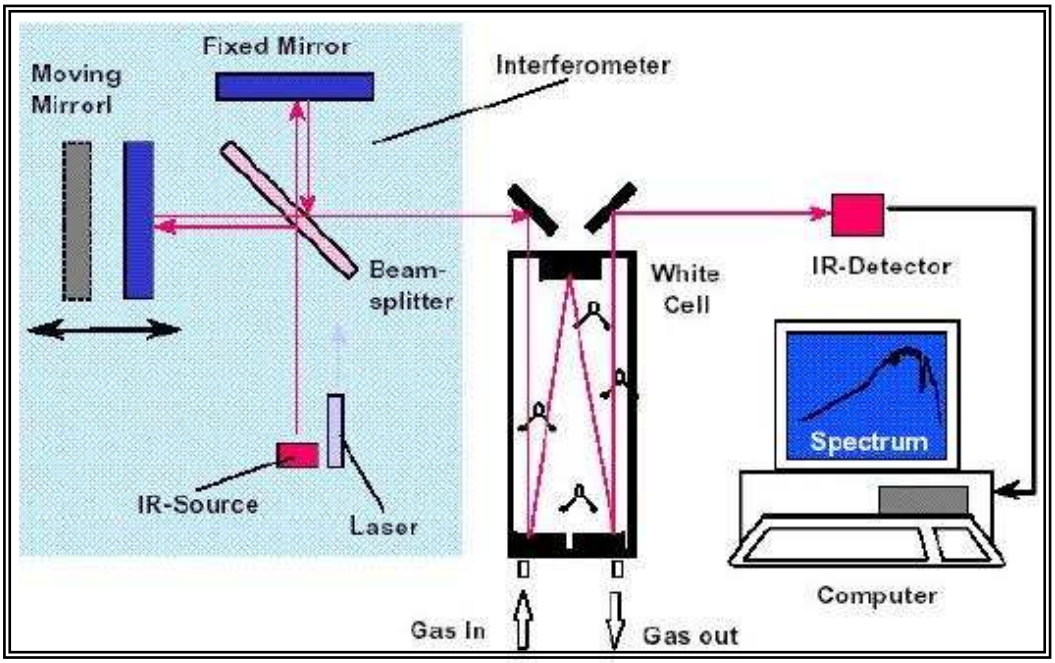

Figure 3.6 : Schematic Diagram of FTIR

A beam of infrared light (wavelength ~ 0.7-500 μm) is focused on the sample using all reflective optics. Depending on the sample composition, differing amounts of light are absorbed a different wavelengths. This pattern of light absorption is unique for almost every organic compound (except optical isomers) and many inorganic compounds. From the pattern of light absorbed, identification of the composition (qualitative analysis) can be made. With additional control over the sample thickness or sampling depth, the intensity of the individual absorbing components can be used to perform quantitative analysis (amount of each compound present). User-provided reference samples aid in positive substance identification and

compositional verification. FTIR can be used to identify chemicals from spills, paints, polymers, coatings, drugs, and contaminants. FTIR is perhaps the most powerful tool for identifying types of chemical bonds (functional groups). The wavelength of light absorbed is characteristic of the chemical bond as can be seen in this annotated spectrum. A Shimadzu IRPrestige-21 FTIR spectrometer was used to record the spectra in the mid IR region, (i.e. 400 – 4000 cm^{-1}) as shown in figure below.

Figure 3.7 : Photograph of Shimadzu IRPrestige-21 FTIR spectrometer

3.5. CV (Cyclic Voltammetry):

The PHE200Physical Electrochemistry Software is used with a Gamry Potentiostat to perform in-depth studies of the structure of the electrode interface and the mechanisms of electrochemical reactions. The PHE200 brings Cyclic Voltammetry and other recognized electrochemical research techniques to the Gamry user. The PHE200 is a useful tool for fundamental studies, sensor development, small-scale energy storage devices, electrophysiology, etc.

The PHE200 incorporates the following electrochemical techniques:

- Cyclic Voltammetry Cyclic Voltammetry
- Linear Sweep Voltammetry Linear Sweep Voltammetry
- Chronoamperometry Chronoamperometry
- Repeating Chronoamperometry Repeating Chronoamperometry
- Multiple- Multiple---Step Chronoamperometry Step Chronoamperometry Step Chronoamperometry
- Chronopotentiometry Chronopotentiometryiometry
- Repeating Chronopotentiometry Repeating Chronopotentiometry
- Chronocoulometry Chronocoulometry
- Controlled Potential Coulometry Controlled Potential Coulometry

Like most Gamry software, the PHE200 and a Gamry Potentiostat use the Framework for data acquisition and the Echem Analyst for data analysis. Gamry electrochemical techniques, therefore, have a common look-and-feel. Moving from one technique to another is easy.

3.5.1. Cyclic voltammetry:

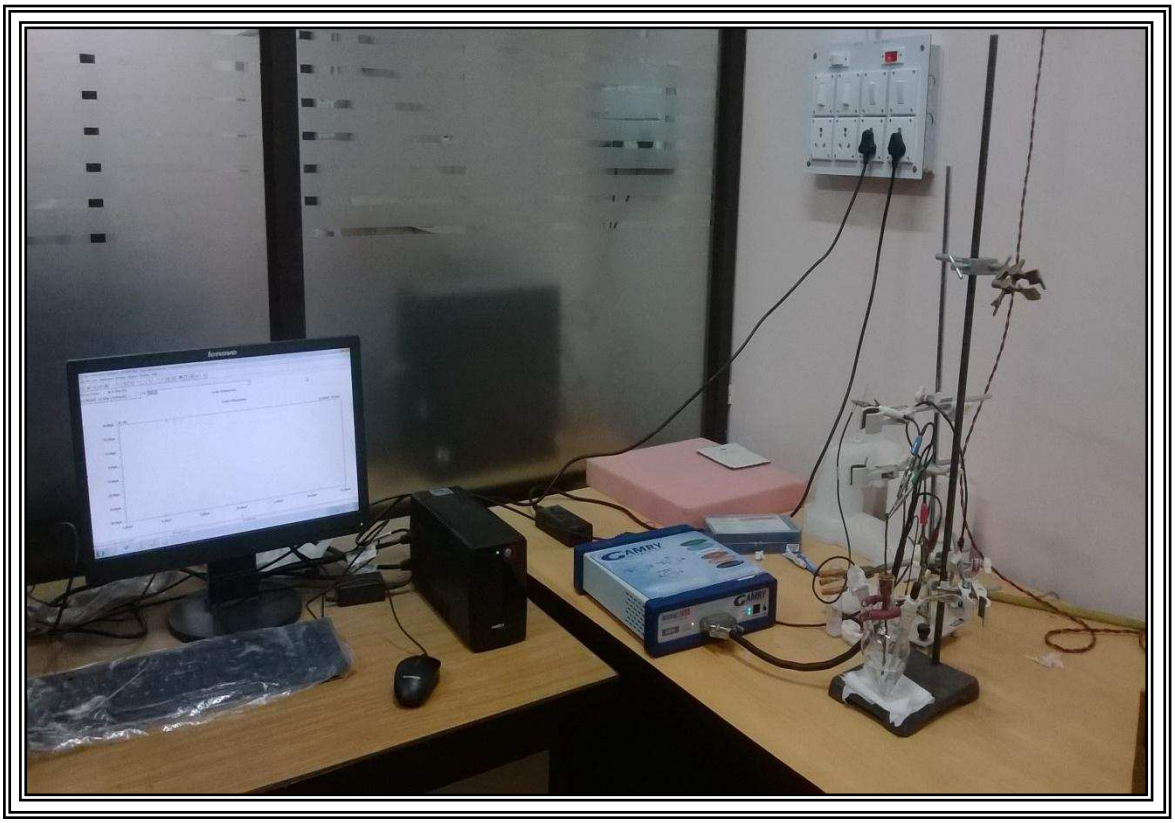

Figure 3.8 : Photograph of Cyclic Voltammetry

Cyclic Voltammetry is among the world's most commonly used techniques for studying electrochemical systems. The potential limits are defined with the Initial E, Scan Limit 1, Scan Limit 2, and Final E. For both a single cycle and a multiple cycle CV, the scan proceeds from one potential to the limit. One can define the potentials as absolute voltages or by their relationship to the Open-Circuit Potential. The scan rate (mV/s) is determined by the interval between data points (sample period) and the Step Size (mV):

Scan rate (mV/s) = Step Size (mV)/ sample period (s).....(3.4)

The minimum sample period may be as low as 3.3 µs. The maximum Scan Rate is a function of Step Size. For example, the maximum scan rate with a 2 mV step

is 600 V/s. Higher steps provide faster scan rates, but at the expense of resolution. Step sizes greater than 10 mV are likely to result in unsatisfactory data. The mode of the current measurement during a CV experiment may be specified by the user as auto-ranging or fixed. Auto-ranging is most convenient – the Gamry Potentiostat can select the most appropriate current range. Auto-ranging, however, should only be used for relatively low scan rates (less than 100 mV/s). Higher scan rates require fixed mode in which the user enters the maximum current and the PHE200 sets the appropriate current range. Current interrupt works great as long as the scan rate is less than 50 mV/s. Current Interrupt is simply turned on with the radio button and the PHE200 takes it from there. For higher scan rates, positive feedback is required if one want to compensate for IR drop. The age-old nemesis of positive feedback, of course, is selecting the proper amount of feedback. As usual, Gamry takes a totally new approach. We use Electrochemical Impedance Spectroscopy to measure the uncompensated resistance of the cell. We make the EIS measurement at a high frequency to make sure the resistance is valid (the limiting impedance at high frequency is the solution resistance). That impedance is employed as the solution resistance in positive feedback IR compensation. One use that resistance and the current range to apply the correct amount of positive feedback to make sure your applied potential is accurate, but not so much that the potentiostat is pushed into oscillation.

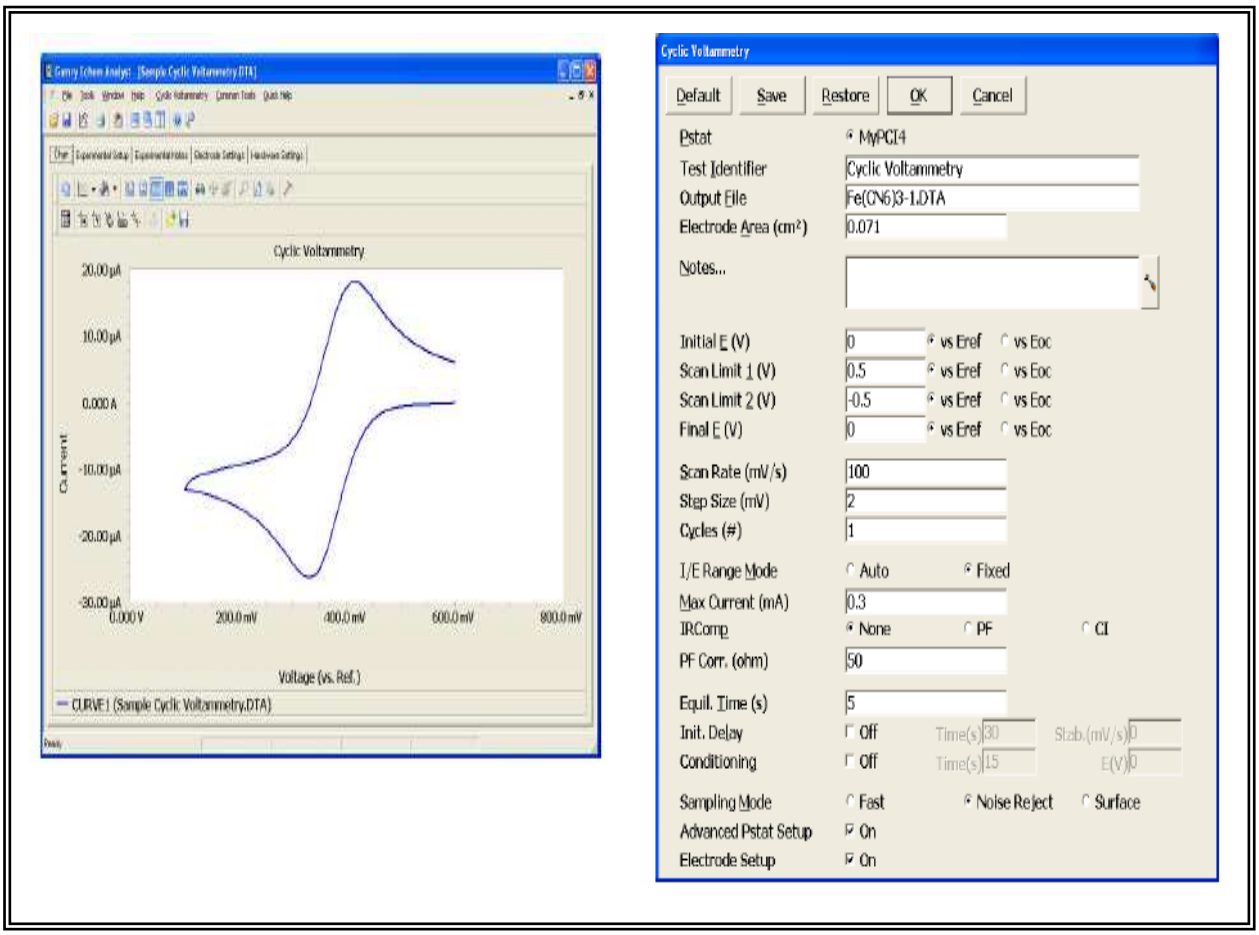

Figure 3.9 : View of the PHE200 Physical Electrochemistry Software

3.6. LCR meter:

This device can perform variable measurement frequencies over broad ranges. The 3522-50 can provide DC or 1 mHz to 100 kHz for measurements, and the 3532-50 can provide 42 Hz to5 MHz, with precise ±0.08% basic accuracy. With this high performance, along with their ease of use, broad set of functions and low price, these LCR measurement instruments achieve outstanding cost performance. These instruments are especially suitable for laboratory applications such as for evaluating operating characteristics, and with their 5 ms fastest response, versatile interface options and comparator functions, they are also ideal for a broad range of production line applications.

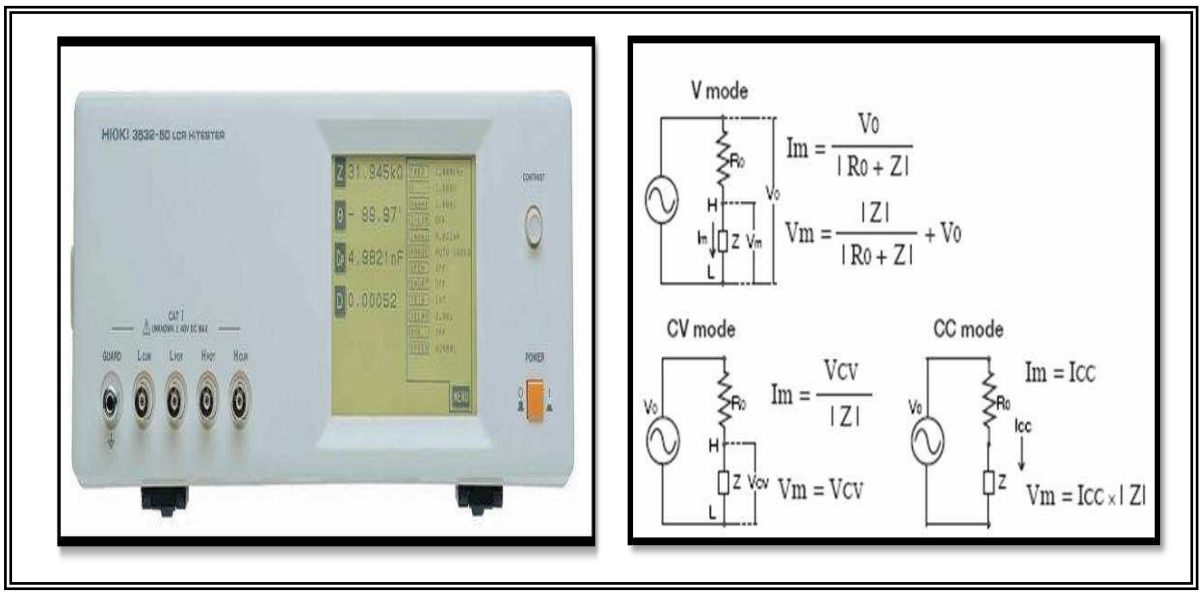

Figure 3.10 : LCR Meter and its Mode of Operation

Chapter 4:

Synthesis and Characterization of amorphous carbon nanotubes based nanocomposites with polypyrrole and bismuth ferrite

4. Synthesis and Characterization of amorphous carbon nanotubes based nanocomposites with polypyrrole and bismuth ferrite

4.1. Detailed Synthesis Procedure:

Synthesis of Amorphous CarbonNanotube (aCNT) :

Ferrocene and ammonium chloride were mixed (in the ratio 1:2) thoroughly in a mortar and taken in an alumina boat. The boat was placed in an air furnace at a temperature 250°C for 30 minutes. The boat was covered by a mica sheet to avoid the immediate evaporation of ferrocene. After heating, the sample was allowed to cool naturally and the obtained black powder was collected from the boat. Then the collected black powder was washed repeatedly by diluted HCl and deionized water and finally dried at 80°C for 24 hours.

Synthesis of Bismuth Ferrite (BFO) :

Bismuth nitrate ($Bi(NO_3)_3{\cdot}5H_2O$) and iron nitrate ($Fe(NO_3)_3{\cdot}9H_2O$) were weighed in stoichiometric proportions and 4.202 g of citric acid ($C_6H_7O_8$) were added to the mixture as a chelating agent. Then the mixture was dissolved in deionized water to make a solution. After the formation of a clear solution, ethylene glycol was added under vigorous stirring. The obtained light yellow coloured solution was kept undisturbed for 1~2 days to form a gel. The as synthesized gel was heated in a box furnace at a temperature of 180°C for 30 minutes. Subsequently, the collected powders were was rinsed repeatedly with diluted nitric acid (HNO_3) and deionized water and finally dried at 80°C for 24 hours.

Synthesis of Polypyrrole(PPy) :

The synthesis of polypyrrole was carried out by the chemical polymerization of pyrrole monomer at the temperature of 0-5°C. In a beaker 20ml of deionized (DI) water and 0.0612ml of HCl were taken and then sonicated. Afterwards the beaker was kept in ice-bath which was constantly maintained at a temperature between 0-5°C. Pyrrole monomer (0.01 mol) was added to this solution. Now, in another beaker 12.5ml deionized water and 0.82g of ammonium persulfate (used as oxidants) were taken and sonicated. After sonication, when a solution is formed, then it was kept undisturbed in ice-bath for few minutes. Then this solution was poured dropwise in the pre-treated solution while constant stirring and it is kept untroubled for 24 hours. After that, the obtained dark coloured sample was washed repeatedly by methanol and deionized (DI) water until it is colourless and finally dried at 80°C for 24 hours. It was named by PPy.

Synthesis of BFO-PPy composite:

Formation of a nanocomposite of BFO and PPy was carried out using in-situ chemical polymerization of pyrrole monomer with aCNTs. Ammonium persulfate (APS) ($(NH_4)_2S_2O_8$, 0.82g) as oxidants for polymerization of pyrrole was added 12.5 mlofDI water. The mixture was taken in a beaker which was then sonicated to dissolve the oxidant and kept in ice-bath at a temperature 0-5°C.In another beaker, a suspension of BFO (0.1 mmol) was made with pyrrole monomer (0.01 mol) in a solution of 25 ml of DI water and 0.076 ml of HCl and then kept in ice-bath after sonication. After that APS solution was slowly added dropwise into the BFO-pyrrole suspension with constant stirring and kept unaltered for 24 hours at ice-bath (0-5°C). After the polymerization was over, the BFO-PPy powder formed was filtered and

rinsed with DI water and methanol until the filtrate was colourless. The prepared powder was then dried in air-oven at 80°C for 24 hours and it was denoted by BPy.

Synthesis of aCNT-PPy composite:

Formation of a nanocomposite of aCNT and PPy was carried out using in-situ chemical polymerization of pyrrole monomer with aCNTs. Ammonium persulfate (APS) ($(NH_4)_2S_2O_8$, 0.82 g) as oxidants for polymerization of pyrrole was added 12.5 mlofDI water. The mixture was taken in a beaker which was then sonicated to dissolve the oxidant and kept in ice-bath at a temperature 0-5°C. In another beaker, a suspension of aCNT (0.06 g) was made with pyrrole monomer (0.01 mol) in a solution of 25 ml of DI water and 0.076 ml of HCl and then kept in ice-bath after sonication. After that APS solution was slowly added dropwise into the aCNT-pyrrole suspension with constant stirring and kept unaltered for 24 hours at ice-bath (0-5°C). After the polymerization was over, the aCNT-PPy powder formed was filtered and rinsed with DI water and methanol until the filtrate was colourless. The prepared powder was then dried in air-oven at 80°C for 24 hours and it was denoted by CPy.

Synthesis of aCNT-BFO-PPy composite :

In-situ chemical polymerization of pyrrole monomer with suspension of aCNT and BFO had resulted into the formation of aCNT-BFO-PPy nanocomposite. Ammonium persulfate (APS) ($(NH_4)_2S_2O_8$, 0.82 g) as oxidants for polymerization of pyrrole was added 12.5 ml of DI water. The mixture was taken in a beaker which was then sonicated to dissolve the oxidant and kept in ice-bath at a temperature 0-5°C. In another beaker, a suspension of aCNT (0.06 g) was made with pyrrole monomer (0.01

mol) and BFO (0.1mmol) in a solution of 25 ml of DI water and 0.076 ml of HCl and then kept in ice-bath after sonication. After that APS solution was slowly poured dropwise into the (aCNT, BFO and pyrrole) suspension with constant stirring and kept unaltered for 24 hours at ice-bath (0-5°C). After the polymerization was over, the aCNT-BFO-PPy powder formed was filtered and rinsed with DI water and methanol until the filtrate was colourless. The prepared powder was then dried in air-oven at 80°C for 24 hours. The suspension of aCNT, BFO and pyrrole was made with three modifications by altering the amount of BFO :

1. The molar concentration of BFO was 0.1mmol. The prepared composite was named as CBPy.
2. The molar concentration of BFO was doubled i.e 0.2mmol. The prepared composite was named as CBPy2.
3. The molar concentration of BFO was tripled i.e 0.3mmol. The prepared composite was named as CBPy3.

Electrochemical sample preparation:

The working electrode was prepared by using the mixture of 80 wt% active material, 15 wt% carbon-black and 5wt% PVDF binder followed by the dropwise addition of an organic solvent N,N-dimethylformamide(DMF) to the afore-mentioned mixture upon continuous stirring to get slurry. After this the slurry mixture was coated on Ni foam substrate and dried in air-oven at 80°C for 24 hours. After drying the active electrode material was pressed to make better adhesion and compactness of material to substrate. The cell consists of three electrode system. The active material as

working electrode, whereas platinum as counter electrode and saturated calomel electrode (SCE) as reference electrode and an electrolyte of 1 M Na_2NO_3 aqueous solution were used. Cyclic voltammetry and EIS (Electrochemical impedance spectroscopy) were performed on a Gamry Instruments (Interface 1000). Cyclic voltammetry was recorded in the voltage range from -1 to 1 at scan rate of 15, 25, 50, 100, 150, and 200 mV s^{-1}cycle no 1. The current density and specific capacitances were measured based on the active mass of the material in the working electrode. All electrochemical measurements were carried out with three electrode system at room temperature.

4.2. Characterization of prepared samples:

The as-synthesized samples were characterized by X-ray diffraction (XRD, Rigaku Ultima III) using CuK_α radiation of wave length λ = 1.54 Å for the structural information. Identification of the phases was done with the help of the Joint Committee on Powder Diffraction Standards (JCPDS) files. The Fourier transformed infrared spectra were recorded on a Shimadzu-8400S FT-IR spectrometer using a KBr-disc method. The detailed morphological feature of all the prepared samples were investigated by field emission scanning electron microscopy (FESEM, Hitachi, S-4800) and high resolution transmission electron microscope (HRTEM, JEOL-JEM 2100).

4.2.1. XRD Analysis:

The synthesized nanoparticles were characterized by using the room temperature powder X-ray diffraction with filtered 0.154 nm Cu Kα radiation for their phase analysis. The prepared samples are scanned in a continuous mode from 10°–80°.

The XRD analysis of $BiFeO_3$ (BFO) powder is shown in the Figure 4.1(g). The prominent peaks in XRD plots are indexed to various hkl planes of BFO, indicating formation of BFO which are in good agreement with JCPDS Card number 20-169. Besides these prominent peaks, some other peaks of low intensity are also observed, which do not belong to BFO

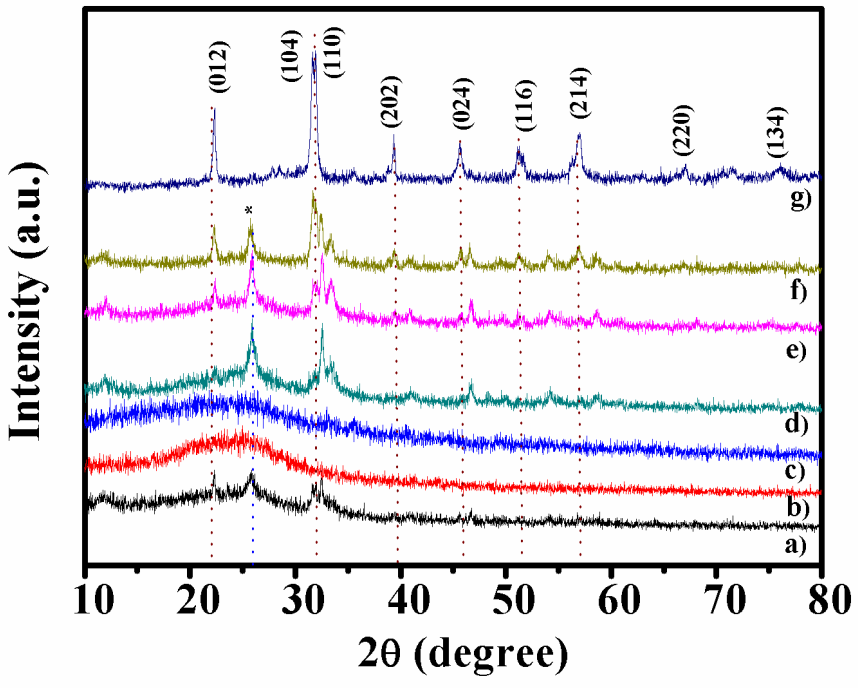

Figure 4.1 : XRD pattern of BPy (a), PPy (b), Cpy (c), CBPy (d), CBPy2 (e), CBPy3 (f), BFO (g)

The presence of PPy is also confirmed by XRD result, as shown in Figure 4.1(b). A characteristic peak of PPy is centered around 24.6° (Partch et al.1991), which can be assigned to the repeat unit of pyrrole ring, implying the polymer chain is highly oriented. The broad feature of the peak reveals the amorphous nature[1, 2]. This characteristic peak of PPy is marked by '*' in the aforesaid figure.

In Figure 4.1(c) the composite CPy shows a hump in-between 20° to 30° due to the amorphous nature of CNT. The sharpening of characteristic peak of PPy in the XRD pattern of other samples (Figure 4.1(a, d, e, f) may be due the crystalline nature of BFO. In addition, the typical peaks of BFO are also present in the composites with a slight shift which is shown in Figure 4.1(a, d, e, f). Hence, the presence of the BFO and PPy in the composites can be confirmed by XRD analysis.

4.2.2. FESEM analysis:

The surface morphologies of the as-prepared samples were examined with the help of Field Emission Scanning Electron Microscope (FESEM). The FESEM images of Bpy, PPy, BFO and CPy are depicted in the Figure 4.2(a-d) respectively

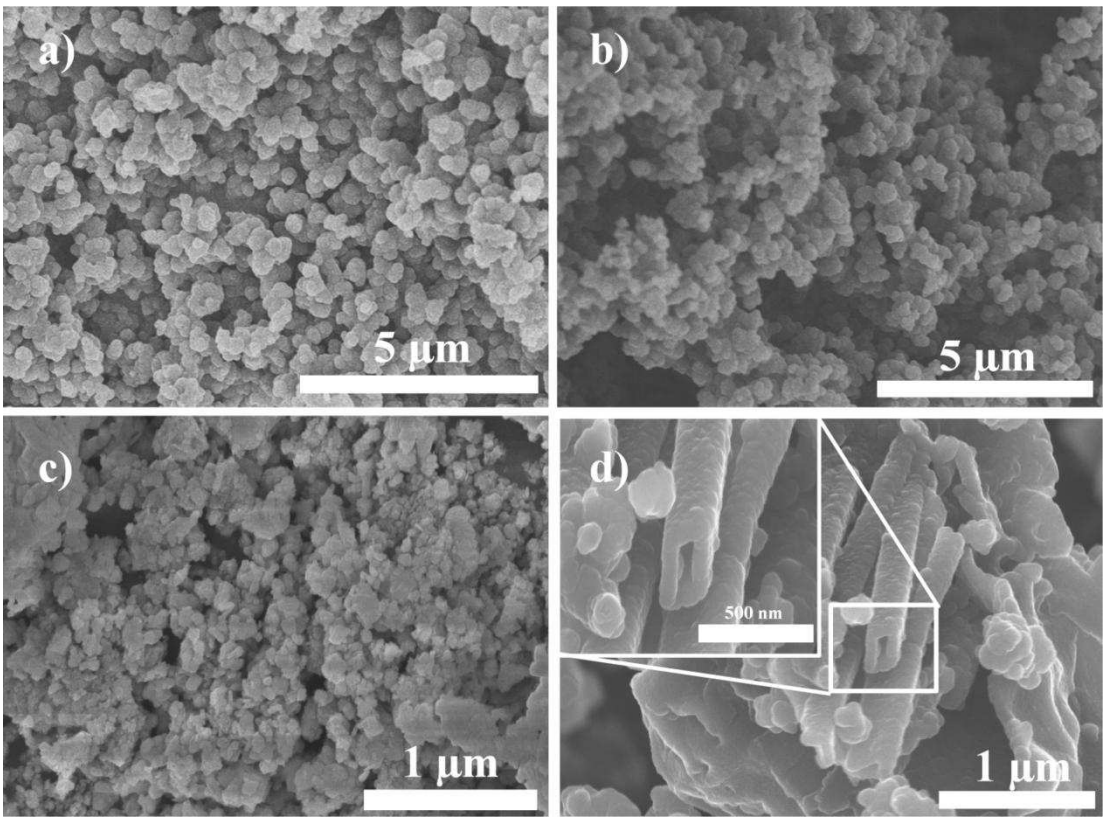

Figure 4.2 : Typical FESEM images of BPy (a), PPy (b), BFO (c) and CPy (d).

In Figure 4.2(a) PPy coated BFO are shown. From the Figure 4.2(b) clearly, spherical structure of pure PPy matrix can be identified. In Figure 4.2(d), PPy is tightly coated onto the surface of each amorphous CNT (aCNT). The average outer diameter of the composite is about 250 nm which can be easily obtained from the inset.

The surface of aCNT is coated with conducting polymer (PPy). The aCNT-BFO-PPy composite prepared by in-situ polymerization in this study form a coaxial core-shell nanostructure which is apparent from the Figure 4.3(a-c).

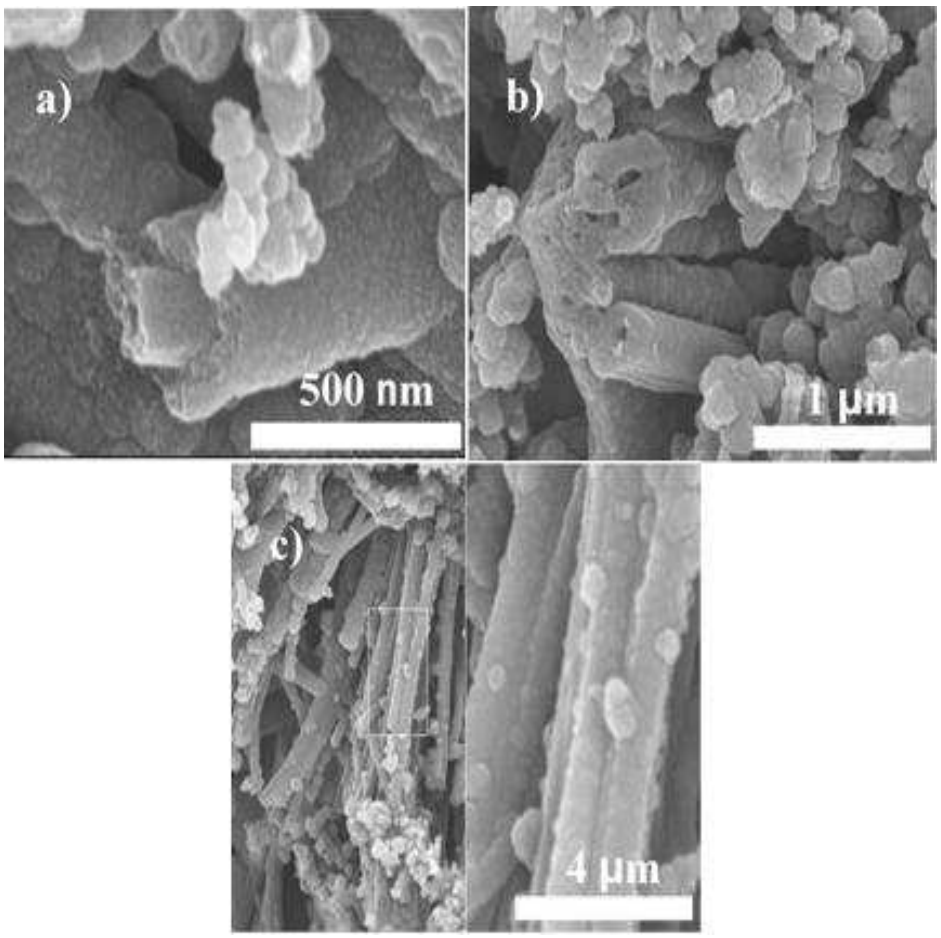

Figure 4.3 : Typical FESEM images of CBPy (a), CBPy2 (b), CBPy3 (c).

The particles on the exterior which are supposed to be BFO are scarcely distributed on the coaxial core-shell surface. The BFO particles are agglomerated and poorly dispersed in the matrix of carbon-polymer nanocomposites. Besides the dimension of the BFO particles are smaller as compared to the other constituents in the as-synthesized samples. The average outer diameter of the composite is about 250 nm and the corresponding inner diameter is about 70-100 nm (Figure 4.3(a)). This result further explained in the later section of this chapter.

4.2.3. TEM analysis:

To prepare the sample grid, TEM samples were dispersed in ethanol and sonicated for 5-10 min using bath sonicator to get well dispersion. Then the few micro-leters of solutions were dropped on carbon grids gently and then dried properly. The grids are dried in open air at room temperature for 24 h. High Resolution Transmission Electron Microscope (HRTEM) images were obtained with a JEOL (200 kV) HRTEM after 48 h of sample preparation.

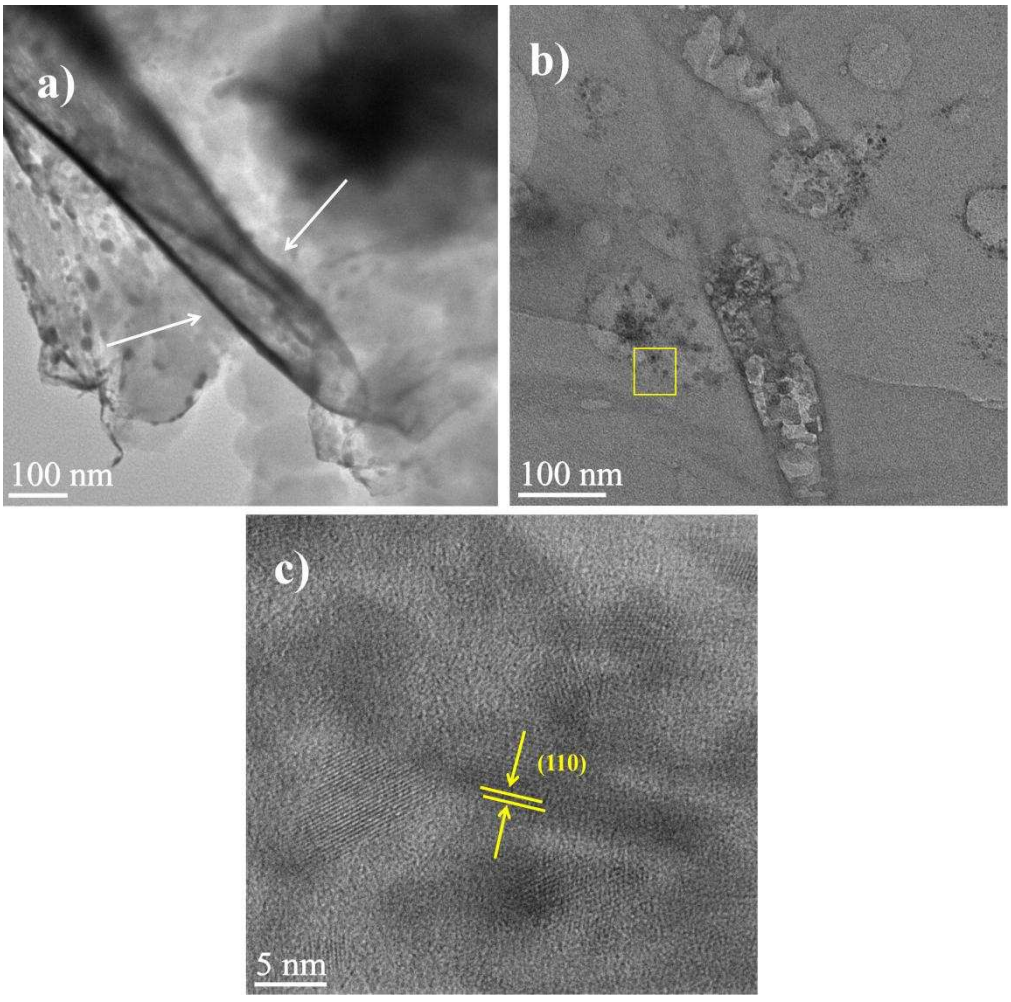

Figure 4.4 : Typical HRTEM images composites (a,b) and lattice image of BFO (c).

High resolution TEM images justifies the nanocomposite consist of BFO, PPy and aCNT. The BFO particles are distributed all over the aCNT indicated in yellow

box along with the PPy. The lattice image of BFO crystal has been shown in the Figure 4.4(c). Black coloured BFO particles are dispersed non-uniformly all over shown in the Figure of 4.4(b). In this figure lattice plane (110) of BFO is indicated in yellow lines which is further assured by XRD analysis. Along the length of aCNTs the conducting polymers have been coated forming a co-axial core shell like structure. The average diameter of aCNTs is near about 70 nm depicted from HRTEM.

4.2.4. FTIR Spectra:

As shown in Figure 4.5, two characteristic IR peaks together with some weak peaks appeared for BFO. The sample has one sharp and one wide IR peaks, which correspond to the stretching vibrations of C-H and –OH. The IR wide peaks located at 3456 cm^{-1} was assigned to the stretching vibrations of structural hydroxyl (OH) groups. The IR peak located at 1382 cm^{-1} was attributed to the symmetry bending vibration of C–H. The IR peaks below 1000 (432, 457, 466, 490, 563, 818, 833) were corresponding to the vibrations bonds of Bi–O or Fe–O[3].

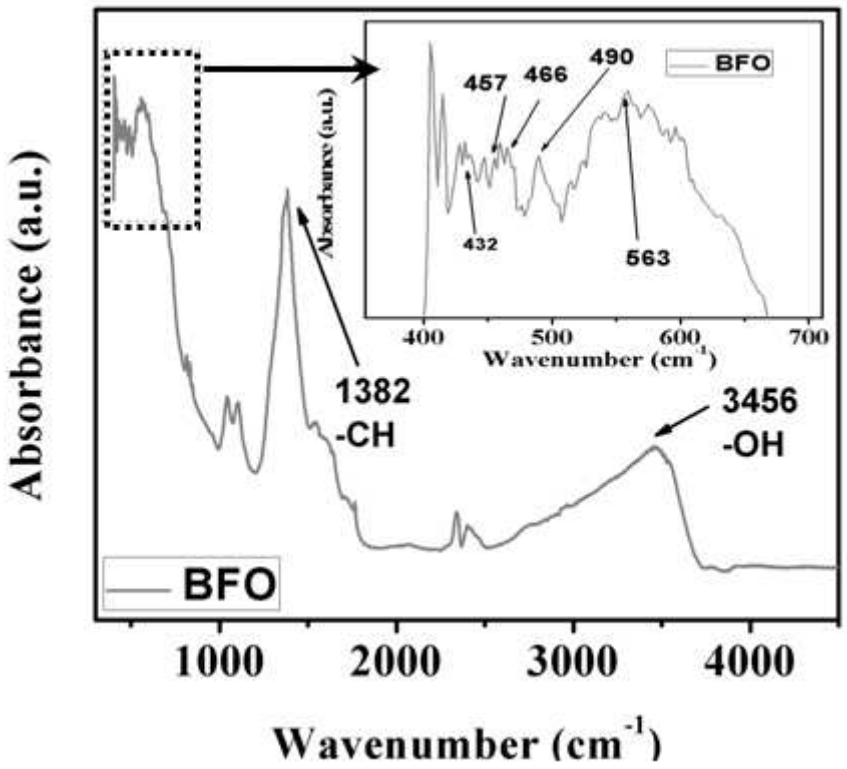

Figure 4.5 : FTIR spectra of pure BFO. Magnifield image of the selected portion (inset).

The chemical structure of the samples is confirmed by FT-IR analysis. The FT-IR spectrum of pure PPy (Figure 4.6(c)) shows a C–C stretching band at 1567 cm^{-1}, a conjugated C–N stretching band at 1488 cm^{-1}, a = C–H in-plane deformation band at 1316 cm^{-1}, a N–H in-plane deformation band at 1039 cm^{-1} and two doping-induced bands at 1210 cm^{-1} and 919 cm^{-1} corresponding to C–N stretching vibration and C–H out-of-plane vibration, respectively [4, 5]. In addition, the high ratio of the integrated peaks of 1540 cm^{-1} against 1446 cm^{-1} represents a long π-conjugation length of the PPy backbone.

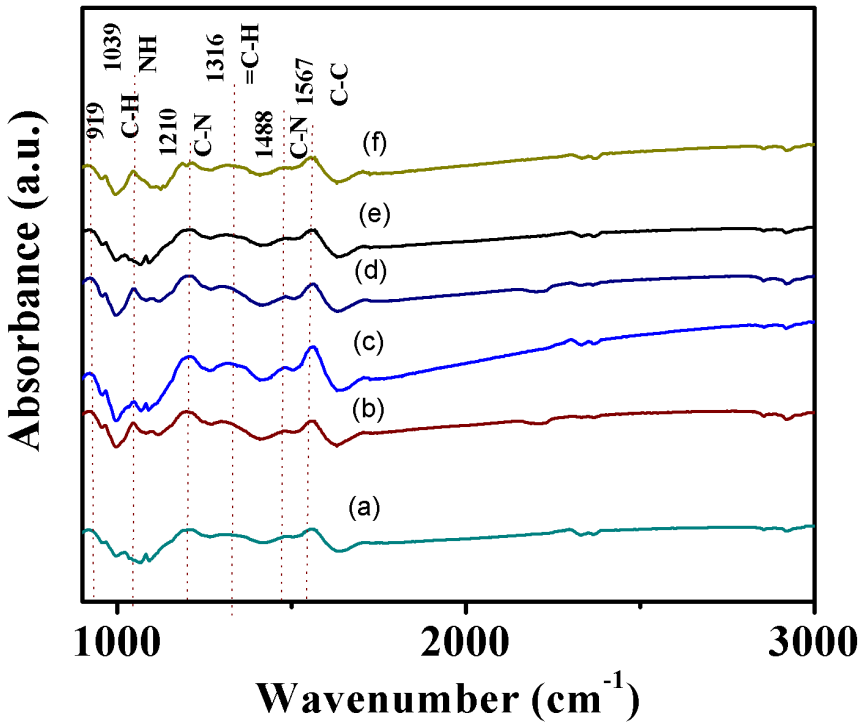

Figure 4.6 : FTIR spectra of CBPy (a), CBPy3 (b), PPy (c), CBPy2 (d), BPy (e), CPy (f).

The typical peaks of PPy are also present in the composites with a slight shift indicating the interaction among the constituents which is shown in Figure 4.6(a, d, e, f). The presence of corresponding bonds in the composites confirms the existence of PPy in the synthesized samples.

References:

1] Jian-Gan Wang, BingqingWeiandFeiyu Kang, (Communication) RSC Adv., 4 (2014) 199.

[2] T K Vishnuvardhan, V R Kulkarni, C Basavaraja and S C Raghavendra,Bull. Mater.Sci., 29 (2006) 77.

[3] Yongming Hu, LinfengFei, Yiling Zhang, Jikang Yuan, Yu Wang, and Haoshuang Gu , Journal of Nanomaterials, 2011 (2011) 6.

[4] L. Pan, L. Pu, Y. Shi, S. Song, Z. Xu, R. Zhang and Y. Zheng, Adv. Mater., 19 (2007) 461.

[5] H. S. Kim, D. H. Park, Y. B. Lee, D. C. Kim, H. J. Kim and J. Joo, Synth. Met., 157 (2007) 910.

Chapter 5:

Electrical and Electrochemical properties investigation of the amorphous carbon nanotubes –polypyrrole-bismuth ferrite nanocomposites

5. Electrical and Electrochemical properties investigation of the amorphous carbon nanotubes–polypyrrole-bismuth ferrite nanocomposites:

I-V characteristics measurements were performed by HIOKI 3522-50 LCR meter at room temperature. The detailed electrochemical measurements of all the samples were examined by in a one-compartment cell with a potentiostat or galvanostat (Gamry framework) at room temperature.

5.1. I-V Characteristics:

5.1.1. I-V Characteristics of the prepared samples :

In order to investigate the electrical properties (I-V Charasteristics), pellets of all the synthesized samples were made by a pelletizer taking approximately same amount of sample. These pellets were coated on both sides by silver paste, in order to make the parallel plate capacitor geometry. Already the ohmic nature of silver paste contacts has been confirmed by different researchers [1, 2]. Copper wires were attached on both sides by the silver paste in order to create two terminal network. Then the copper wires were connected by two terminals of HIOKI 3522-50 LCR Meter. The LCR meter was connected for voltage bias, and the current was read to measure current-voltage characteristics. All the measurements were performed with HIOKI 3522-50 LCR Meter at room temperature.

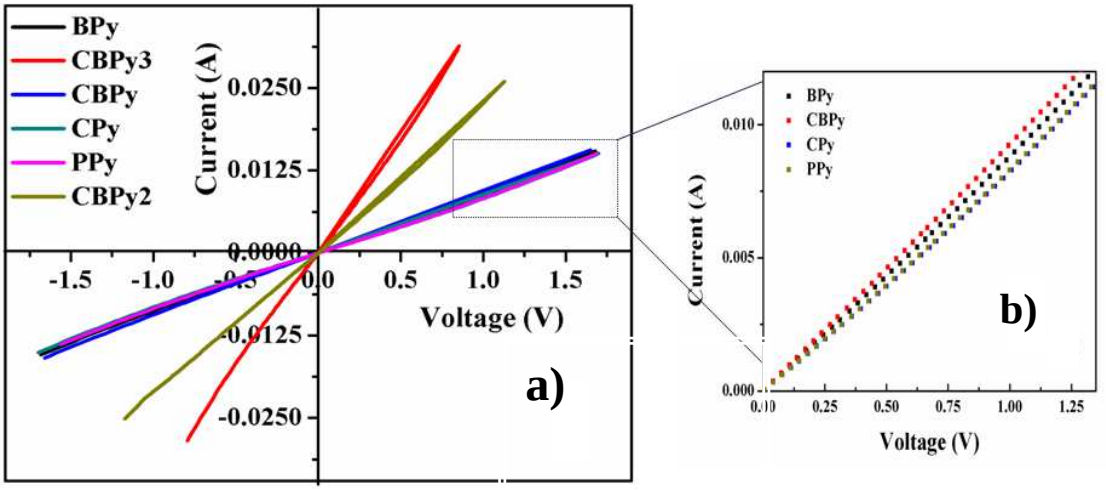

Figure 5.1 : I-V Characteristics of as-prepared samples (a), magnified image of the marked curve (b).

The I-V Characteristics of all the synthesized samples show a linear pattern. The current–voltage curves of the aCNT/PPy nanocomposites followed Ohm's law, reflecting the metallic character of the composites. From the Figure 5.1(a), it is observed that the line curve of CBPy3 sample (red line) is the steepest i.e it shows highest conductance among the other curves which may be attributed to the molar concentration of BFO. It can be concluded from the above figure, that as the molar concentration of BFO in the polymer-aCNT composites increases, conductance also increases i.e decrease in resistance. The variation slope of the curves shows as follows: CBPy3 > CBPy2 > CBPy > Cpy. From Figure 5.1(b), it can be seen that CBPy has a higher slope (lesser resistance) than BPy, CPy and pure PPy. The reason for this trend is still unknown to some extent. Many research works have been in progress in order to find a suitable explanation[3]. The increase of few ohms of resistance in case of CBPy may be due the amorphous nature of CNT. The possible reasons may be due to presence of defect states, loss of hybridization in amorphous CNT etc.

Table 5.1 : The calculated electrical parameters of the prepared samples

Sample	**Radius (cm)**	**Thickness (cm)**	**Area (cm^2)**	**Resistance (Ω)**	**Resistivity (Ωm)**	**Conductivity (S/m)**
PPy	0.7	0.13	3.08	116.822	27.233	0.03612
BPy	0.7	0.15	3.08	111.982	22.994	0.04349
CPy	0.7	0.23	3.08	117.786	15.775	0.06339
CBPy	0.7	0.29	3.08	106.496	11.310	0.08841
CBPY2	0.7	0.20	3.08	46.061	7.097	0.1409
CBPy3	0.7	0.16	3.08	28.776	5.540	0.1805

The electrical parameters are calculated from the slope of the I-V Characteristics and are represented in the above table. It is seen that, conductivity increases with the increase in BFO concentration in the nanocomposites. The conductivity of all the prepared samples is plotted in a bar chart shown in Figure 5.2.

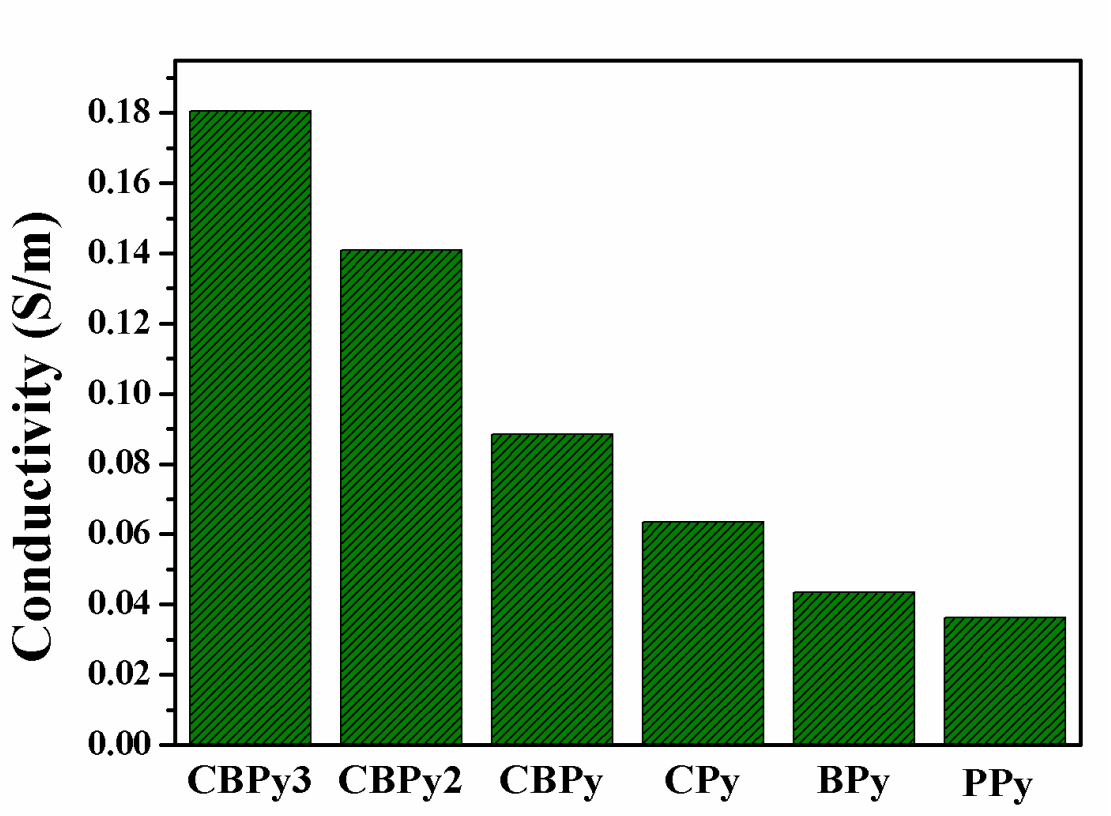

Figure 5.2 : Chart representing conductivity of the prepared samples.

I-V Characteristic represents the transport phenomenon of free electrons of the sample. Here, the voltage was applied to the ends of the pellet and the corresponding current was noted down. Another kind of transport phenomenon exists in the domain of electrochemistry which can be studied with the help of Cyclic Voltammetry. The later transport phenomenon is demonstrated by the movement of ions in the electrolyte. Voltage was applied across the two terminals (SCE and Working electrode) and corresponding current was measured with respect to the counter electrode.

The results of I-V and electrochemical measurements of different samples are opposite to each other. The sample showing good I-V characteristics exhibits poor

electrochemical behaviour. In order to examine this trend, we have investigated the transport phenomenon of ions of the samples by electrochemistry.

5.2. Electrochemical analysis:

5.2.1. CV study of as synthesised samples:

The specific capacitance of the electrode can be calculated according to the following equation[4]:

$$C = \frac{\int I.dV}{mvV}$$

.....(5.1)

where'I' is the response current density (A cm^{-2}), 'V' is the potential(V), 't' is the potential scan rate (mV s^{-1}) and 'm' is the mass of the as synthesised composites in the electrodes. Figure 5.3 shows the CV curves of CNT, pure BFO, PPy, CPy, BPy, CBPy, CBPy2 and CBPy3 composite at 100 mVs^{-1}. Figure 5.4 shows CV curves of individual composites in same voltage window and same scan rate. The CV shape of the composites shows a relatively regular rectangle without obvious redox peaks and a rapid current response to voltage reversal at each end potential, which indicates that composites mainly possess electrical double-layer capacitance. As for these composites, there are some of redox peaks in CV curve, attributed to the redox transition of pyrrole between a semiconducting state to conducting state which results in the redox capacitance.

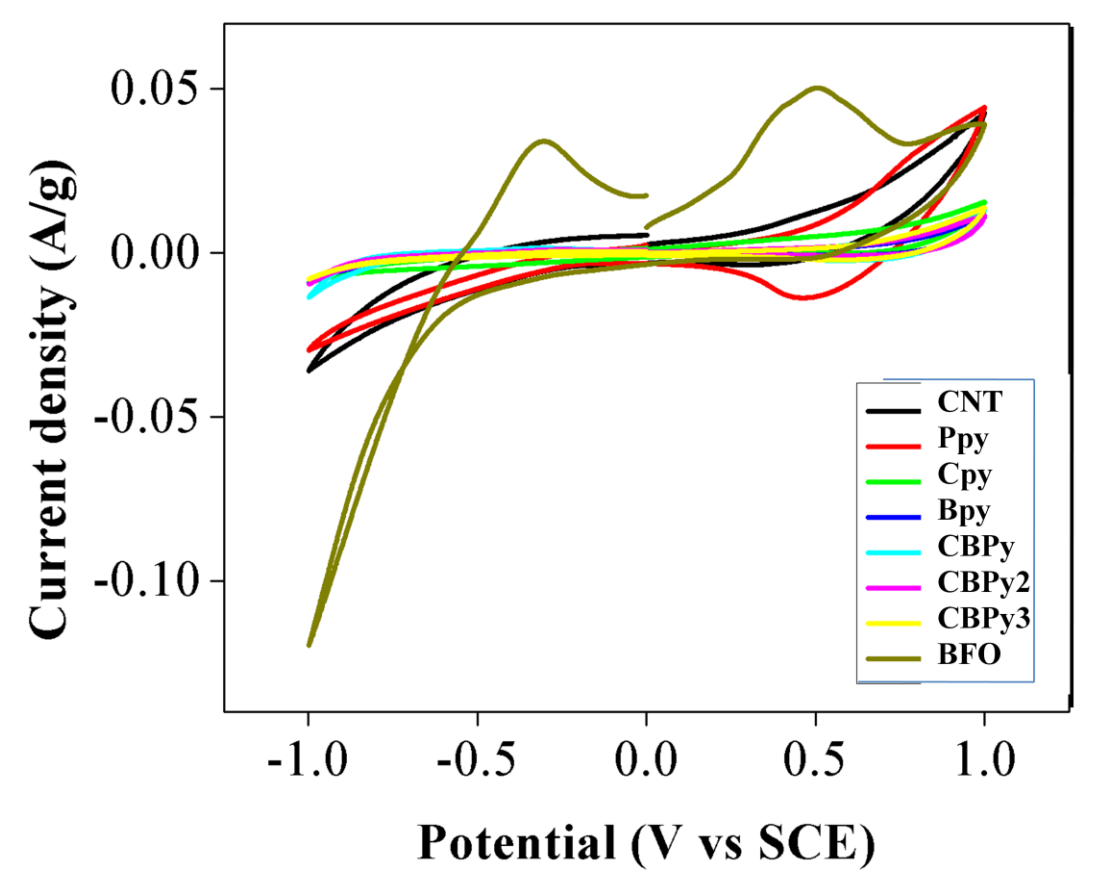

Figure 5.3 : Combined CV plots of all synthesised samples at 100mVs^{-1}.

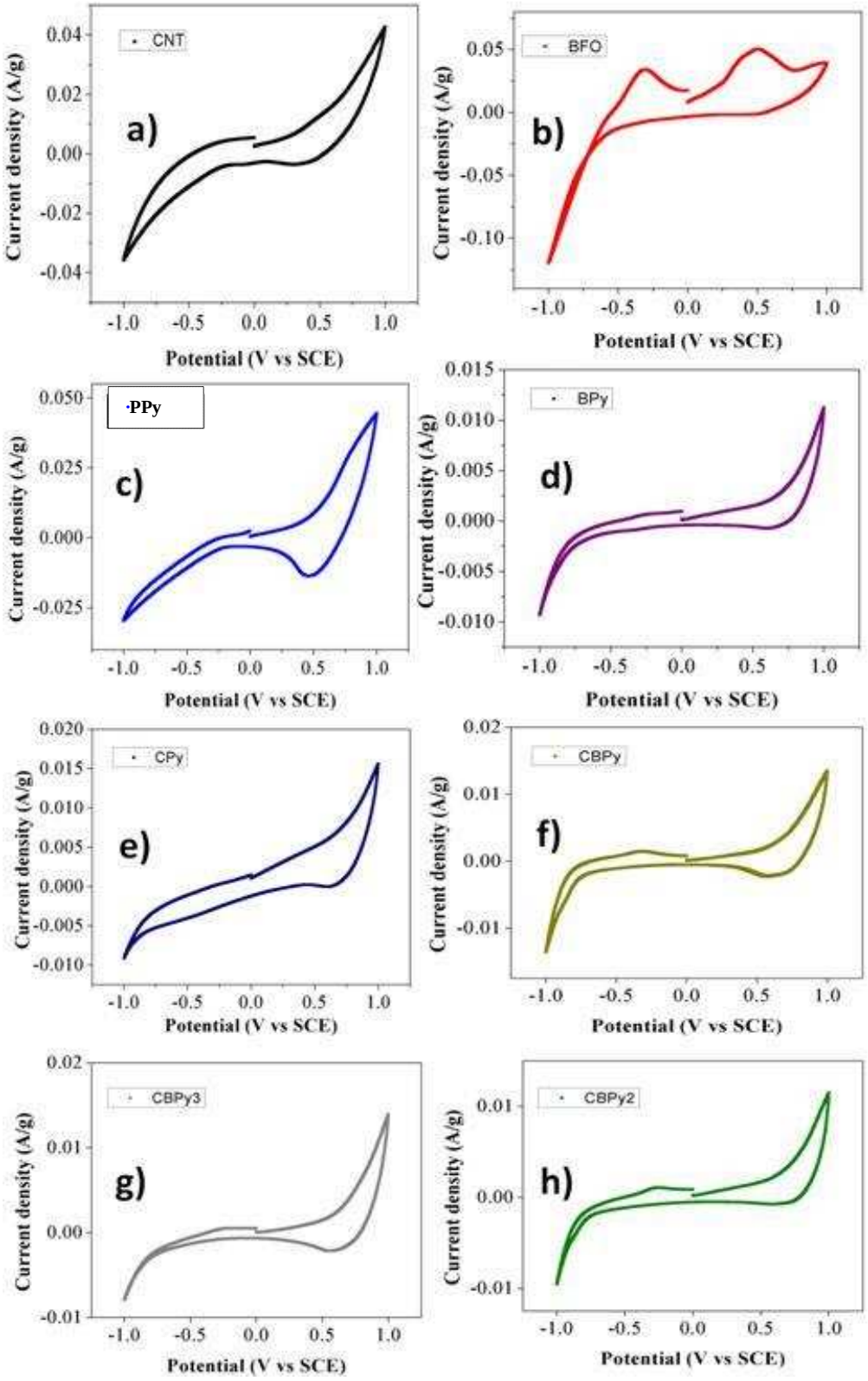

Figure 5.4 : CV plots of all synthesised samples (a) CNT (b) BFO (c) PPy (d) BPy (e) CPy (f) CBPy (g) CBPy2 and (i) CBPy3 at voltage window -1 V to +1 V at 100 mVs^{-1} for cycle no. 1.

As described in previous section of CV the dependency of Specific capacitance on different scan rates, here we observed the shift of cathodic and anodic peaks towards higher and lower regions[5] respectively of as synthesised individual samples of ours represented in Figure 5.5 to Figure 5.12 clearly for the scan rates 5, 15, 25, 50, 100, 150 and 200 mV s^{-1} for cycle no. 1 for sweep range -1 V to +1 V. The peak current at different scan rates is proportional to the square root of the scan rate $v^{1/2}$ which infers the reaction kinetics is controlled by the diffusion steps [6, 7]. Furthermore the rate of increment of current with higher scan rates has also been studied here. The current amount is also increased of CV plots as scan rate of samples were varied from low to high in contrast with specific capacitance. The dispersion of nanoscale pyrrole on CNT reduces the diffusion and migration length of the electrolyte ions during the electrolysis process and increases the electrochemical utilization of pyrrole. Besides, BFO and CNT in the composite can also provide better electron transfer path due to their excellent conductivity which enhances the conductivity of pyrrole. The plot of specific capacitances with different scan rate has been depicted in the Figure 5.13.

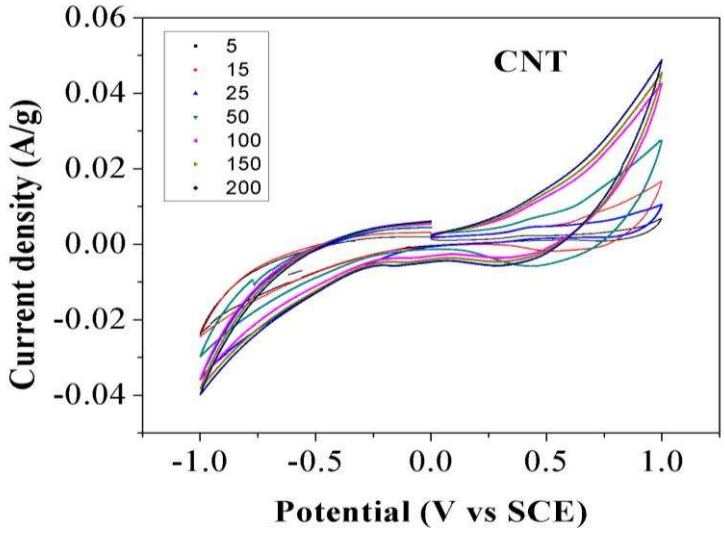

Figure 5.5 : CV plots of CNT at voltage window -1 V to +1 V at 5, 15, 25, 50, 100, 150 and 200 mV s^{-1} for cycle no. 1.

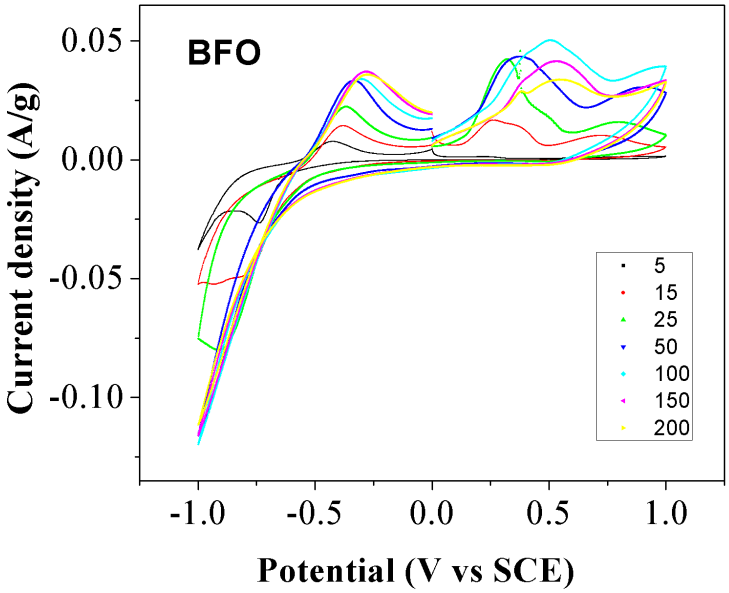

Figure 5.6 : CV plots of BFO at voltage window -1 V to +1 V at 5, 15, 25, 50, 100, 150 and 200 mV s^{-1} for cycle no. 1.

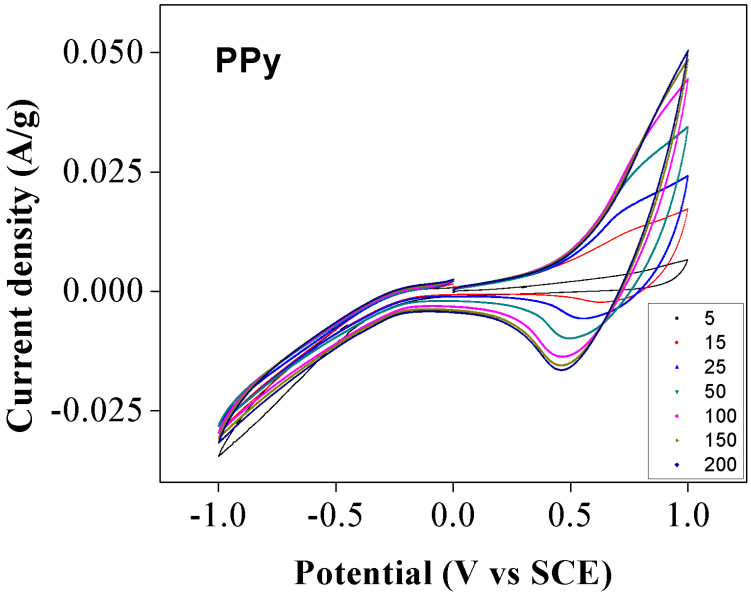

Figure 5.7 : CV plots of polypyrrole at voltage window -1 V to +1 V at 5, 15, 25, 50, 100, 150 and 200 mV s^{-1} for cycle no. 1.

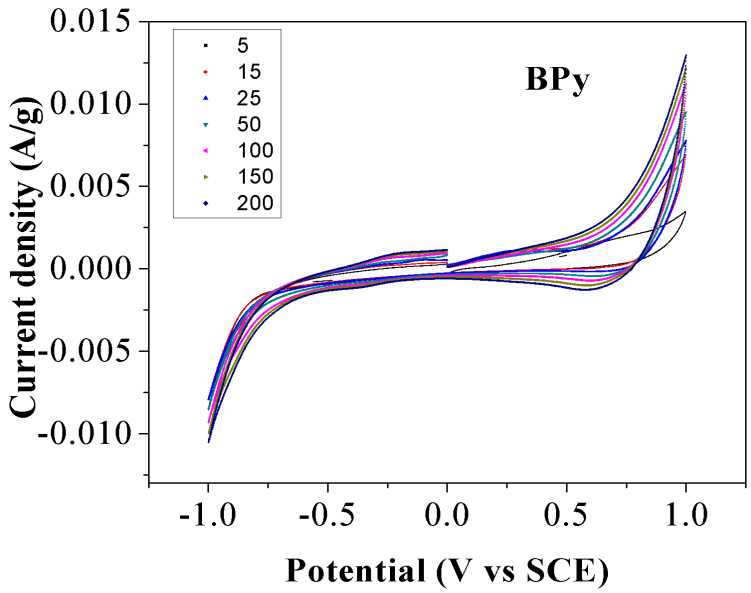

Figure 5.8 : CV plots of BPy at voltage window -1 V to +1 V at 5, 15, 25, 50, 100, 150 and 200 mV s^{-1} for cycle no. 1.

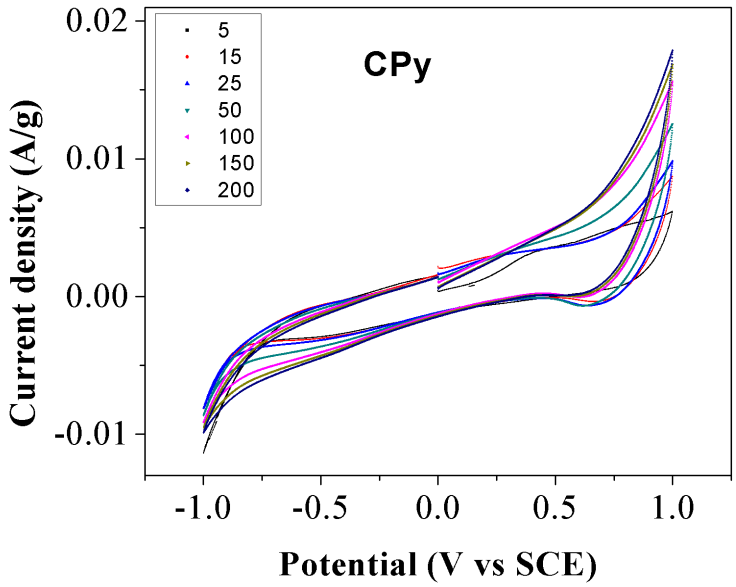

Figure 5.9 : CV plots of CPy at voltage window -1 V to +1 V at 5, 15, 25, 50, 100, 150 and 200 mV s^{-1} for cycle no. 1.

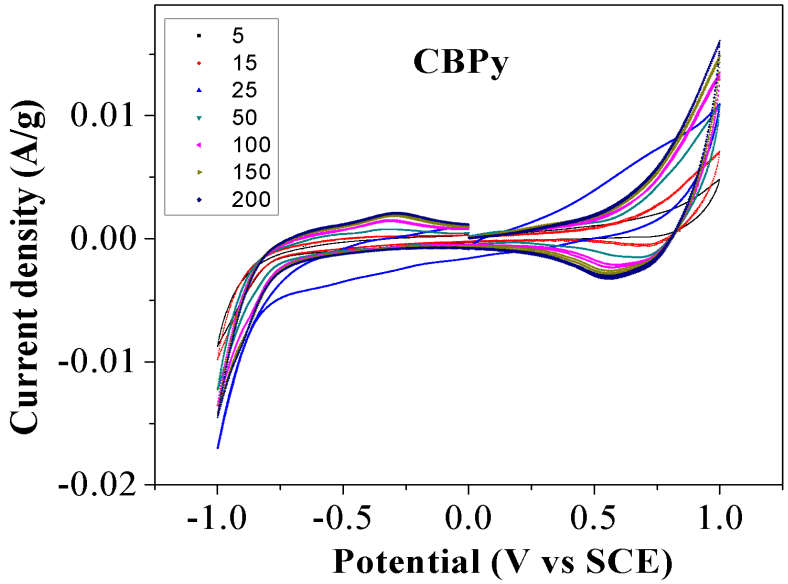

Figure 5.10 : CV plots of CBPy at voltage window -1 V to +1 V at 5, 15, 25, 50, 100, 150 and 200 mV s^{-1} for cycle no. 1.

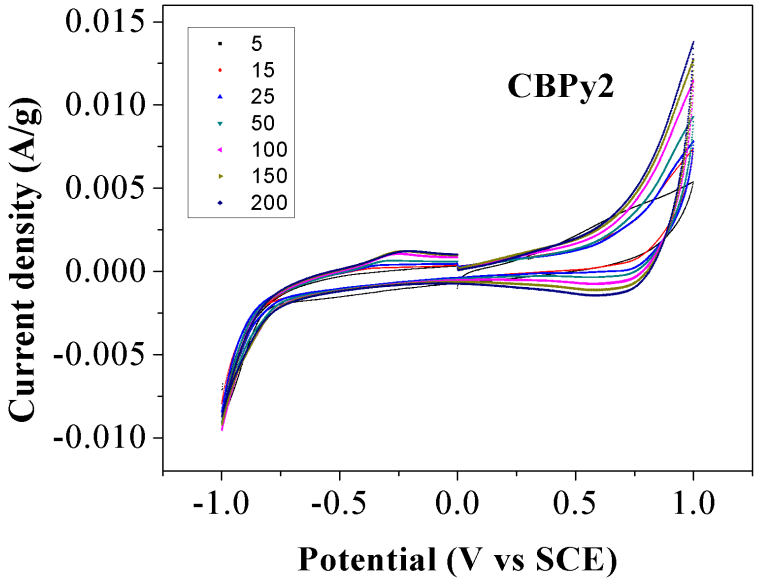

Figure 5.11 : CV plots of CBPy2 at voltage window -1 V to +1 V at 5, 15, 25, 50, 100, 150 and 200 mV s^{-1} for cycle no. 1.

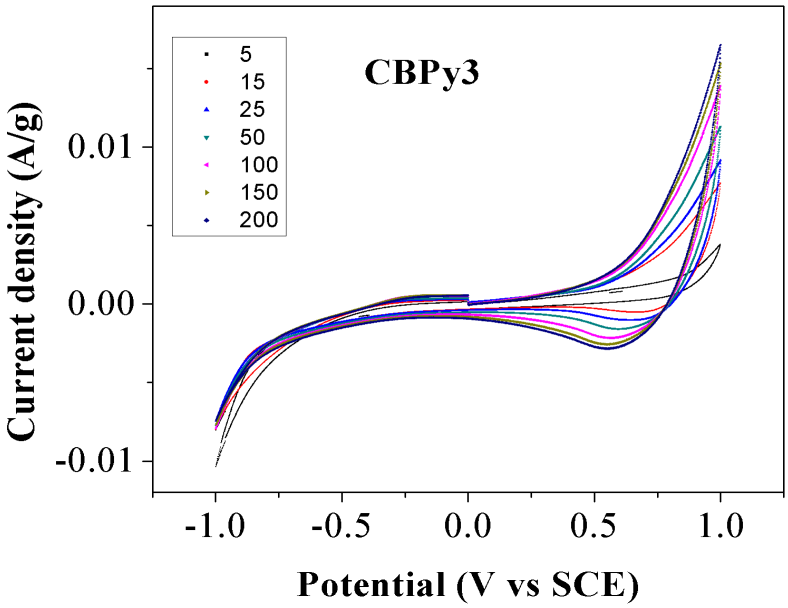

Figure 5.12 : CV plots of CBPy3 at voltage window -1 V to +1 V at 5, 15, 25, 50, 100, 150 and 200 mV s^{-1} for cycle no. 1.

Figure 5.13 shows the variation in the specific capacitance of CNT, BFO, pure polypyrrole and BPy, CPy, CBPy, CBPy2 and CBPy3 composite as a function of scan rates. It can be observed that the specific capacitance of Pyrrole is much higher than that of CNT and pure BFO and composites at the same scan rates. The maximum specific capacitance of 1.69 Fg^{-1} is obtained at a scan rate of 15 mVs^{-1} for CBPy3composite compared to 0.61 and 0.5 Fg^{-1} for CBPy2 and CBPy respectively. The greatly enhanced specific capacitance is due to the synergistic effect between CNT and BFO. In addition, the small pyrrole can exhibit enhanced electrode/electrolyte interface areas, providing high electroactive regions and short diffusion lengths[4], which can ensure the high utilization of Pyrrole.

The specific capacitances calculated for different as synthesised samples for same voltage range and cycle no 1 at different scan rates from the eq. 5.1 are tabulated below.

Table 5.2 : Specific capacitances of samples

Sample name	Specific capacitance (F/g)	Scan rate
CNT	0.5	5
	2.59	15
	12.7	25
	8.7	50
	4.92	100
	3.59	150
	2.84	200
PPy	0.304	5
	3.9	15
	18.75	25
	8.75	50
	3.7	100
	2.32	150
	1.62	200
BFO	43	5
	20	15
	19	25
	11	50
	4.707	100
	3.39	150
	2.41	200
BPy	0.055	5
	1.13	15
	0.85	25
	0.53	50
	0.32	100
	0.28	150
	0.21	200
CPy	0.051	5
	0.4	15
	0.87	25
	0.5	50
	0.28	100
	0.185	150
	0.14	200
CBPy	0.101	5
	0.5	15
	1.1	25
	0.4	50
	0.26	100
	0.21	150
	0.165	200
CBPY2	0.025	5
	0.61	15
	0.6	25

	0.35 0.24 0.16 0.142	50 100 150 200
CBPy3	0.00196 1.69 1.67 1.03 0.67 0.5 0.4	5 15 25 50 100 150 200

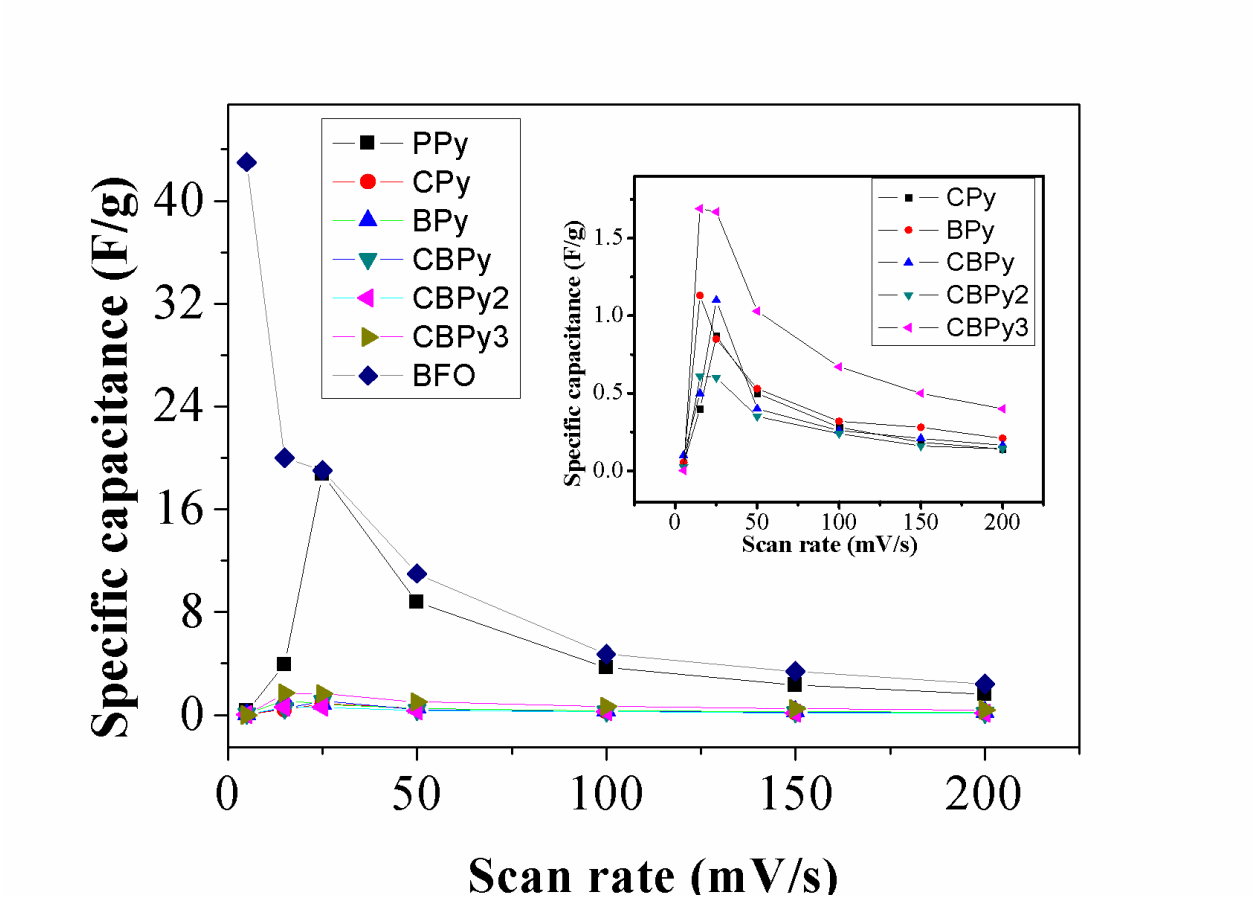

Figure 5.13 : Specific capacitance vs scan rate plots of samples at voltage window -1 V to +1 V at 5, 15, 25, 50, 100, 150 and 200 mV s^{-1} for cycle no. 1.

5.2.2. Nyquist plots of as-synthesised samples:

EIS Nyquist plots an extremely powerful and sensitive characterization technique for probing the electron-transfer kinetics. The Nyquist plots are semicircle in nature at high frequency region and show sloping straight line at low frequency region. The semicircle in high frequency region is due to the electrode/electrolyte interface charge transfer that represents to electrochemical controlled process[8]. The inclined straight line represents at low frequency range represents diffusion controlled process of ions in electrolyte to the surface of electrode. EIS measurements were carried out to compare the charge transfer resistances of different samples and composite as synthesized which are shown in Figure (5.14 and 5.15). BFO electrode provides smallest semicircle size that indicates an effective separation of photogenerated electron−hole pairs and fast interfacial charge transfer to the electron donor or acceptor in the Figure 5.14(c). It suggests that a more effective separation of photogenerated electron−hole pairs which may enhance the photocatalytic activity. Whereas, CNT and polymer show wider semicircles than BFO (Figure 5.14(a,b)). In comparison with the precursor materials the as prepared composites CPy, BPy, CBPy, CBPy2 and CBPy3 have exhibited semicircles of bigger size in the Figure 5.14(d-h) which demonstrates the faster diffusion rates of ions at the electrode/electrolyte interfaces. Thus these results also assure the higher rate of recombination of charged particles. Figure 5.15 represents the combined plot of nyquist plots of all as prepared samples from which it is clearly apparent that all the samples are not showing EIS characteristics in same range. It might have been inferred from the graph above mentioned the conductivity property of the as prepared samples are differed from each other which is also discussed in the section of Current-Voltage.

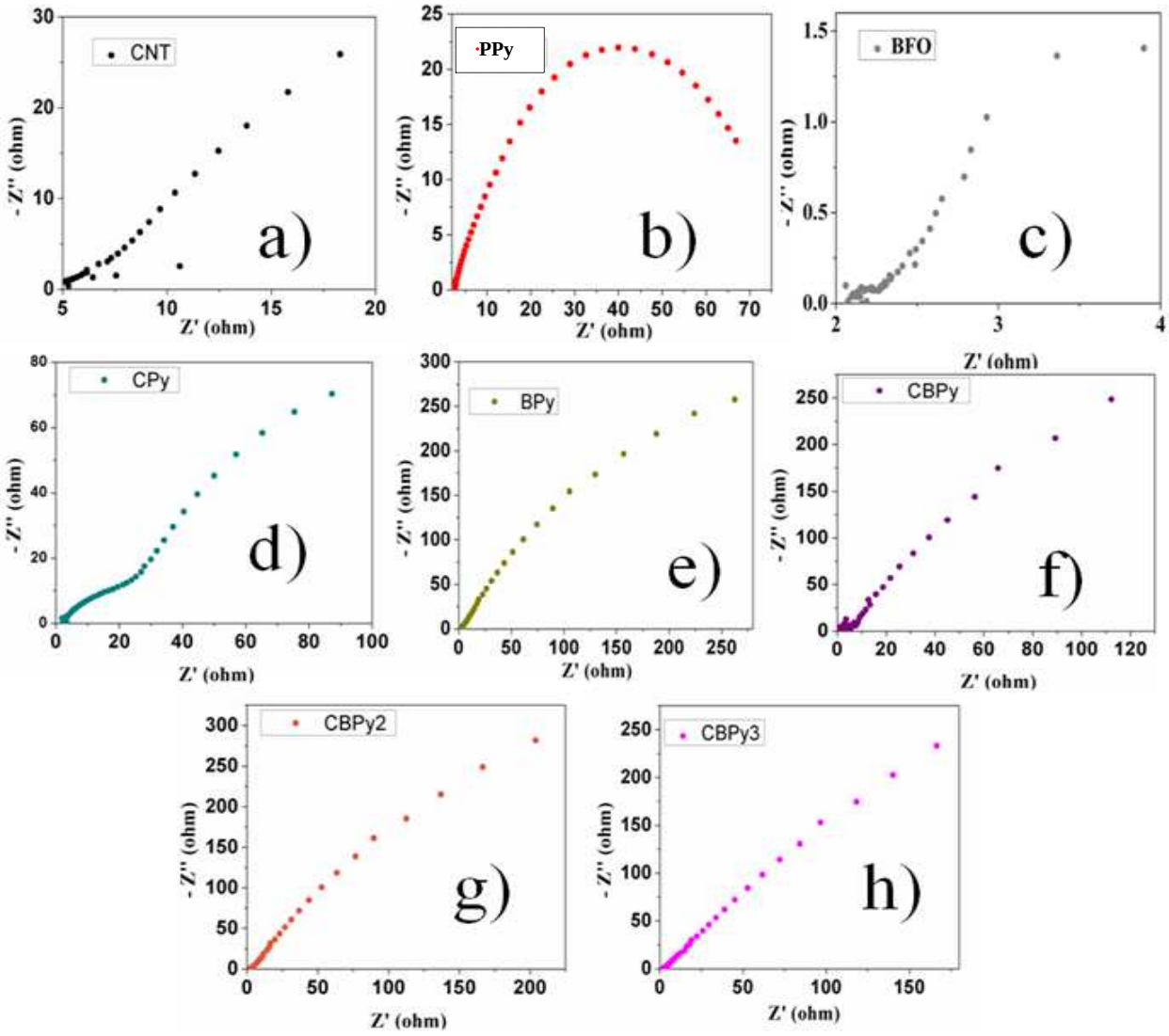

Figure 5.14 : Nyquist plot of as synthesised samples

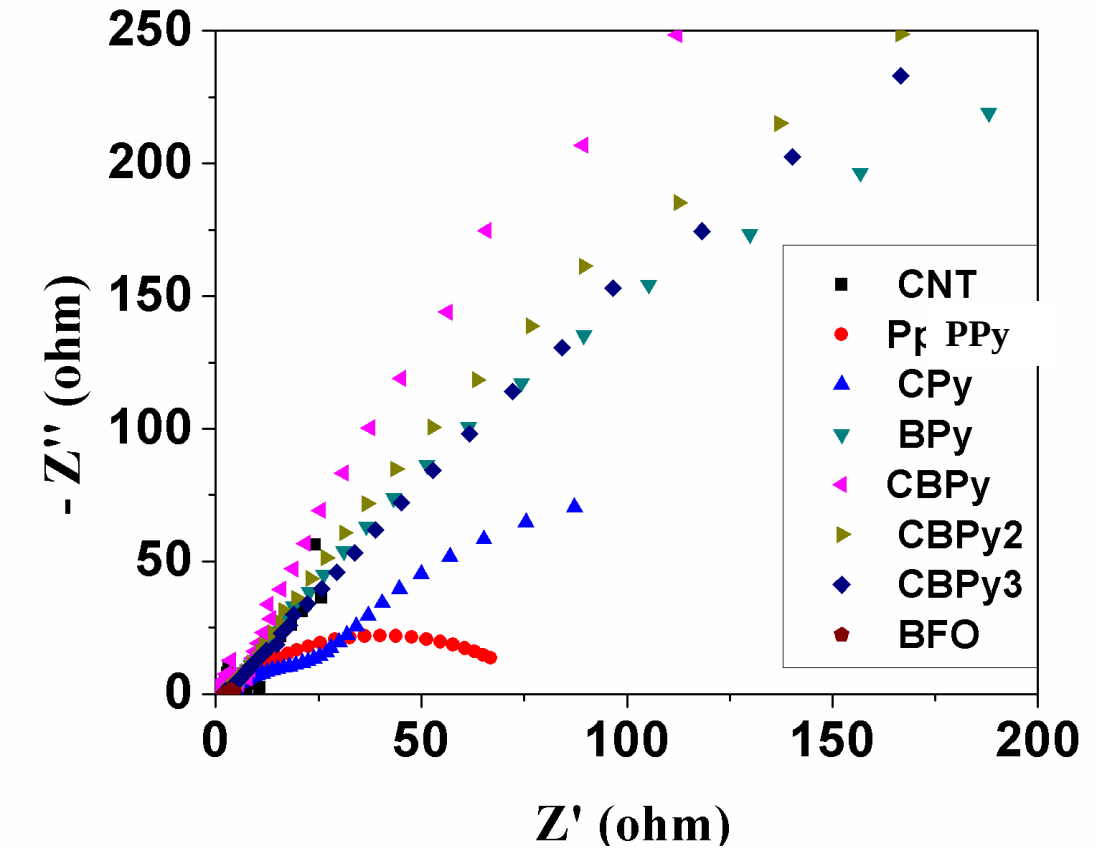

Figure 5.15 : Combo Nyquist plot of as synthesised samples.

5.2.3. Bode Plots of the samples:

Further, the composite and pure precursor material films were studied by EIS and for this reason the working electrodes was placed in a cell in such a way that only 0.5 cm^2 area of the working electrode was exposed to the solution. EIS studies were performed at open circuit potential, in an aqueous solution of 1 M Na_2NO_3 at 25 ºC. It is noted that EIS measurements were repeated more than 2 times to ensure reproducibility. The resulting Bode plots for CNT, PPy, BFO, CPy, BPy, CBPy, CBPy2 and CBPy3 systems are shown in Figure 5.16 to 5.24. Bode diagrams point

out also the capacitive behaviour in concordance with Nyquist plots (see in comparison Figure 5.14 and Figure 5.15).

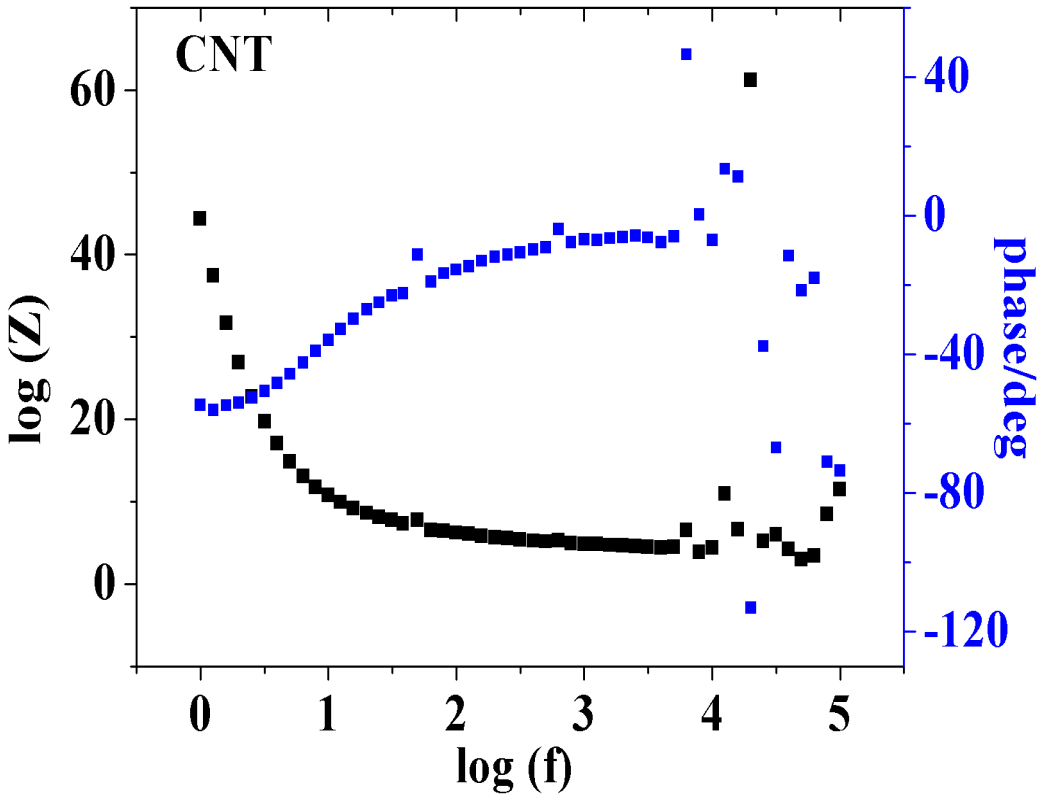

Figure 5.16 : Bode plot of CNT

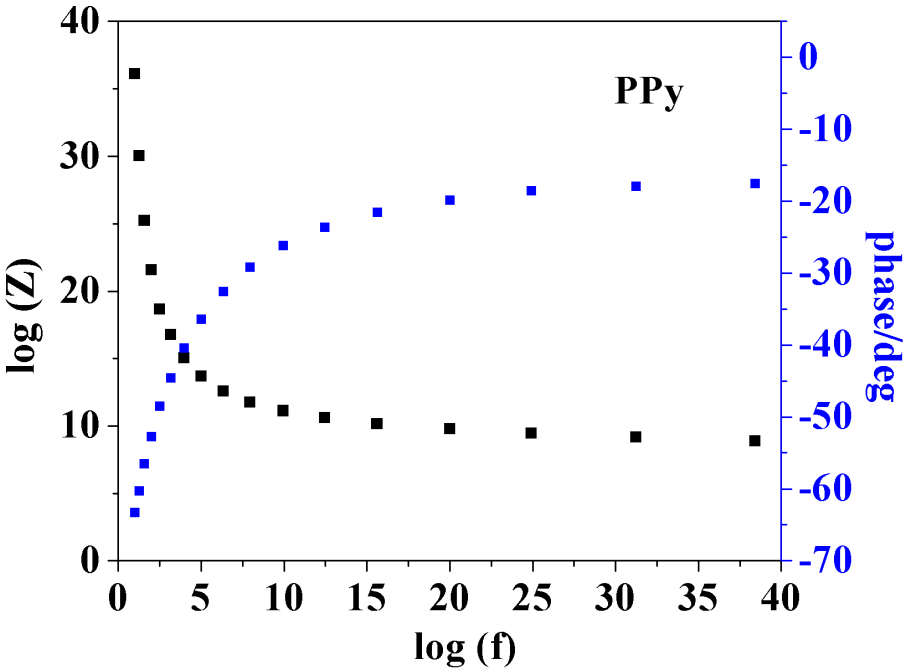

Figure 5.17 : Bode plot of PPy

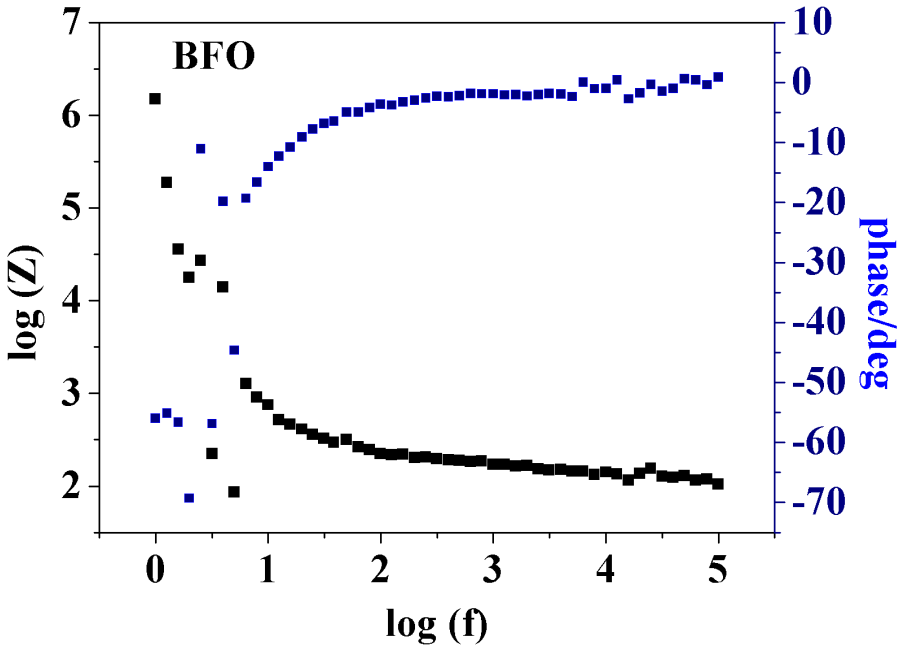

Figure 5.18 : Bode plot of BFO

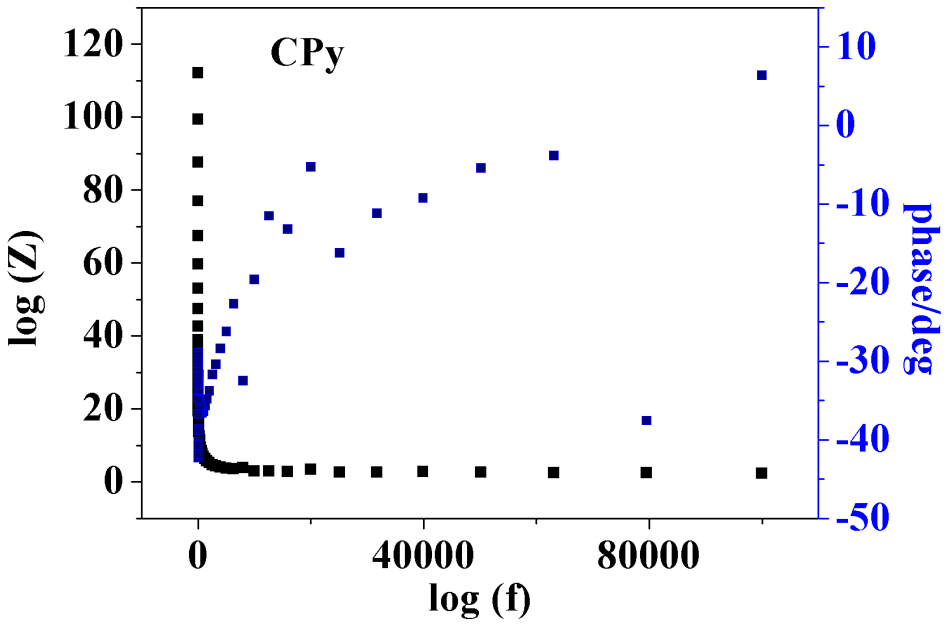

Figure 5.20 : Bode plot of CPy

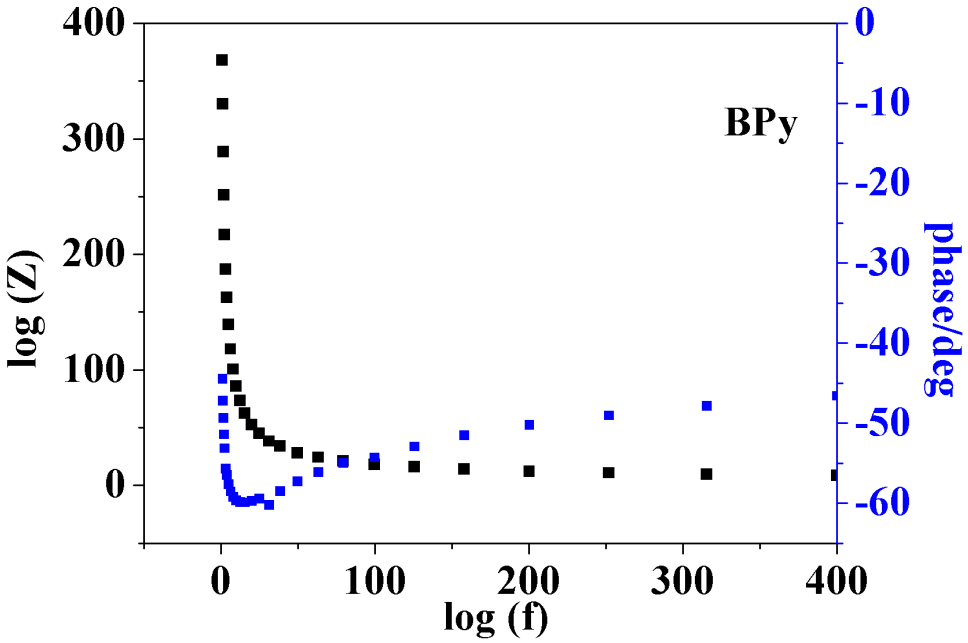

Figure 5.21 : Bode plot of BPy

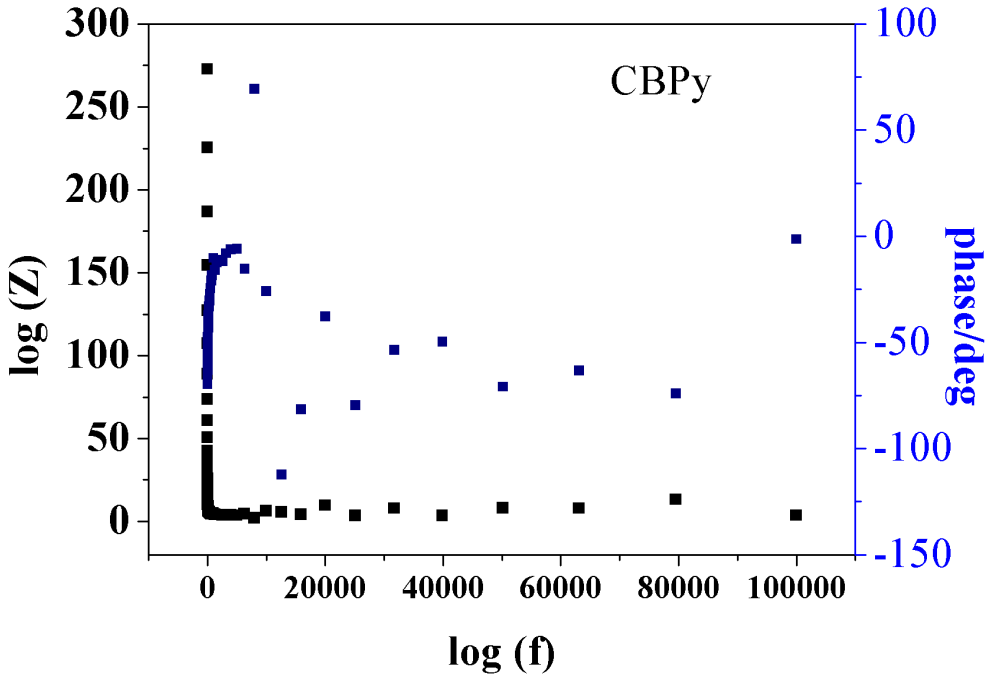

Figure 5.22 : Bode plot of CBPy

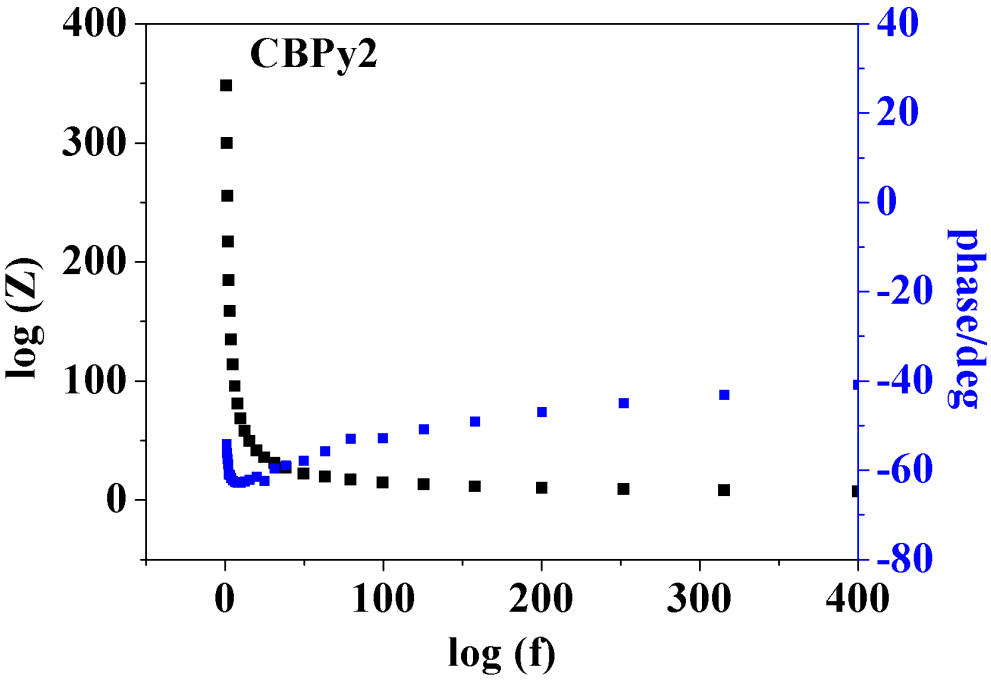

Figure 5.23 : Bode plot of CBPy2

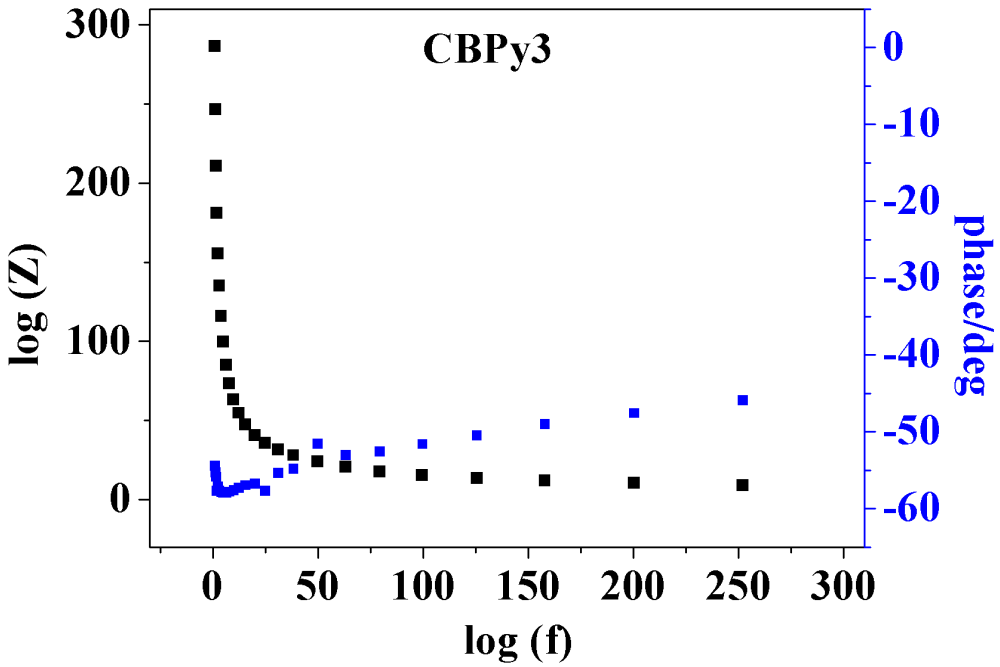

Figure 5.24 : Bode plot of CBPy

References :

[1] Tate J, Ju HL, Moon JC, Zakutayev A, Richard AP, Russell J, McIntyre DH, Phys Rev B 80 (2009) 165.

[2] Banerjee AN, Chattopadhyay KK, Appl Surf Sci 225 (2004) 243.

[3] Peter Kr. Petrov, Vaijayanti R. Palkar, Alexander K Tagantsev, Hsin-I Chien, K. Prashanthi, Anna-Karin Axelsson, S. Bhattacharya, Neil McN Alford, J. Mater. Res. 22 (2007) 2183.

[4] Jun Yan, Tong Wei, Bo Shao, Zhuangjun Fan, Weizhong Qian, Milin Zhang, Fei Wei, 48 (2010) 487.

[5] Jinwei Xu, Yunfei Wang, Zonghui Li, W.F. Zhang, Journal of Power Sources 175 (2008) 903.

[6] L.J. Fu, H. Liu, H.P. Zhang, C. Li, T. Zhang, Y.P. Wu, H.Q. Wu, J. Power Sources 159 (2006) 219.

[7] L. Kavan, M. Kalb, M. Zukalova, I. Exnar, V. Lorenzen, R. Nesper, M. Gratzel, Chem. Mater.16 (2004) 477.

[8] Zhang H, Cao GP, Wang WK, Yuan KG, Xu B, Zhang WF, Electrochim Acta, 54 (2009) 1153.

Chapter 6:
Grand Conclusion and Future Scope

6. Grand Conclusion and Future Scope:

6.1. Grand Conclusion:

Mainly in this work three different composites as prepared CBPy, CBPy2 and CBPy3 are synthesized via simple low temperature chemical synthesis. In the chemical synthesis CNT, BFO and conducting polymer are used as precursors. This procedure consists of in-situ polymerisation process.

Some of the characterisation procedures have been done successfully for the analysing of samples TEM, FESEM, XRD, FTIR, I-V & CV have been done. According to those different observations have been gathered which are analysized thoroughly.

According to TEM study the produced samples are wrapped with polymer and BFO is dispersed poorly along the length direction of main mother material aCNT. From the HRTEM images, coatings of polymer (pyrrole) on aCNT are clearly seen. FESEM images clearly have depicted the core-shell like co-axial structures of as prepared composites. From FTIR study the compositional comparison among composites and pure materials has been studied. From XRD plots structure and plane orientations of composites have been studied. For the application purpose current-voltage characteristic and electro-chemical study have been performed to compare as prepared samples. CBPy3 is highest conductive sample than CBPy2 and CBPy.

In the electrochemical investigation of samples shows good results of our samples where it is apparent from the results that CBPy exhibits most capacitive nature than the two other composites. Furthermore, nyquist and bode plots of the samples are also carried out to assure the electrochemical characteristics in more detail.

6.2. Future scope:

CNT has proved itself such an excellent material in the field of carbon based research for it's different novel properties. Hence it is being used in various ways for application purpose in the area of electronics, Biology, Chemistry, Medical and many more. It has drawn the interests of many research groups all over the world due to its enormous properties and application. Now with the incorporation of different material such as doping, attachments with CNT are being investigated widely in order to enhance its properties leads to wider and broader application purpose. On CNT almost all it's properties & features have already been investigated. According to them the newest approaches in this topic are still very surprising like electrochemical analysis. Still from this point of view if some main drawbacks about CNT could have been eliminated then it will add new possibility to flourish this field. In this thesis as discussed earlier the simple methods to synthesize three composites have been tried. Furthermore, comparisons among two different properties of the produced samples have been investigated such as I-V &CV.